NASA CONTRACTOR REPORT

EXPERIMENTAL VERIFICATION OF LOW SONIC BOOM CONFIGURATION

by Antonio Ferri, Huai-Chu Wang, and Hans Sorensen

Prepared by
NEW YORK UNIVERSITY
Bronx, N.Y. 10453
for

NATIONAL AERONAUTICS AND SPACE ADMINISTRATION • WASHINGTON, D. C. • JUNE 1972

1. Report No.	2. Government Accession No.	3. Recipient's Catalog No.
NASA CR-2070		

4. Title and Subtitle	5. Report Date
EXPERIMENTAL VERIFICATION OF LOW SONIC BOOM CONFIGURATION	June 1972
	6. Performing Organization Code

7. Author(s)	8. Performing Organization Report No.
Antonio Ferri, Huai-Chu Wang, and Hans Sorensen	NYU-AA-71-19
	10. Work Unit No.

9. Performing Organization Name and Address	11. Contract or Grant No.
A. Ferri & H. C. Wang New York University, Bronx, NYC 10453 H. Sorensen, Aeronautical Institute of Sweden, Bromma, Sweden	NGL-33-016-119
	13. Type of Report and Period Covered
12. Sponsoring Agency Name and Address	Contractor Report
National Aeronautics and Space Administration Washington, D. C. 20546	14. Sponsoring Agency Code RAA

15. Supplementary Notes

16. Abstract

A configuration designed to produce near field signature has been tested at M = 2.71 and the results are analyzed, by taking in account three-dimensional and second order effects. The configuration has an equivalent total area distribution that corresponds to an airplane flying at 60,000 ft. having a weight of 460,000 lbs. and 300 ft length. A maximum overpressure of 0.95 lb/ft^2 has been obtained experimentally. The experimental results agree well with the analysis. The investigation indicates that the three-dimensional effects are very important when the measurements in wind tunnels are taken at small distances from the airplane.

17. Key Words (Suggested by Author(s))	18. Distribution Statement
Sonic boom measurements or near field configurations at M = 2.7.	Unclassified - Unlimited

19. Security Classif. (of this report)	20. Security Classif. (of this page)	21. No. of Pages	22. Price*
Unclassified	Unclassified		$3.00

*For sale by the National Technical Information Service, Springfield, Virginia 22151

CONTENTS

LIST OF FIGURES

EXPERIMENTAL VERIFICATION OF LOW SONIC BOOM CONFIGURATION

by

Antonio Ferri[†] and Huai-Chu Wang[††]
New York University
Bronx, New York 10453
and
Hans Sorensen[†††]
Aeronautical Institute of Sweden

I. Introduction

Airplanes flying at supersonic speed produce "sonic booms" on the ground. Sonic boom reflected on the ground is felt by people as a "startling noise," and the present levels and shapes of the overpressures are highly objectionable. The sonic boom is unavoidable for vehicles having lift and cruising in horizontal flight. Therefore, the direction to follow in order to attempt to minimize the unacceptability on the part of the people is to decrease the main source of annoyance which is largely connected with the presence of shock waves.

The results of an analytical and experimental investigation are presented and discussed herein, and have been performed in order to determine configurations that present a reduction of shock wave strengths with respect to values produced in present configurations, and to validate results of

---

† Director, Aerospace Laboratory, and Astor Professor of Aerospace Sciences
†† Research Scientist
††† Head of the Trisonic Tunnel, Aeronautical Institute of Sweden

approximate analysis by means of experimental results. The investigation also is useful for developing satisfactory prediction methods.

The investigation indicated that the analysis and experiments are in good agreement, and that sonic booms having the first shock strength of the order of 1 lb/ft^2 as predicted by the analysis are measured in the experiments. The investigation indicates some of the difficulties encountered in extrapolating near field data at large distances. The experiments have been performed at the Aeronautical Research Institute of Sweden, by the research group directed by Professor M. Landahl and Dr. G. Drougge, and have been performed by using a new experimental technique developed by the group[1] based on the higher order analysis developed by M. Landahl, I.L. Ryhming, and others[2]. The model has been designed by a research group at the Aerospace Laboratory of New York University, as a part of an investigation on low boom configurations.[3,4] The latter group also performed the analysis of the experimental results described in this report. The work has been carried out under two NASA Grants: (1) NGR 52-120-001, assigned to the Aeronautical Research Institute of Sweden; and (2) Grant NGL 33-016-119, assigned to New York University. The experiments have been performed by H. Sorensen of the Aeronautical Institute of Sweden. The analyses have been performed by a team under the direction of Professors Ferri and Ting, which includes besides the authors, Mrs. F. Kung, Messrs. M. Siclari and A. Agnone. This report discusses the results corresponding to an angle of attack close to the selected flight conditions for the SST, and at another slightly higher angle of attack.

II. Definition of the Problem

Prediction of sonic boom signatures at large distances from the airplane is based mainly on the Whitham second order analysis.[5,6,7,8] The aircraft is represented by a distribution of multipoles and lifting elements derived from the airplane's geometry on the basis of linearized supersonic theory. The asymptotic solution is expressed in terms of the cross-sectional area distribution. $S(x\theta)$ is a function of the distance x and azimuthal angle θ of an equivalent body of revolution, and an equivalent cross-sectional area that represents an equivalent linear lift distribution. The pressure variations produced by a vehicle are strongly nonlinear near the vehicle; however, the nonlinear effects decrease rapidly moving away from the airplane. Therefore, at some finite distance from the airplane surface, linear theory is generally valid locally. Then the only nonlinear effects to be considered are the effects related to the variation of the speed of sound that when combined with the local variation of velocity of fluid produces distortions of the signal with respect to linear Mach waves. This second order effect is cumulative and therefore must be considered when propagation of disturbances at a large distance is investigated. The Whitham theory takes into account these effects and permits us to determine the propagation of waves from a region where the disturbances produced by the vehicle are already sufficiently small, so that linear theory applies.

The analysis permits us to extend the signal produced by the airplane to regions far from the airplane, provided that the disturbance produced by the airplane is known in a region where such disturbances are already small. The analytical determination of such disturbances is extremely difficult,

especially at high Mach numbers. The linear theory that is the most adaptable type of analysis available for three-dimensional flow, cannot be used for the purpose of relating the shape of the airplane to the signature produced in the near field, because it neglects higher order effects both in the definition of the local intensity of the signal, and in the decay and shape of the wave propagation.

Experimental methods, where the wind tunnels are used as analog machines to define the signals at some distance from the vehicle, open a promising way to solve this problem because they do not have the limitations of the linearized theory.[9,10,11] Such approaches, however, have other limitations that only recently have been recognized.[12] The most direct approach for eliminating many of the uncertainties due to the simplifications introduced in the analysis to determine the actual signature of an airplane at some distance from the airplane, is to measure the complete signature experimentally. At Mach numbers on the order of 2 to 3, the disturbances produced by good L/D configurations at distances of the order of a few body lengths from the model are extremely small; therefore, linear theory applies here. The experimental approach proposed by NASA[9], and used extensively for sonic boom determination, has been to build a model and to determine experimentally the disturbances produced at some distance from the airplane and then extrapolate the measured signal to the required height of flight by means of the Whitham theory. The concept is surely valid, and therefore presents one of the most direct ways of obtaining accurate information. However, it has been shown[12] that in applying the concept that more attention should be given to the type of measurements performed, and to the interpretation of the experi-

mental data, before such methods can give completely satisfactory results for configurations producing weak sonic boom signatures as required for future airplanes. One of the basic simplifications of the Whitham theory is that at large distances from the body, the details of the spanwise distribution of the sources of disturbances are not important provided that the span of the vehicle is very small with respect to the distance considered. Then, the airplane can be substituted by an equivalent axially symmetric body in any of the meridional planes around the axis of the body considered. This approximation has been introduced in the past, and used in the extrapolation of experimental measurements to large distances. Because of these simplifications, the measurements have been performed only in the meridian plane normal to the plane of the airplane wing. These measurements have been used to determine by means of the Whitham theory, an axially symmetric body equivalent to the airplane configuration which is used to determine the sonic boom at large distances. This approach introduces two approximations: the first is that the region where the measurements are made is sufficiently far from the model, so that the disturbances are small; the second is that all dimensions normal to the axis of the airplane, including also the spanwise dimensions, are negligible with respect to such a distance so that the three-dimensional effects are neglected. Both assumptions are acceptable if the regions of the measurements are sufficiently far away from the model; however, the distance required for the validity of the first approximation is not the same distance required for the validity of the second. For airplanes having good performances, and wings of practical span, the first requirement can be satisfied at much smaller distances than the second.

In practice, distances from the model of the station where measurements are performed cannot be too large because of practical experimental difficulties. The precision of the measurements decreases sharply with an increase of distance because of the finite sensitivity of the instruments. Furthermore, the size of available wind tunnels and the size of the model required for the tests limits the ratio between distance of measurements and length of the model. Another important difficulty is due to the fact that the flow field produced by a wind tunnel is not absolutely uniform. In any wind tunnel, a nonuniformity of a few percent in Mach number exists. Such nonuniformities correspond to waves that interact with the wave pattern produced by the model. When these disturbances interact with the flow field, an error is introduced that is cumulative along the waves carrying disturbances from the model to the plane of measurement. The strength of the waves that is produced by the model at a very large distance from the model is only slightly larger than the waves due to nonuniformities existing even in the most uniform wind tunnel. Therefore, the error introduced is proportionally larger at larger distances. This error tends to increase with Mach number. Thus, a compromise must be reached between accuracy required and distance of the measurement where a single measurement is acceptable.[12]

The problem can be reduced substantially by the introduction of more complex techniques for obtaining experimental data, and extrapolating the results. Two different approaches have been proposed; one by the first author of this report[12] where the measurements are performed in a plane located at some distance from the model parallel to the plane where the sonic boom signal must be determined. The deviations of the stream surface

normal to the plane are measured in a region inside the shock generated by the front tip of the airplane. Such deviations are determined along several straight lines parallel to the flow direction to cover all of the flow inside the shock. A stream surface is defined by the measurements that can be substituted for the airplane. Such a stream surface where the flow disturbances are small is equivalent to the vehicle placed above. Then, the Whitham analysis as applied by Walkden,[13] is used directly to determine sonic boom at the required distance from this surface. The Whitham theory applies for this extrapolation provided that the disturbances are small, so that locally the linear theory is sufficiently accurate. In this type of an approach, the deviation of the stream surface is measured experimentally by measuring the stream deviation in a plane parallel to the ground in the entire region inside the front Mach cone. Therefore, the precision of this method depends on the compromise of two opposite requirements: (1) the accuracy of the linearized theory which increases with the distance from the body; and (2) the precision of measurements which decreases when the distance increases. However, three-dimensional effects are accounted for accurately. The experiments presented here tend to indicate that a satisfactory compromise can be obtained for these two opposite requirements even if the measurements are performed at very small distances from the body.

The present experiments have been performed by using the second method proposed by Landahl, Ryhming, Sorensen, and Drougge.[1] Here, the streamline deviation is measured for several streamlines starting on a cylindrical tube placed around the model having the axis parallel to the wind, and at small distances from the axis. In the experiments performed, the distance is

smaller than the length of the model. The deviation of each streamline of this tube is measured locally in several meridian planes. Two angles are measured: one gives the deviation in the meridian plane; and the second gives the deviation on the cylinder normal to the meridian plane. These data are used to determine at the axis of the cylinder the F function that is used in the Whitham theory, by means of higher order approximation that takes into account second order terms in the disturbance components and higher order terms in the curvature according to a theory developed by the proposers of the method.

This method permits us to use smaller distances from the models than the other; however, it requires differentiation of the measured deviation which is difficult to do. In addition, the analysis assumes that the three-dimensional and thickness effects are small so that the disturbances can be extrapolated at the axis of the body. This last condition can produce F functions that are not singly valued. Both approaches are improvements with respect to the standard method, especially at Mach numbers of 2 or 3.

III. Experimental Techniques

The experiments were conducted in the Trisonic Tunnel of the Aeronautical Institute of Sweden, FFATUM 500, at Mach number 2.718.[1] The tunnel has a square test section of 50 x 50 cm^2 with perforated walls for the transonic speed range and a flexible wall nozzle which allows the Mach number to be varied continuously between 1 and 4. It is a blowdown tunnel, which may be operated with a stagnation pressure up to 12 atmospheres, and a stagnation temperature range of $300^{o}K$ - $400^{o}K$. A schematic design of the tunnel is shown in Fig. 1.

Pressure measurements were performed on the model at 2.6° and 3.2° incidence at two positions along the tunnel axis. The flow field measurements were conducted at two radial distances from the model axis corresponding to 0.271 and 0.558 times the length of the model in meridian planes spaced at 5° intervals from the plane of symmetry in the range between 0° and 90°. The meridian planes are defined by the angle θ with respect to the plane of symmetry. The pressures were recorded almost simultaneously, since the time between the individual measurements were $1 - 10^{-4}$ sec. Schlieren photographs were taken of the flow field generated by the model and the pressure probe.

The absolute level of accuracy of the results is very difficult to establish, because of the combined effects of the many possible sources of error. A number of precautions were taken, however, to reduce the magnitude and probability of significant errors. The facility instrumentation consists primarily of higher sensitivity pressure measurement devices for determining both stagnation and reference pressures. These pressures were calibrated carefully preceding the investigation. The free-stream properties are considered accurate within the following limits:

$$M_{\infty} \qquad \pm 0.01$$

$$p_{t,\infty} \qquad \pm 0.1\%$$

The precision with which local flow quantities can be determined is estimated by the Laboratory to be as follows:

		Errors at $M_\infty = 3.0$
M_1		$\pm$ 0.07
$p_{t,1}$		$\pm$ 1.0 %
ε	$=<$	$\pm 0.10^\circ$
σ	$=<$	$\pm 0.10^\circ$

The values of the errors in angles quoted here do not include the influence of the nonuniform flow on the probe. As it will be discussed later, the interaction of the shock with the subsonic flow in front of the probe, produces locally large errors; therefore, there such a type of measurement is not accurate. In addition some small influence due to Mach number gradients has been found experimentally. A report on such an influence will be made available later by the FFA group. However such effects are small and do not affect the results presented here. In order to analyze such effects, a comparison between measured and calculated values was performed for the front part of the model that is axially symmetric. The calculations performed by means of a numerical program based on a three-dimensional characteristic analysis is as accurate as the numerical approximation. The comparison that will be presented later, indicates that the estimated value of the error for ε and σ is larger than the maximum differences found between the measured and calculated values.

The definition of the angles σ and ε, the support of the model, and the dimensions and point for rotation of the model are shown schematically in Fig. 2. The angles σ and ε were measured by means of a probe as shown in Fig. 3.

IV. Description of the Model

In references 3 and 4, configurations have been investigated that

according to approximate analyses should produce sonic booms much lower than present configurations for equivalent conditions of flight. In order to determine the validity of such conclusions, and in parallel to experiments with the more accurate experimental techniques, one of these configurations has been selected for the tests. The configuration selected is shown in Fig. 4, where the dimensions correspond to the model tested. The wing is swept back at 72°. The wing profile has 2% thickness and is a symmetrical circular arc profile. The fuselage shape has a circular cross section; detailed dimensions of the fuselage area as a function of the distance are given in Table I.

In the analysis it has been assumed that the fuselage is sharp at the front and rear tips,and that the wing profile is also sharp at the trailing and leading edges. The construction of the model had required some modification on the wing leading edge and fuselage front tip, and on the rear part of the fuselage. The modification introduced at the leading edge is required in order to avoid local separation. The modification at the rear part of the fuselage is required because of the presence of the support. The support increases the equivalent area in the rear part of the vehicle, and therefore affects the sonic boom because it changes the final value of the equivalent area distribution.

In order to eliminate such effects, the equivalence between lift and cross-sectional area has been utilized, and a correction on the planform of the wing has been introduced. The area of the wing has been reduced in the region where the fuselage cross section is different from the design. The

reduction of wing area has been calculated to balance the increase of cross-sectional area from the reduction of lift and volume for a C_L of the wing of 0.060, at M = 2.70.

The design of the model is shown in Fig. 5, where the important differences between the model used in the analysis and in the tests are shown. The configuration does not have a vertical tail because of the advisability of constructing a simple model. The volume due to the vertical tail has been included as an equivalent increase in volume of the fuselage. Actually, the vertical tail increases the equivalent length and is useful in decreasing the intensity of the rear shock. This effect is not important for this set of tests because the main interest is directed to the determination of the front shock, in view of the difficulty of obtaining representative measurements from the rear shock.

The configuration selected does not represent a realistic airplane configuration. However, the total equivalent area distribution produced by the model tested at the selected C_L, has been selected from a more realistic airplane configuration where the requirements of the volume and lift distribution have been selected from practical configurations. This configuration is shown in Fig. 5b. There are two reasons for the selection of the different configurations shown in Fig. 5, corresponding to the same total equivalent area. The first is of an analytical nature. The configuration shown in Fig. 5b is more complex; therefore, an approximate analysis that takes into account three-dimensional and nonlinear effects is not possible. Then an iteration procedure would be required, where the wind tunnel is used as an analog machine to select accurately the details of the configuration that

correspond to the equivalent area selected. The second is of an experimental nature; a minimum fuselage diameter was imposed by the balance. This required a reduction of the wing thickness and in increase of fuselage volume.

Once a configuration has been obtained that gives low sonic boom, criteria are available to introduce changes that permit selecting an equivalent practical configuration similar to the configuration shown in Fig. 5b.

V. Possibility of Obtaining Information on the Rear Shock from Wind Tunnel Tests

The measurements in a wind tunnel of the rear shock produced by a model of this type are not indicative of the actual phenomena because of the lack of similarity. The presence of the sting, the difference in the size of the wake, and the lack of representation of the engine jets introduce severe errors in the intensity of the rear shock. The engines produce jets that mix with the outside flow producing a displacement thickness equivalent to substantial area changes. Figure 6 indicates the equivalent area variation due to the jet downstream of one of the engines for an SST configuration which has four General Electric engines fully expanded. The total equivalent cross-sectional area for a complete airplane at cruise is of the order of 800 ft^2. The difference between flight conditions and tunnel conditions in wake displacement thickness produces effects of the same order. These effects can be included in the analysis and have been included in the results presented in reference 4; however, they are difficult to simulate in small scale experiments of the type described here, and require a more complex research program than is required for the measurements of the front shock.

VI. Results of the Analysis

The configuration presented has been analyzed for flight conditions at cruise for an airplane having a length of 300 ft in full scale. An airplane of this dimension has 10,000 ft^2 of wing area. The volume of the fuselage is 44,000 ft^3, while the wing span is 58.8 ft and the wing volume 10,000 ft^3.

The analysis of the sonic boom has been performed for the conditions corresponding at cruise at 60,000 ft, M = 2.70, and total weight equal to 460,000 lbs. The analysis has been performed following the method outlined by Carlson[4], which transforms the lift in an equivalent area. The lift has been determined by means of linear theory with some approximate second order corrections. The extrapolation of signature to ground level has been performed by means of the variable density program developed in reference 15. Figure 7 indicates the contribution of the equivalent area distribution of the different components. Table 1 gives the same information. The sonic boom signature obtained from the analysis is shown in Fig. 8 where four meridian planes are considered. The cut-off angle is around 60^o. For comparison, the constant pressure analysis for average pressure equal to:

$$P_{average} = \sqrt{P_{sea\ level}\ P_{60,000\ ft}}$$

has also been performed. The results are shown in Fig. 9 where the reflection coefficient K is equal to 1.8. The analysis indicated that the front

shock for the weight assumed is of the order of 0.94. The ground reflection coefficient used in the analysis is 1.8. The area curve corresponding to the sonic boom in Fig. 8, is a smooth curve corresponding to sharp leading edges for the wing. The wing of the actual model produces a detached shock because the leading edge has been rounded. Therefore, some perturbations in the equivalent area distribution will be produced by this change. It is difficult to predict the actual intensity of these perturbations; however, the qualitative trend of the effects of such disturbances can be predicted. The round leading edge will produce initially stronger pressure rises than the sharp leading edge followed by an overexpansion. This is equivalent to a more rapid increase of the variation of the cross-sectional area in the region where the wing starts followed by a more gradual variation. The wing starts roughly at 50% of the length. The variations of the type of curves indicated in a and b of Fig. 10 can be expected. The sonic boom signature for these two distributions has been calculated. The results indicate that these local small perturbations tend to produce signatures that have two shocks of about the same intensity, Fig. 11.

The calculations have been performed initially for a weight of 460,000 lbs, at M = 2.70. The experiments have been performed at M = 2.72, and a $C_L = 0.055$, and $C_L = 0.066$ corresponding to the angle 2.6^o and 3.2^o. These conditions would correspond to a total airplane weight of 430,000 lbs and 520,000 lbs. Then the condition of $C_L = 0.055$ is close to the design conditions. The sonic boom for these two conditions has been calculated and is shown in Fig. 12. The effects of small local perturbations as shown

in Fig. 13 are also indicated.

VII. Review of the Experimental Data

The experimental data made available for the analysis are presented in Figs. 14 to 19. Figure 14 presents the measured values of ϵ at r/L = 0.271 for different values of θ, while Fig. 15 presents the values of σ for the conditions. Figures 16 and 17 present the same quantities for the distance r/L = 0.558. For several values of θ, measurements are available for more than one position of the model along the axis of the tunnel. Figures 18 and 19 present the results for θ = 0 and r/L = 0.272 and 0.558 for the different positions. The figure indicates that the change of position does not affect the experimental results, giving an indication of the uniformity of the flow. Similar configurations on σ and ϵ at the two distances but for α = 3.2 are given in Figs. 20, 21, 22, 23. As shown in the figures, the disturbances at $\frac{r}{L}$ = 0.558 and $\alpha = 2.6^{\circ}$ are extremely small; therefore, here linear theory applies for this case.

In addition, Schlieren pictures are available for all of these conditions. Figures 24a and 24b give the Schlieren photographs at φ = 0 and φ = 90, for $\alpha = 2.6^{\circ}$, and Figs. 25a and 25b for $\alpha = 3.2^{\circ}$. The photographs permit us to locate accurately the position of the shocks, and therefore help in the interpretation of the experimental results.

VIII. Corrections Introduced on the ϵ and Justification for the Corrections

The probe that measures the angles ϵ and σ has a diameter of 3 mm and has a spherical nose. The probe produces a shock and the flow region downstream of the shock near the orifices is subsonic. The calibration of the probe is based on the assumption that the flow in front of the shock is

fairly uniform and the angle is determined on the basis of the assumption that a small inclination of the flow direction with the axis of the probe corresponds to the equal rotation of the pressure distribution around the axis of the probe. This assumption is correct everywhere if the flow is continuous because the probe is small. However, the situation changes when an external shock interferes with shock of the probe in the subsonic region. Consider Fig. 26 where the probe and the shock in the external flow are represented schematically. Interference with the calibration starts when the probe is behind the external shock, in position a, and continues until the probe has crossed the shock and is at position b.

Experiments have been performed[16] where this phenomenon has been investigated at higher Mach number. In Fig. 27 taken from reference 16, the effects on the pressure distribution due to the interaction are shown. The variation of pressure distribution, due to the interaction when the sphere is in front of the external shock is very large (case c of Fig. 27). In this case if the pressure distribution is used to determine angles on the basis of a uniform flow calibration, then the measurement would indicate incorrectly that a large flow deviation exists in front of the probe. When the sphere is behind the external shock, then the interference produces an opposite effect, decreasing the value of the actual deviation. Because of these effects, the points measured in the vicinity of the shocks have been discounted and the diagram shown in Fig. 28 has been used for the analysis. In this diagram the position of the shocks have been determined very accurately from the Schlieren pictures. The peak deviation behind the shock has been obtained from the measurements of the shock inclination, and the

flow properties in front of the shock.

In Figs. 29 and 30, the value of c calculated by means of three-dimensional characteristics are shown, and compared with the experimental data. The differences are extremely small and can be due either to small differences in geometry between the model and the shape used for the calculation or to measurements or calculation accuracy. Because the data of the sets of tests agree well, the first assumption seems to be more probable

In order to determine the importance of some of the details of the pressure distribution, two alternate curves, 1 and 2 of Fig. 28 have been used in the analysis. Curve 1 considers only one shock, while curve 2 considers the existence of two shocks. The second shock is produced by the discontinuity in slope between fuselage and support.

IX. Description of the Method of Analysis Used

The method used for the analysis has been described in reference 1 and has been developed by M. Landahl, I. Ryhming, H. Sorensen, and G. Drougge of the Aeronautical Research Institute of Sweden. In order to simplify the reading of this paper, the important features of the method are summarized here by reproducing a section of the report of reference 1.

According to reference 2, the perturbation velocity components at large distances from a three-dimensional body in supersonic flow are given to second order by

$$u_2 = \frac{\rho_\infty}{\rho} \; u(x_o, r_o, \theta_o) \tag{1}$$

$$v_2 = \frac{\rho_\infty}{\rho} \; \frac{r_o}{r} \; v(x_o, r_o, \theta_o) \tag{2}$$

$$w_2 = w(x_o, r_o, \theta_o) = \frac{1}{r_1} \varphi_\theta \tag{3}$$

where u_2, v_2, w_2 are the second-order components referred to a cylindrical coordinate system, θ_o is the meridian plane angle and r_o is the radial distance from the wind axis.

$$x = x_o - Kr_o v - M^2 \varphi + Kr_o \frac{\partial w}{\partial \theta} \tag{4}$$

$$r = r_o \left(1 - Ku - \frac{K}{\beta} \frac{\partial w}{\partial \theta}\right) \tag{5}$$

$$\theta = \theta_o - 2K \frac{\partial u}{\partial \theta}, \quad K = \frac{(\gamma+1)M^4}{2\beta^2}, \quad \beta^2 = M^2 - 1 \tag{6}$$

and u, v, w are the corresponding values according to linearized theory and their potential is φ. For large distances the following expansions were shown to hold:

$$F(y;\theta) = \frac{2r_o}{\beta} v + \frac{3\varphi}{8r_o} - \frac{\varphi_{\theta\theta}}{2r_o} \tag{7}$$

$$u = -\frac{v}{\beta} - \frac{1}{2r_o} \varphi \tag{8}$$

$$w = -\frac{F_{\theta_o}}{r_o \, 2\beta r_o} \tag{9}$$

$$\varphi_2 = \varphi - Kr_o uv \tag{10}$$

$$y = x - \beta r + kr^{\frac{1}{2}} F + \left(M^2 - \frac{K}{4}\right) \varphi - K\varphi_{\theta_o} \theta_o \tag{11}$$

$$\theta_o = \theta - \frac{k}{\beta} \frac{F_\theta}{r} \tag{12}$$

where $k = k\,2\beta$

The quantities measured are the flow deflection angles ϵ and σ, along lines of constant r but in different azimuthal planes θ = const. The angle ϵ is related to v_2 as follows:

$$\epsilon = \tan^{-1} \frac{v_2}{1+u_2} \tag{13}$$

or since $u_2 = - v_2/\beta$ to lowest order

$$v_2 = (1 - \frac{\epsilon}{\beta}\ \epsilon + \ldots \tag{14a}$$

From the aximuthal deflection angle σ we obtain

$$w_2 \simeq w\ \sigma$$

or

$$\varphi_\theta \simeq \varphi_{\theta_o} \simeq r\sigma \tag{14b}$$

Thus, φ_{θ_o} can be determined directly from the measurements, and by aid of numerical differentiation of $\sigma(\theta)$ one can also calculate $\varphi_{\theta_o\theta_o}$. From the measurements of $\epsilon(x)$, φ_2 can be determined by numerical integration, since to the order considered

$$\varphi_{2|_{r=\text{const}}} \simeq - \frac{1}{\beta} \int_{\text{shock}}^{x} \epsilon(x')dx' \tag{15}$$

One can next obtain v from (2):

$$v \simeq (1 - M^2u)\ (1- Ku)\ v_2 \simeq (1 + M^2\ \frac{\epsilon}{\beta})\ (1 + K\ \frac{\epsilon}{\beta})\ v_2 \tag{16}$$

Furthermore, (5) gives that

$$r_o \simeq r(1 - \frac{K}{\beta} \epsilon) \tag{17}$$

We have now the quantities needed to calculate F from (7). The Mach line parameter y and the angle parameter θ_o, finally, can then be determined from (11) and (12).

For an axisymmetrical flow field w is zero as well as θ-derivatives. The measurements and the evaluation of the F-function is then simplified, since it is only necessary to consider a single azimuthal plane.

X. Application of the Method to the Present Experiments

The method presented is an improvement with respect to the methods used previously, because it takes into account nonlinear effects which are important in the near field and because it introduces corrections for the near field effects due to three-dimensional phenomena. In applying such a method to the present experiments, two different difficulties have been encountered.

The first difficulty is related to the evaluation of $\varphi_{\theta\theta}$ in equation 7 of the analysis, which required differentiation with respect to θ of the measured quantity σ. Such an operation is difficult to perform accurately, because small errors on the measured values of σ introduce variation of the value of $\varphi_{\theta\theta}$. An attempt has been made first to perform a Fourier analysis of all the measured values, between $\theta = 0$ and 90^o. However, for the front part the experimental accuracy is insufficient, while for the region of the wing where the contribution of $\varphi_{\theta\theta}$ to the final results has significance, the series does not converge. Therefore, a different approach has been used

in the analysis. In the region of the wing the values of σ between 0 and 30° have been plotted as a function of θ, and a curve has been drawn connecting the experimental points. Then the value of $\partial\sigma/\partial\theta$ at $\varphi = 0$ has been obtained from the curve. For the region where the model has axial symmetry, the values of $\partial\sigma/\partial\theta$ given by the analysis have been used. The contribution of $\varphi_{\theta\theta}$ to the F function in this region is negligible. Therefore such an approach is justified. However the contribution of the term is important in the region of the wing indicating the importance of the three-dimensional effects.

The second problem encountered in the determination of the F function is related to the existence of double values of the F function due either to the three-dimensional effects or to rapid expansions (corners) at the surface of the body.[7] This effect is due to the fact that the F function is calculated at the axis and can be understood clearly if a simple configuration is analyzed. Consider, as an example, a cone cylinder at zero angle of attack. At the expansion corner, a family of expansion waves is produced. Fig. 31. If these expansion waves are extrapolated to the axis, then two sets of values corresponding to the same y for the F function in the region AB of the figure. Similar effects exist when the model is three-dimensional. Then waves generated from different points of the model at different r reach the same point in the meridian plane analyzed. In order to obtain some criterion for the solution of this difficulty, a detailed analysis has been performed for the case of the cone cylinder of Fig. 31 for the case, the actual stream deviation ϵ at several values of r can be numerically obtained by means of the method of characteristics. Then it is possible to deter-

mine the F function that corresponds to the ϵ distribution obtained at some distance from the axis, and compare with the F distribution obtained by introducing the discontinuity. Such analysis indicates that the double value should be eliminated by adding and subtracting equal areas in F on the Mach wave from the corner as discussed in reference 7, (see Fig. 31), in the region where multiple values exist. The F function obtained from the data is shown in Fig. 32. Figure 33 shows the F function used in the analysis. The same method of analysis has been used for the data at r/L = 0.271, and for $\alpha = 3.2^{\circ}$. The F function obtained from the data at 0.558 has been used to obtain the sonic boom corresponding to an airplane 300 ft long flying at 60,000 ft, for the C_L of 0.055 which corresponds to a total weight of 430,000 lbs. Figure 34 gives the sonic boom shape obtained from the F function by using the variable pressure program, and Fig. 35 the same results obtained by using constant pressure program corresponding to the square root of the two values at the flight and ground level. The amplification due to the reflection of the ground is assumed to be equal to 1.8 the incoming signal, and is included in the values presented. In order to determine the importance of the three-dimensional and nonlinear effects, the calculations have been repeated, by applying directly the Whitham theory to determine the F function, and neglecting all the higher order terms, curve a and only the three-dimensional effects ($\varphi_{\theta\theta}$) curve b. Figure 36 shows the sonic boom obtained, when these quantities are neglected. The figure indicates that the three-dimensional effects are important at least when r/L is small. A similar calculation has been performed for the data at $\alpha = 2.6^{\circ}$ and r/L = 0.271. The two ϵ distributions for the analysis are as

shown in Fig. 37. The results obtained are shown in Fig. 38. They are very similar to the results of Fig. 35. The position of the second shock is different.

The same analysis has been performed for the data corresponding to $\alpha = 3.2^{\circ}$. This condition corresponds to a vehicle that has a length of 300 ft, weight of 530,000 lbs, flying at an altitude of flight of 60,000 ft. The results are shown in Figs. 39, 40, and 41. Figure 39 gives the distribution of ε at $r/L = 0.558$ used in the analysis. Figure 40 gives the F function calculated and the curve used after being corrected by eliminating the double value, and Fig. 41 gives the shape of the sonic boom derived from the F function.

XI. Conclusions

The experimental investigation performed permits us to reach the following conclusions:

1. Sonic booms having peak values of the order of 1 lb/ft^2 as predicted analytically in reference 3 have been measured. The sonic booms obtained have near field signatures as predicted in reference 3 for cruise conditions and in reference 17 for the acceleration phase. The distribution of equivalent cross-sectional area tested corresponds to an airplane shape that has the volume, length, and lift requirements of a practical airplane configuration; however, substantial additional work is required to investigate if all other aerodynamic requirements related to a practical configuration can be met.
2. The nonlinear and three-dimensional effects are of primary importance for the determination of the correct values of the sonic boom from measurements at small distances from the model.
3. More complex experimental techniques where such effects are determined

are required when near field measurements are made as recommended in references 1 and 12.

4. The experimental method proposed in reference 1 gives satisfactory results.

5. Improvements are still required in the experimental techniques and in the analysis in order to measure and determine with better accuracy all of the required quantities.

REFERENCES

1. Landahl, M., Ryhming, I., Sorensen, H., and Drougge, G.: " A New Method for Determining Sonic Boom Strength from Near-Field Measurements." NASA Third Conference on Sonic Boom Research, NASA SP-255, October 1970, pp. 285-295

2a. Landahl, M., Ryhming, I., and Hilding, L.: "Nonlinear Effects on Sonic Boom Intensity." NASA Second Conference on Sonic Boom Research, NASA SP-180, May 1968, pp. 117-124.

2b. Landahl, M., Ryhming, I., and Lofgren, P.: "Nonlinear Effects on Sonic Boom Intensity." NASA Third Conference on Sonic Boom Research, NASA SP-255, October 1970, pp. 3-15.

3. Ferri, A. and Ismail, A.: "Report on Sonic Boom Studies - Part I - Analysis of Configurations." NASA Second Conference on Sonic Boom Research, NASA SP-180, May 1968, pp. 73-88.

4. Ferri, A.: "Practical Aspects of Sonic Boom Problems." NYU Report AA-70-22, September, 1970, and presented at 7th ICAS Congress, Rome, Italy, September, 1970. Also presented at NASA Third Conference on Sonic Boom Research, NASA SP-255, October 1970, under title "Airplane Configurations for Low Sonic Boom," pp. 255-275.

5. Whitham, G.B.: "The Flow Pattern of a Supersonic Projectile." Comm. Pure Appl. Math., 5:301-48, 1952.

6. Whitham, G.B.: "On the Propagation of Weak Shock Waves." J. Fluid Mech. 1:290-318 .

7. Lighthill, M.J.: "Higher Approximations in Aerodynamic Theory." Princeton University Press, 1960.

8. Hayes, W.D.: "Linearized Supersonic Flow." Ph.D. thesis, California Institute of Technology, microfiche available, North American Aviation, Inc., Aerophysics Lab., Rep. AL-222. Reprinted, Princeton University Aerospace Mech. Sci. Rep. 852.

9. Carlson, Harry W.: "An Investigation of Some Aspects of the Sonic Boom by Means of Wind Tunnel Measurements of Pressures about Several Bodies at a Mach Number of 2.01." NASA TN D-161, 1959.

10. Carlson, Harry W.: "An Investigation of the Influence of Lift on Sonic Boom Intensity by Means of Wind Tunnel Measurements of the Pressure Fields of Several Wing-Body Combinations at Mach Number of 2.01." NASA TN D-881, 1961.

11. Hicks, R., Medoza, J.: "Prediction of Aircraft Sonic Boom Characteristics from Experimental Near Field Results." NASA TM X-1477, 1967.

12. Ferri,A. and Wang, Huai-Chu: "Observations on Problems Related to Experimental Determination of Sonic Boom." NASA Third Conference on Sonic Boom Research, NASA SP - 255, October 1970, pp. 277-284.

13. Walkden, F.: "The Shock Pattern of a Wing-body Combination Far From the Flight Path." Aeronaut. Quart. 9:164-94, 1958.

14. Carlson, H.W.: "The Lower Bound of Attainable Sonic Boom Over-pressure and Design Methods of Approaching This Limit." NASA TN D-1494,October 1962.

15. Hayes, W.D., Haefeli, R.C., and Kulsrud, H.E.: "Sonic Boom Propagation in a Stratified Atmosphere with Computer Program." NASA CR-1299, 1969.

16. Edney, B.: "Anomalous Heat Transfer and Pressure Distributions on Blunt Bodies at Hypersonic Speeds in the Presence of an Impinging Shock." The Aeronautical Research Institute of Sweden, FFA Report 115, February 1968.

17. McLean, Edward F.: "Some Nonasymptotic Effects on the Sonic Boom of Large Airplanes." NASA TN D-2877, June 1965.

Table 1

STATION X(FT)	FUSELAGE RADIUS R(FT)	TOTAL EQUIV.AREA AE	FUSELAGE AREA AF(SQ.FT.)	WING AREA AW(SQ.FT.)	FUSELAGE +WING AFW(SQ.FT.)	LIFT DUE TO FUSELAGE XLEF	LIFT DUE TO WING XLEW	LIFT DUE TO WING+FUSE. XLE	MODEL SCALE STATION XM(IN.)	MODEL SCALE RADIUS RM(IN.)
.00000	.00000	.00000	.00000	.00000	.00000	.00000	.00000	.00000	.000	.000
5.00000	1.03617	3.55640	3.37297	.00000	3.37297	.18343	.00000	.18343	.181	.037
10.00000	1.64482	8.96156	8.49935	.00000	8.49935	.46222	.00000	.46222	.361	.059
15.00000	2.15532	15.38765	14.59399	.00000	14.59399	.79366	.00000	.79366	.542	.078
20.00000	2.61099	22.58173	21.41702	.00000	21.41702	1.16471	.00000	1.16471	.723	.094
25.00000	3.02978	30.40679	28.83848	.00000	28.83848	1.56831	.00000	1.56831	.903	.109
30.00000	3.42136	38.77444	36.77455	.00000	36.77455	1.99989	.00000	1.99989	1.084	.124
35.00000	3.79166	47.62203	45.16580	.00000	45.16580	2.45623	.00000	2.45623	1.265	.137
40.00000	4.14468	56.90239	53.96750	.00000	53.96750	2.93489	.00000	2.93489	1.445	.150
45.00000	4.48325	66.57848	63.14452	.00000	63.14452	3.43396	.00000	3.43396	1.626	.162
50.00000	4.80948	76.62030	72.66841	.00000	72.66841	3.95189	.00000	3.95189	1.807	.174
55.00000	5.12499	87.00248	82.51557	.00000	82.51557	4.48740	.00000	4.48740	1.987	.185
60.00000	5.43107	97.70546	92.66605	.00000	92.66605	5.03941	.00000	5.03941	2.168	.196
65.00000	5.72875	108.70971	103.10272	.00000	103.10272	5.60698	.00000	5.60698	2.349	.207
70.00000	6.01889	120.00000	113.81069	.00000	113.81069	6.18931	.00000	6.18931	2.529	.217
75.00000	6.30049	131.49109	124.70909	.00000	124.70909	6.78199	.00000	6.78199	2.710	.228
80.00000	6.57290	143.10721	135.72608	.00000	135.72608	7.38112	.00000	7.38112	2.891	.238
85.00000	6.83722	154.84836	146.86166	.00000	146.86166	7.98670	.00000	7.98670	3.071	.247
90.00000	7.09435	166.71455	158.11582	.00000	158.11582	8.59873	.00000	8.59873	3.252	.256
95.00000	7.34506	178.70578	169.48857	.00000	169.48857	9.21721	.00000	9.21721	3.433	.265
100.00000	7.58997	190.82203	180.97989	.00000	180.97989	9.84214	.00000	9.84214	3.613	.274
105.00000	7.82964	203.06332	192.58981	.00000	192.58981	10.47351	.00000	10.47351	3.794	.283
110.00000	8.06452	215.42965	204.31830	.00000	204.31830	11.11134	.00000	11.11134	3.975	.291
115.00000	8.29503	227.92101	216.16539	.00000	216.16539	11.75561	.00000	11.75561	4.155	.300
120.00000	8.52152	240.53740	228.13106	.00000	228.13106	12.40633	.00000	12.40633	4.336	.308
125.00000	8.74431	253.27882	240.21531	.00000	240.21531	13.06351	.00000	13.06351	4.517	.316
130.00000	8.95296	266.14528	251.81580	.00000	251.81580	13.69437	.63510	14.32947	4.697	.324
135.00000	9.13796	279.13678	262.33020	.00000	262.33020	14.26617	2.54041	16.80658	4.878	.330
140.00000	9.30072	292.25330	271.75848	.00000	271.75848	14.77890	5.71592	20.49482	5.059	.336
145.00000	9.44239	305.49487	280.10065	.00000	280.10065	15.23257	10.16163	25.39420	5.239	.341
150.00000	9.56392	318.86146	287.35672	.00000	287.35672	15.62717	15.87755	31.50472	5.420	.346
155.00000	9.66600	332.35308	293.52362	.00322	293.52685	15.96255	22.86367	38.82622	5.601	.349
160.00000	9.72976	345.96975	297.40892	1.26696	298.67588	16.17384	31.12000	47.29384	5.781	.352
165.00000	9.74122	359.71144	298.11031	4.74267	302.85298	16.21198	40.64653	56.85851	5.962	.352
170.00000	9.70294	373.57817	295.77173	10.27847	306.05019	16.08480	51.44326	67.52807	6.143	.351
175.00000	9.61763	387.56994	290.59351	17.66304	308.25655	15.80320	63.51020	79.31340	6.323	.348
180.00000	9.48824	401.68673	282.82697	26.63158	309.45855	15.38083	76.84735	92.22818	6.504	.343
185.00000	9.31796	415.92857	272.76670	36.87343	309.64013	14.83373	91.45469	106.28842	6.685	.337
190.00000	9.11026	430.29543	260.74234	48.04102	308.78337	14.17982	107.33224	121.51206	6.865	.329
195.00000	8.86890	444.78733	247.10927	59.75972	306.86899	13.43842	124.48000	137.91842	7.046	.320
200.00000	8.59789	459.40426	232.23829	71.63831	303.87659	12.62970	142.89796	155.52765	7.227	.311
205.00000	8.30156	474.14622	216.50557	83.28044	299.78601	11.77411	162.58612	174.36023	7.407	.300
210.00000	7.98447	489.01323	200.28223	94.29467	294.57690	10.89185	183.54449	194.43633	7.588	.289
215.00000	7.65147	504.00526	183.92436	104.30555	288.22991	10.00226	205.77306	215.77532	7.769	.276
220.00000	7.30760	519.12233	167.76402	112.96305	280.72706	9.12342	229.27183	238.39526	7.949	.264

225.00000	6.95810	534.36443	152.10056	119.95144	272.05199	8.27161	254.04081	262.31242	8.130	.251
230.00000	6.60833	549.73156	137.19335	124.99733	262.19067	7.46092	280.07999	287.54091	8.311	.239
235.00000	6.26364	565.22373	123.25469	127.87677	251.13146	6.70290	307.38939	314.09228	8.491	.226
240.00000	5.92921	580.84093	110.44454	128.42117	238.86571	6.00625	335.96898	341.97522	8.672	.214
245.00000	5.60980	596.58317	98.86529	126.52257	225.38786	5.37654	365.81877	371.19531	8.853	.203
250.00000	5.30930	612.45044	88.55741	122.13829	210.69570	4.81597	396.93877	401.75474	9.033	.192
255.00000	5.03033	628.44274	79.49544	115.29517	194.79061	4.32316	429.32898	433.65213	9.214	.182
260.00000	4.77345	644.56007	71.58379	106.09401	177.67780	3.89290	462.98938	466.88229	9.395	.172
265.00000	4.53641	660.80244	64.65091	94.71567	159.36658	3.51588	497.91999	501.43587	9.575	.164
270.00000	4.31300	677.16985	58.43982	81.43113	139.87094	3.17810	534.12081	537.29891	9.756	.156
275.00000	4.09148	693.66228	52.59094	66.61950	119.21044	2.86003	571.59183	574.45185	9.937	.148
280.00000	3.85181	710.27976	46.61008	50.80186	97.41195	2.53477	610.33305	612.86782	10.117	.139
285.00000	3.55963	727.02227	39.80701	34.70598	74.51299	2.16480	650.34448	652.50928	10.298	.129
290.00000	3.14988	743.88981	31.17004	19.39856	50.56860	1.69510	691.62611	693.32121	10.479	.114
295.00000	2.46332	760.88238	19.06296	6.60478	25.66774	1.03669	734.17795	735.21464	10.659	.089
300.00	0.0	778.00	0.0	0.0	0.0	0.0	778.00	778.00	10.840	0.0

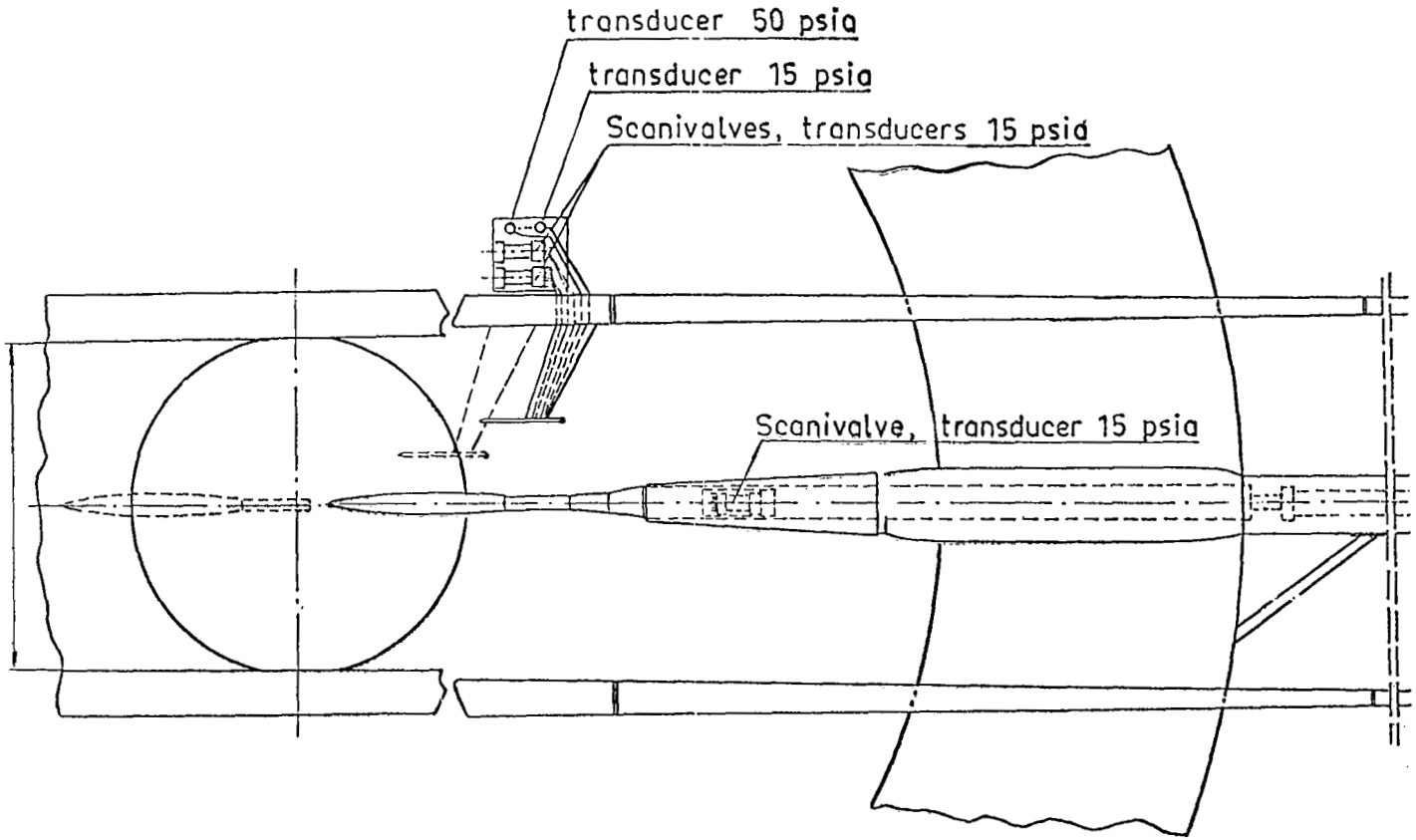

Fig 1. Schematical view of test set-up.

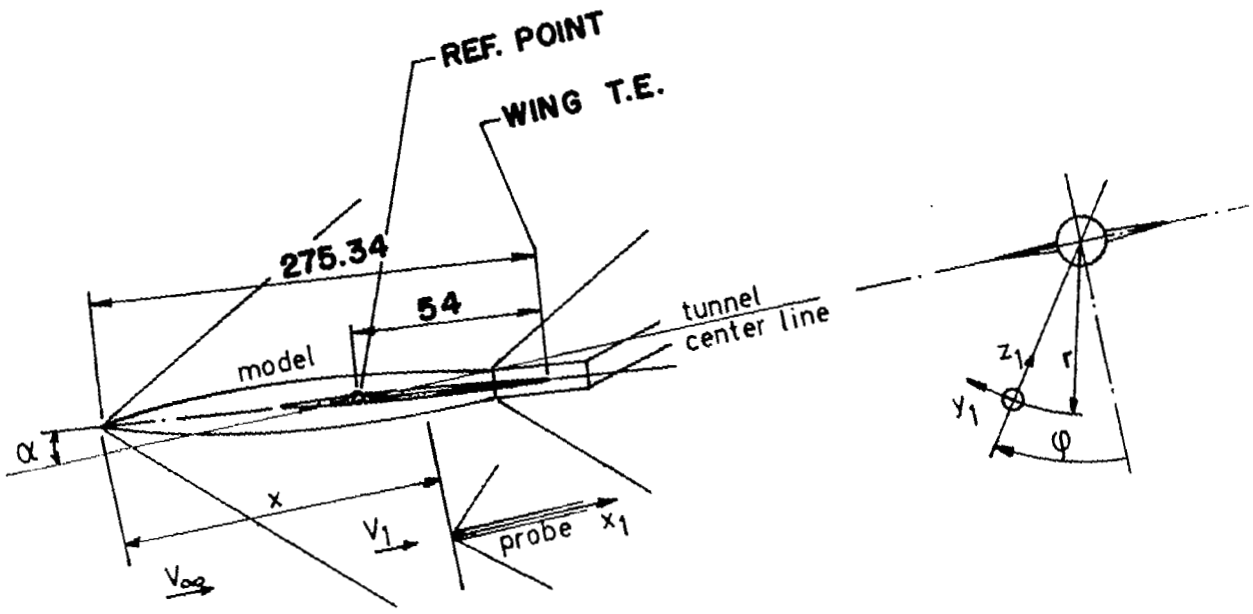

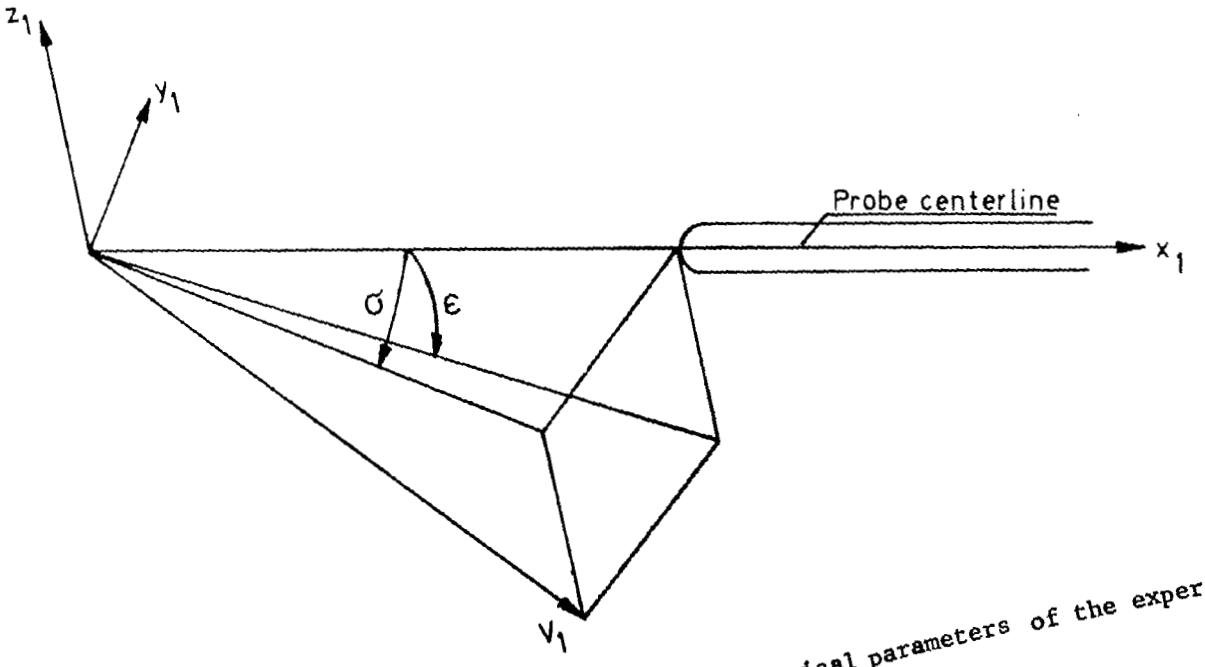

...l indication of geometrical parameters of the exper

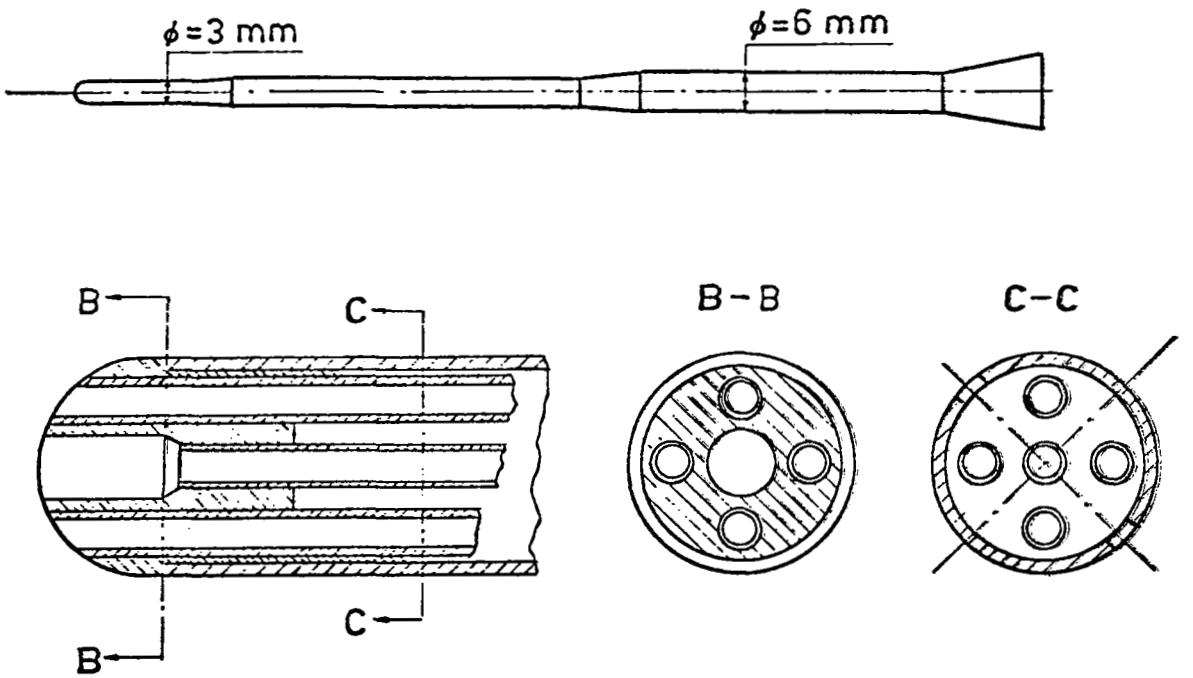

Fig. 3 Design of yaw probe

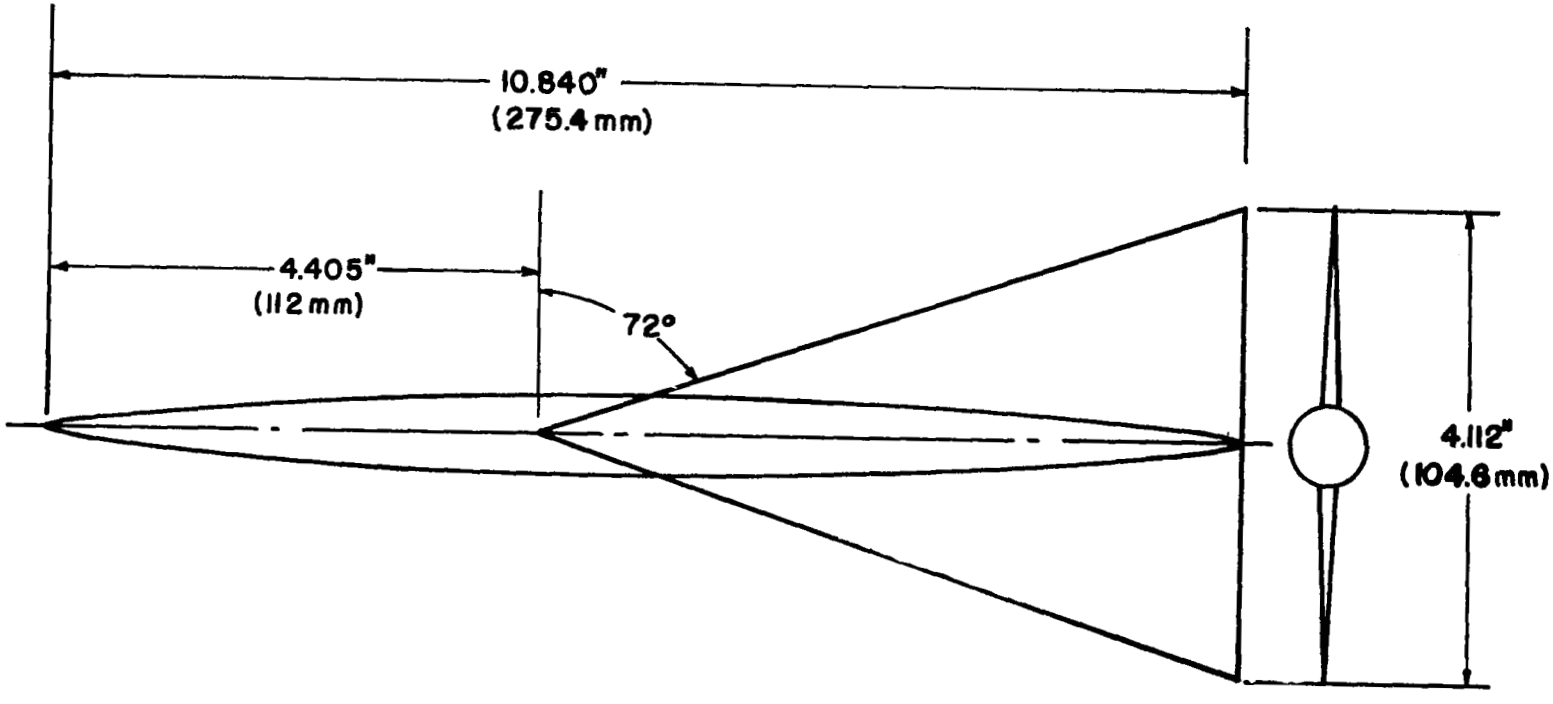

Fig. 4 Design of airplane configuration

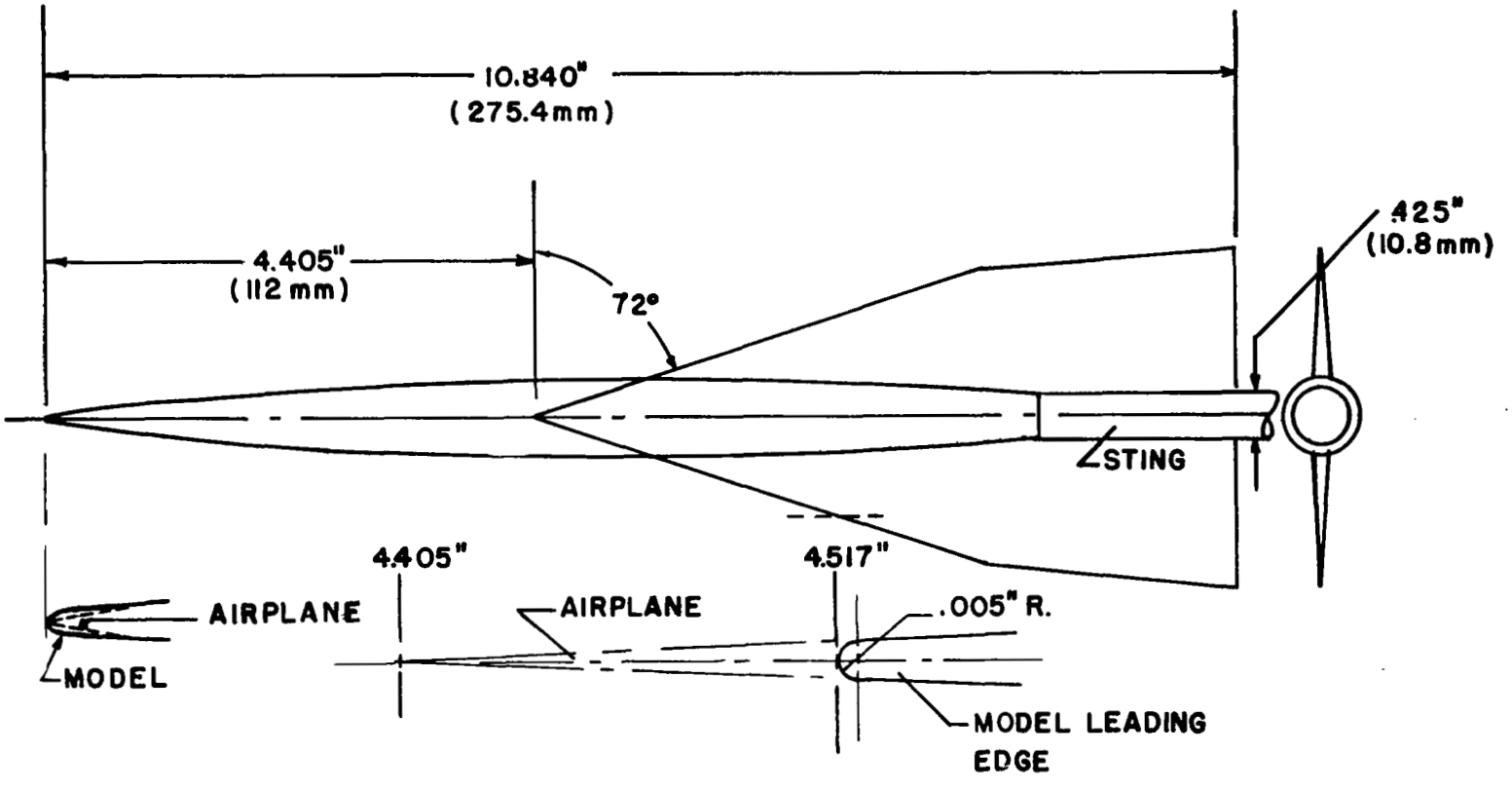

Fig. 5a Model design

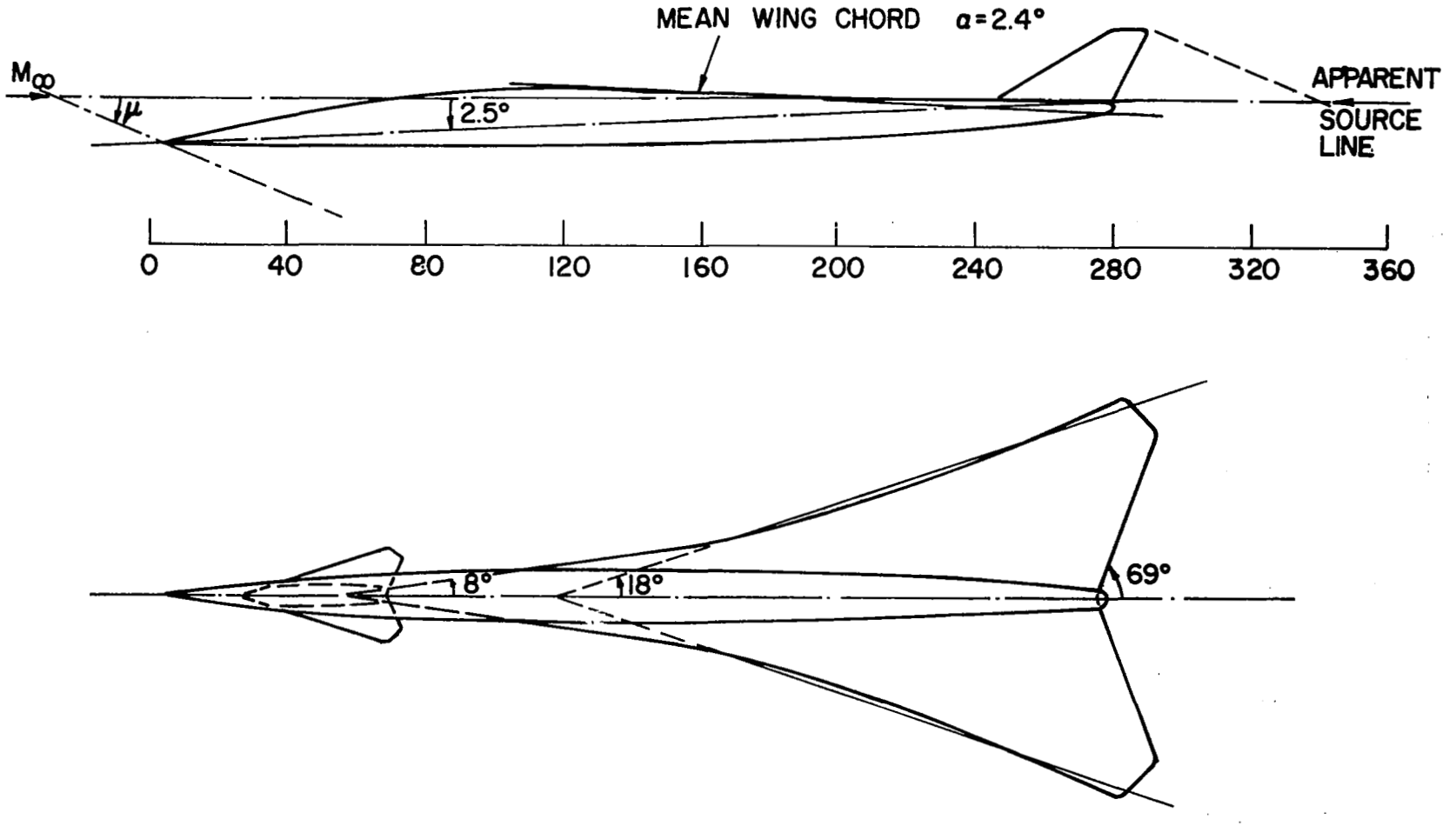

Fig. 5b Airplane configuration corresponding to the area distribution of the model of Fig. 4

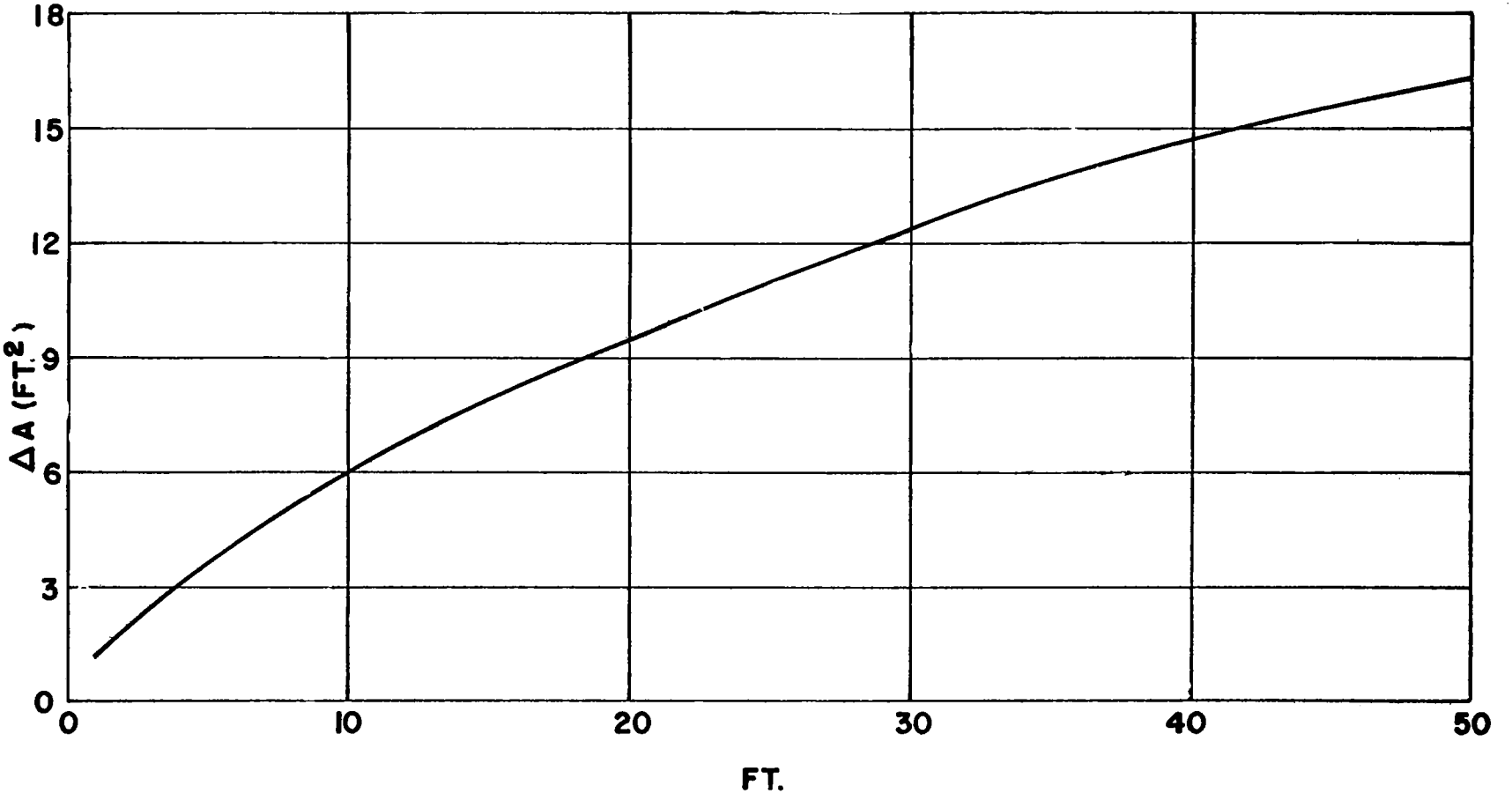

Fig. 6 Variation of Total Equivalent Area Due to the Jet Exhaust of an Engine as a Function of Distance from the Exit of the Jet.

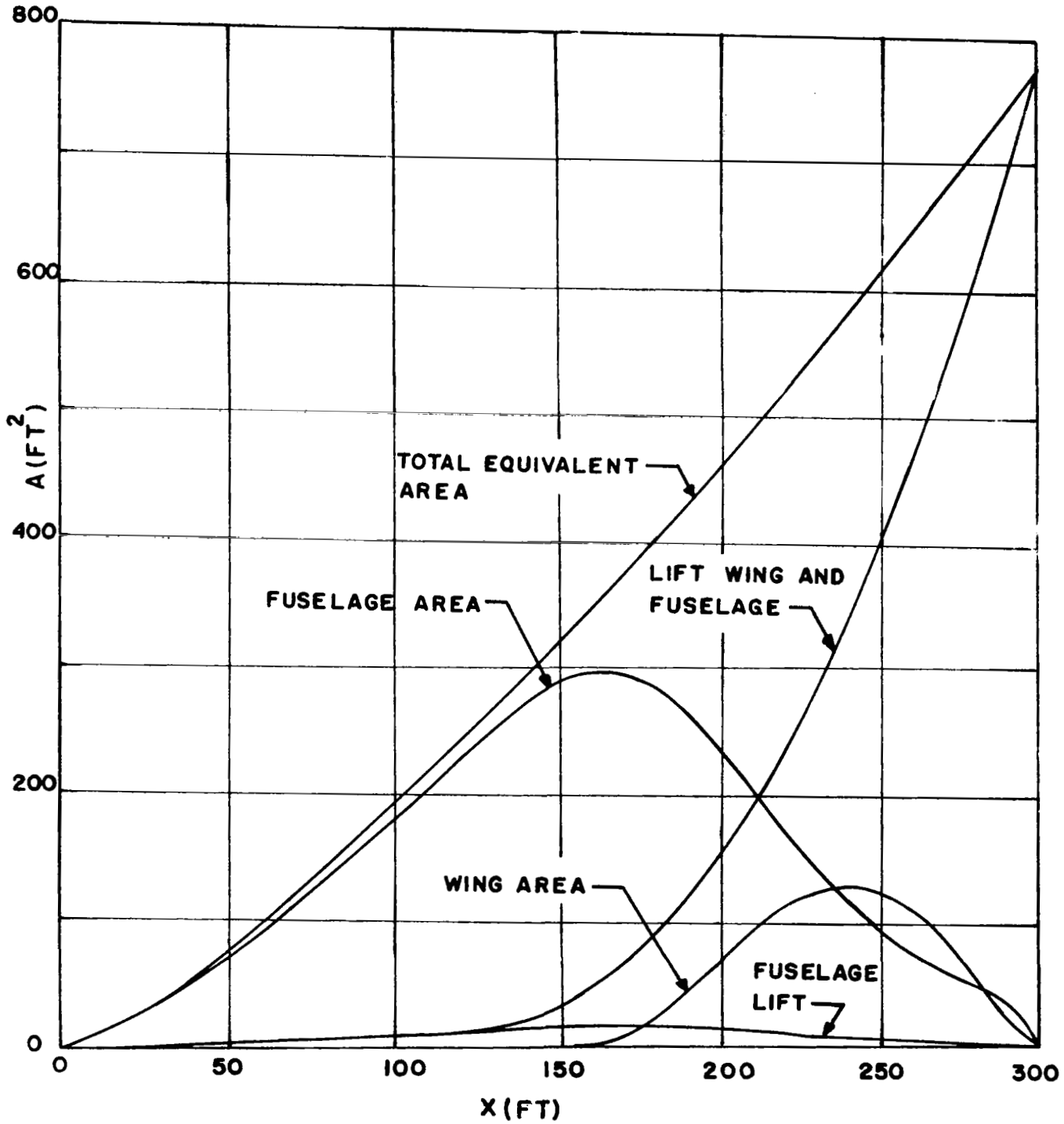

Fig. 7 Equivalent area distribution

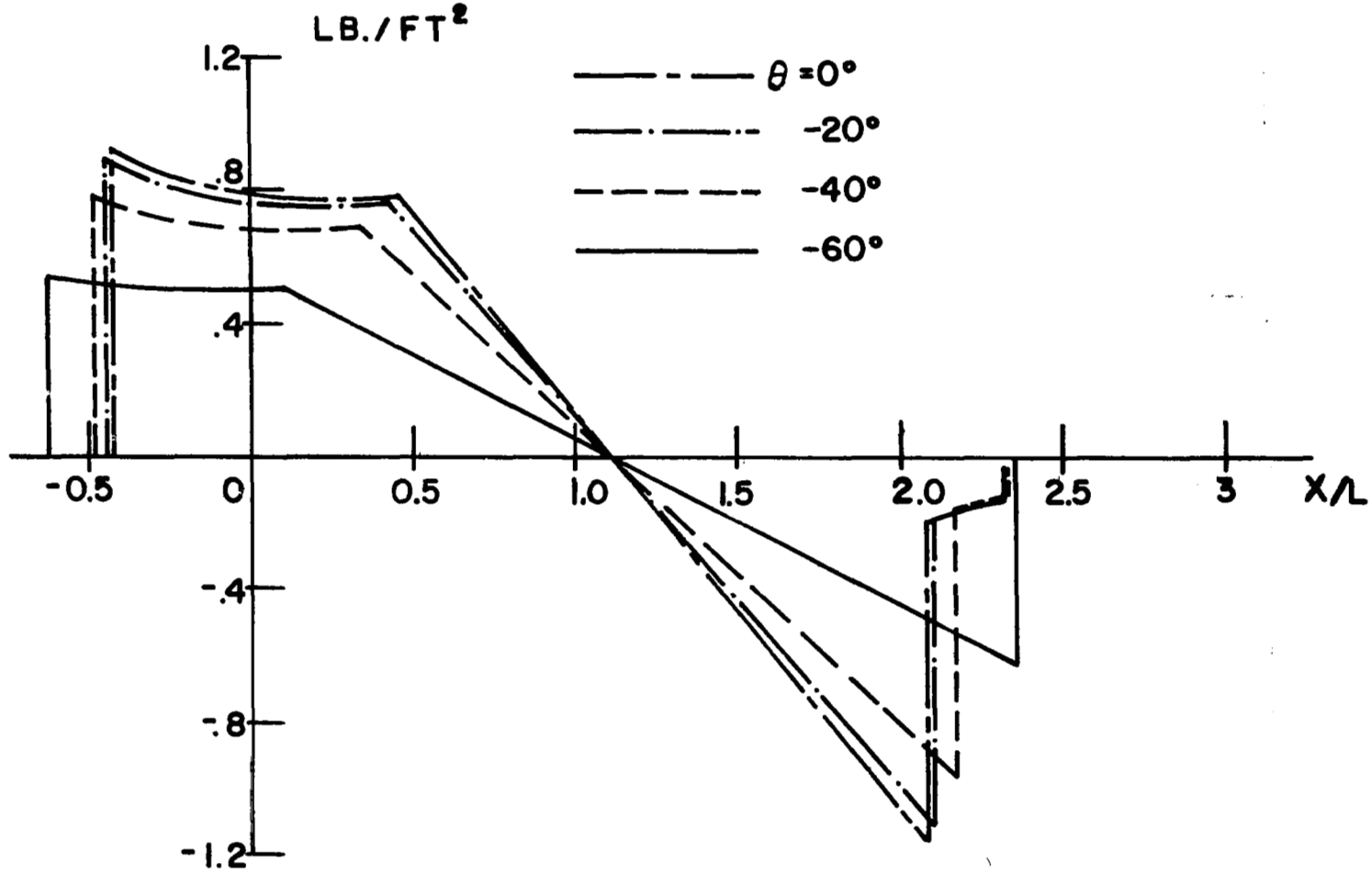

Fig. 8 Sonic boom signature L = 300 ft, h = 60,000 ft, w = 460,000 lb, M = 2.70 variable pressure program

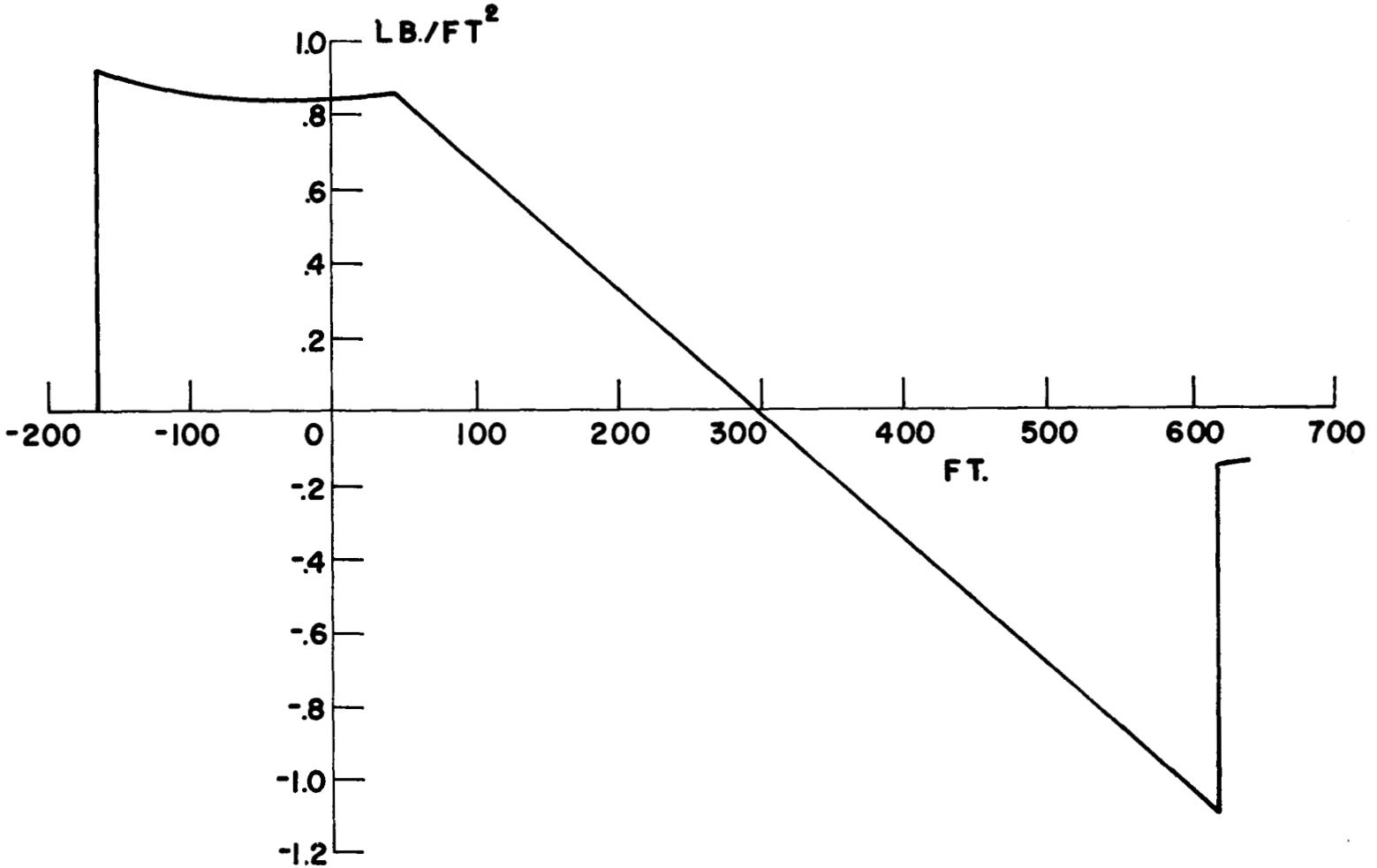

Fig. 9 Sonic boom signature constant pressure program $Kp=K\sqrt{P_{60,000}\ P_{SL}} = 1017$ lbs/ft^2

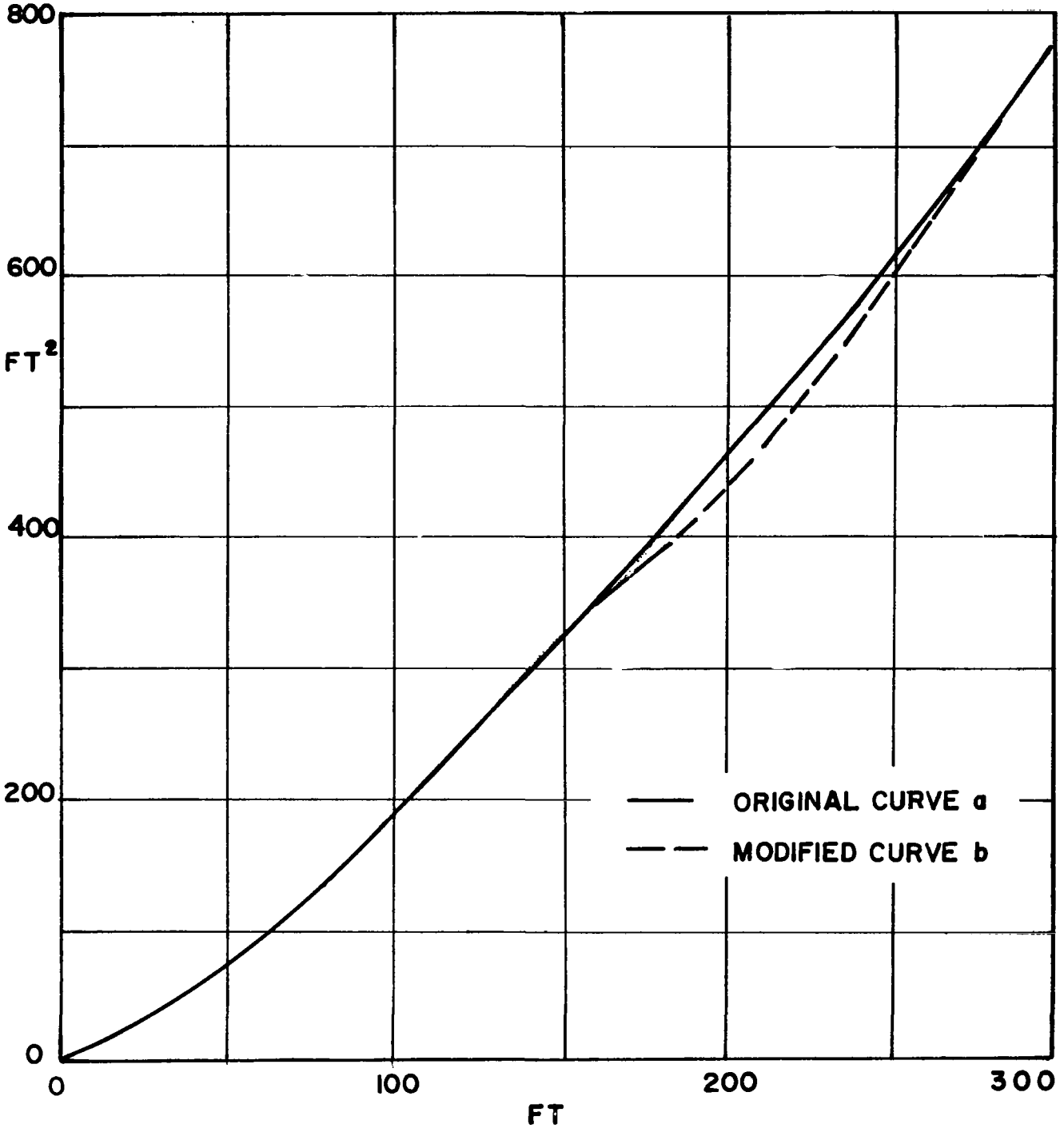

Fig. 10 Perturbation of the area distribution curve M = 2.70, w = 460,000, h = 60,000
L = 300

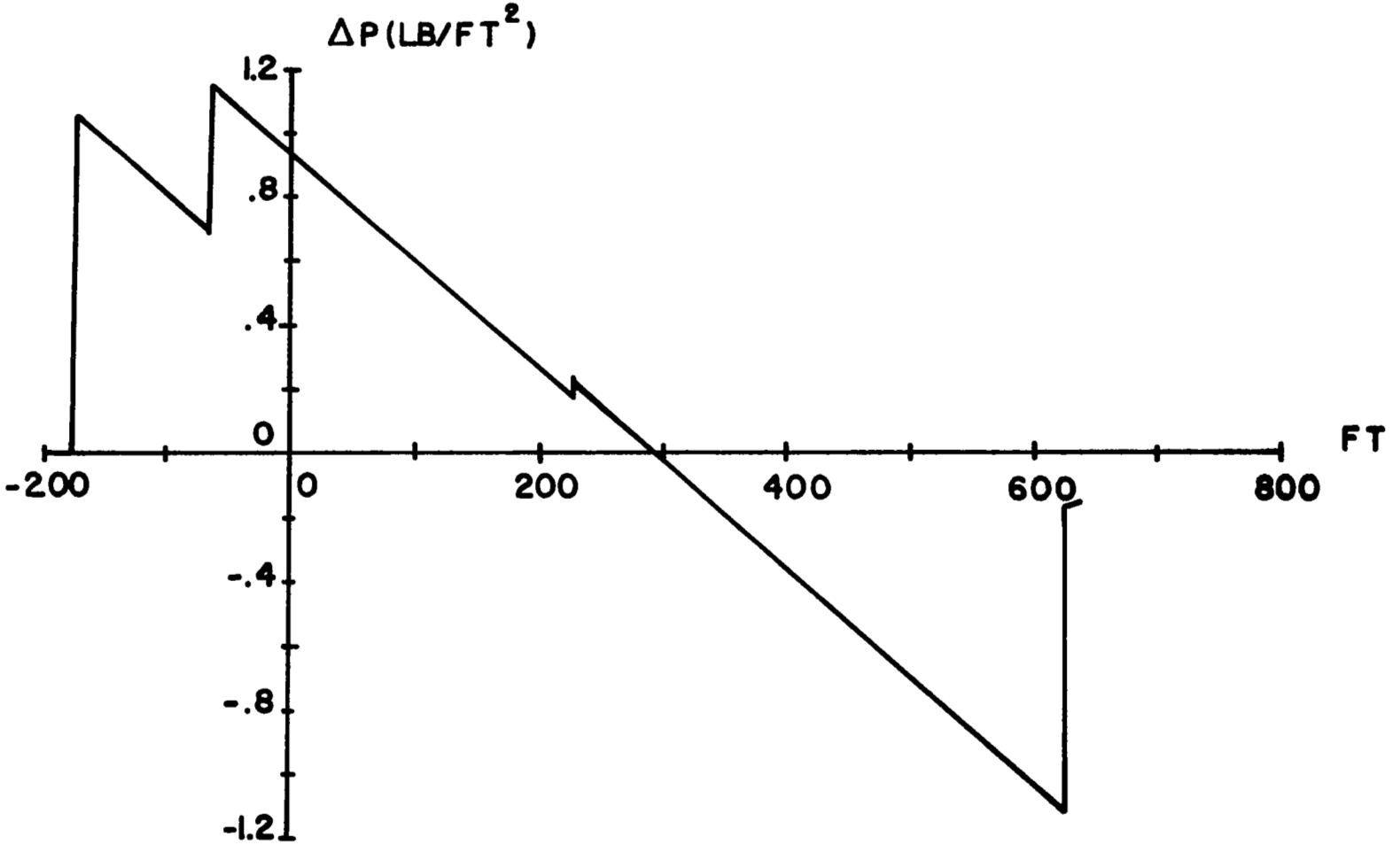

Fig. 11 Sonic Boom Signature Corresponding to Area Curve B of Fig. 10

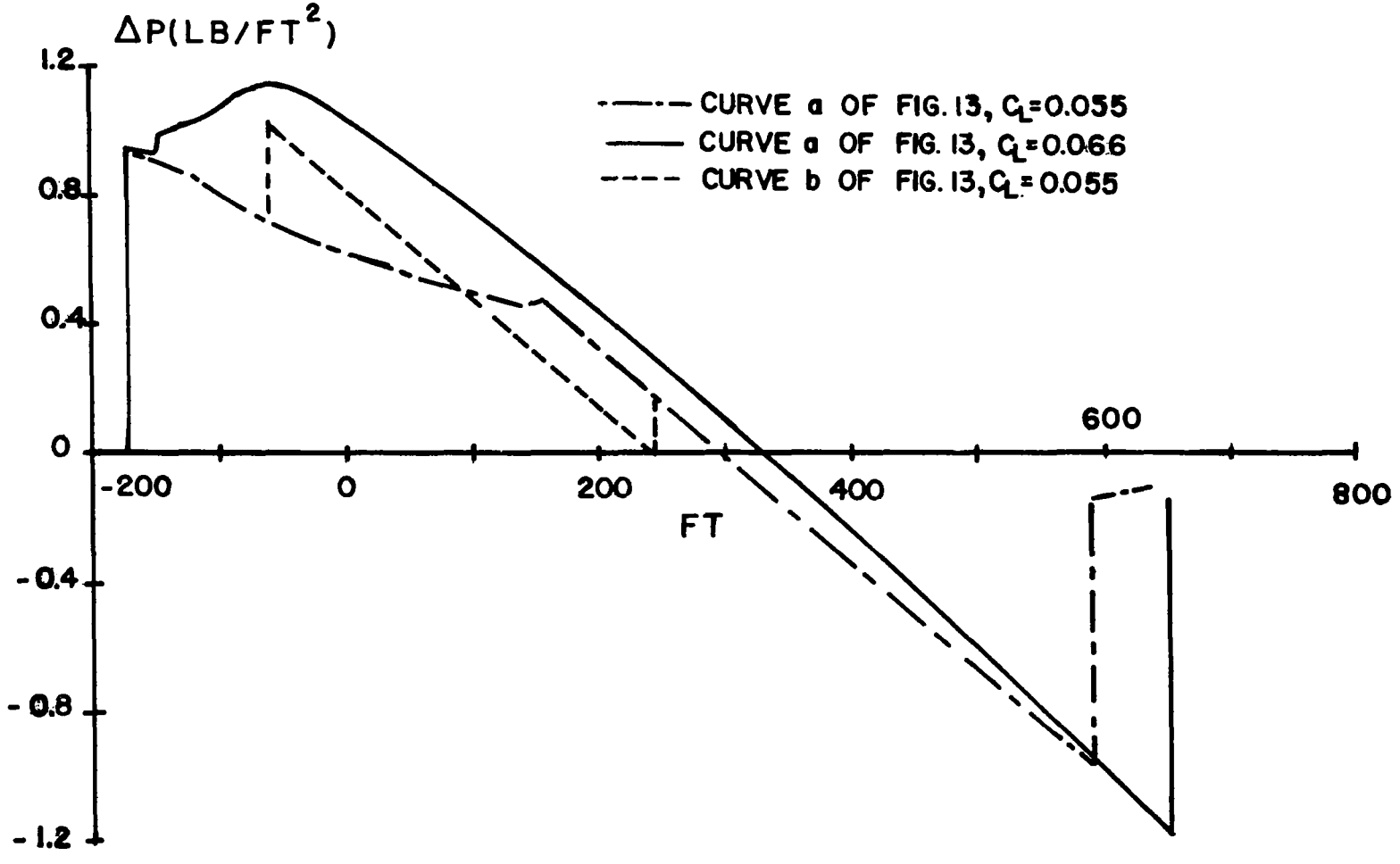

Fig. 12 Sonic boom signature at M = 2.718 L = 300 ft, h = 60,000 ft, W_1 = 430,000 lb (C_L = 0.055)
W_2 = 516,000 lb, (C_L = 0.066)

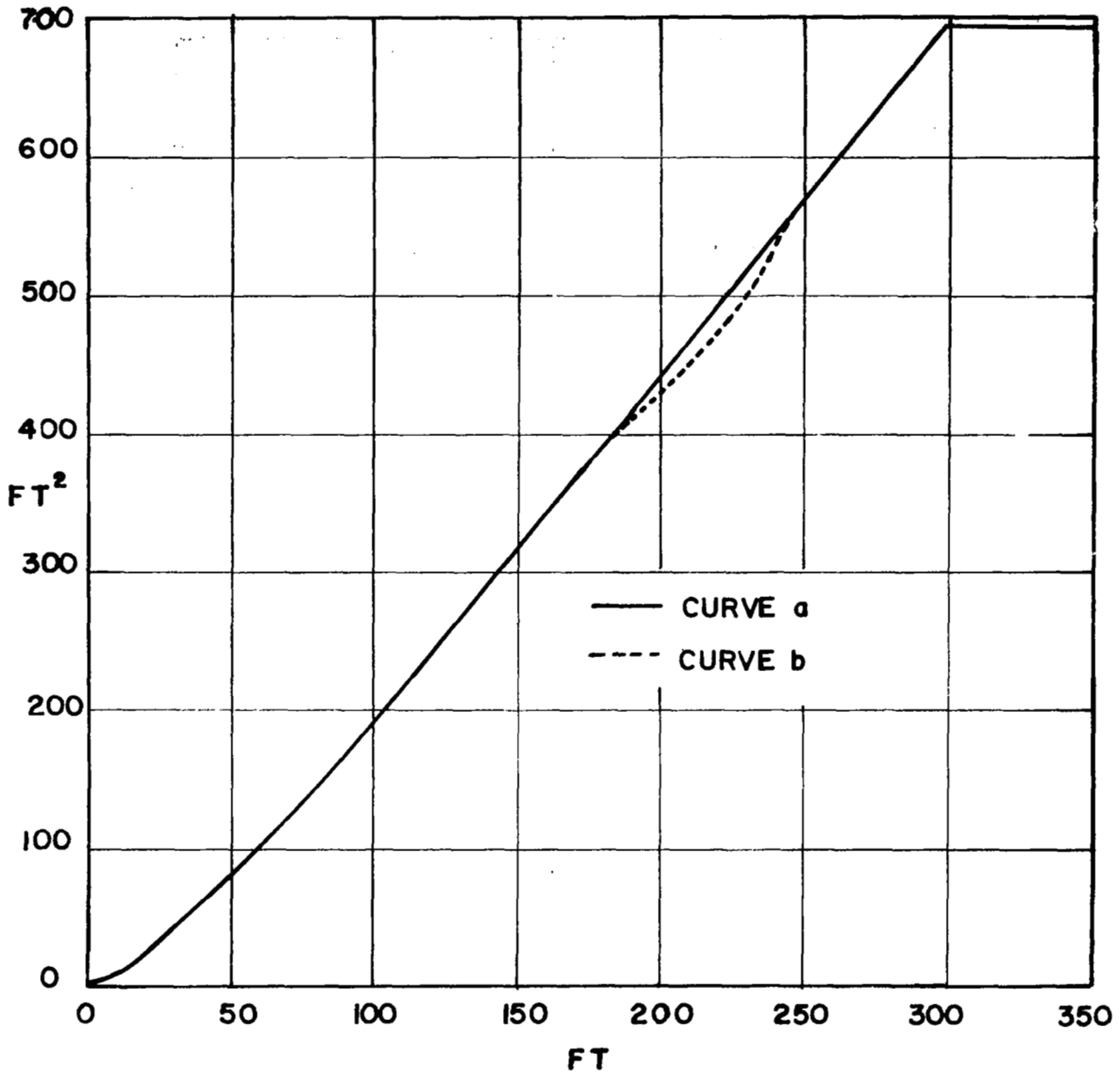

Fig. 13 Variation of equivalent area distribution corresponding to curve c of Fig. 12

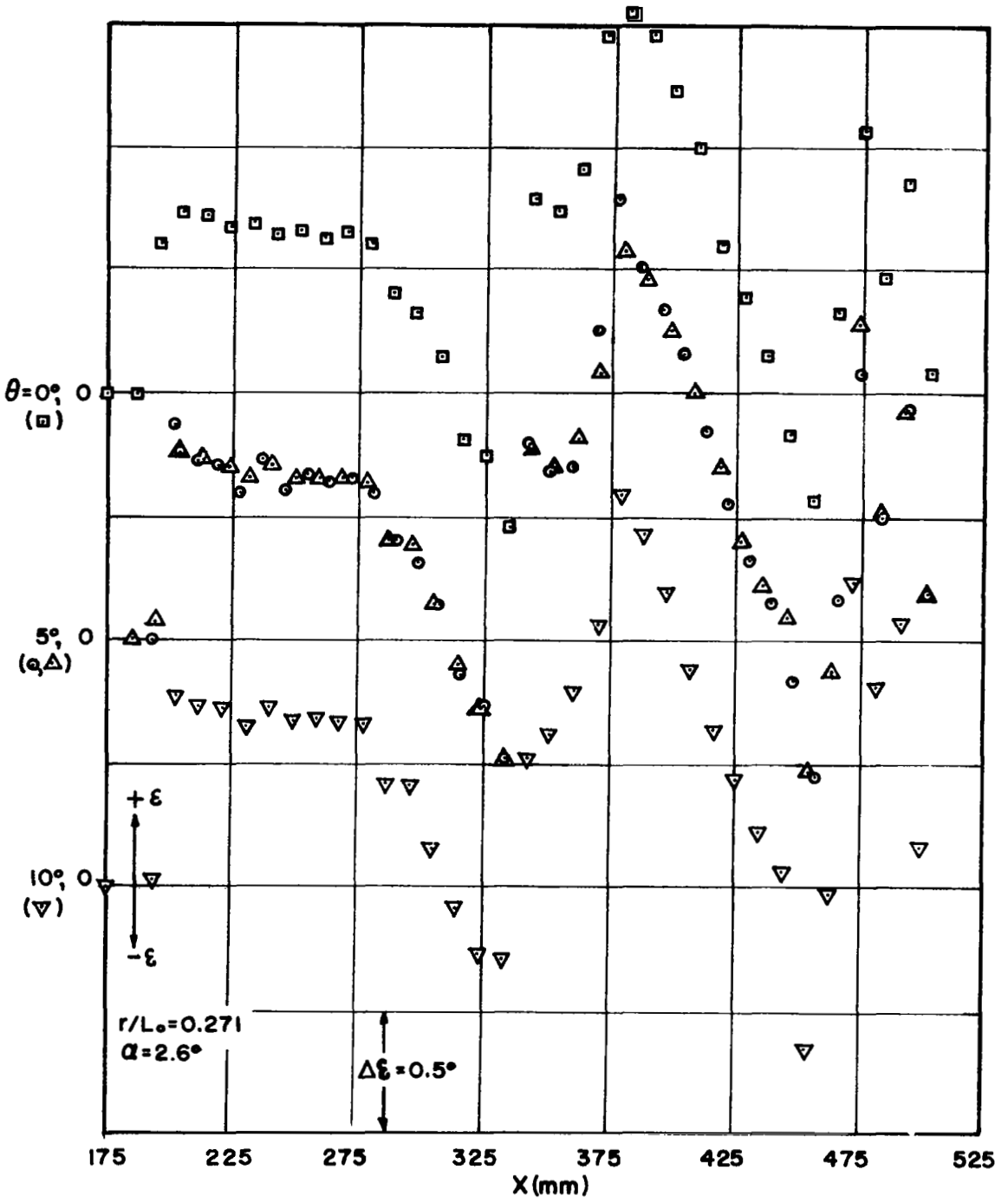

Fig. 14a Experimental values of ε as function of distance at several meridian planes $r/L_o = 0.271$ $\alpha = 2.6^o$

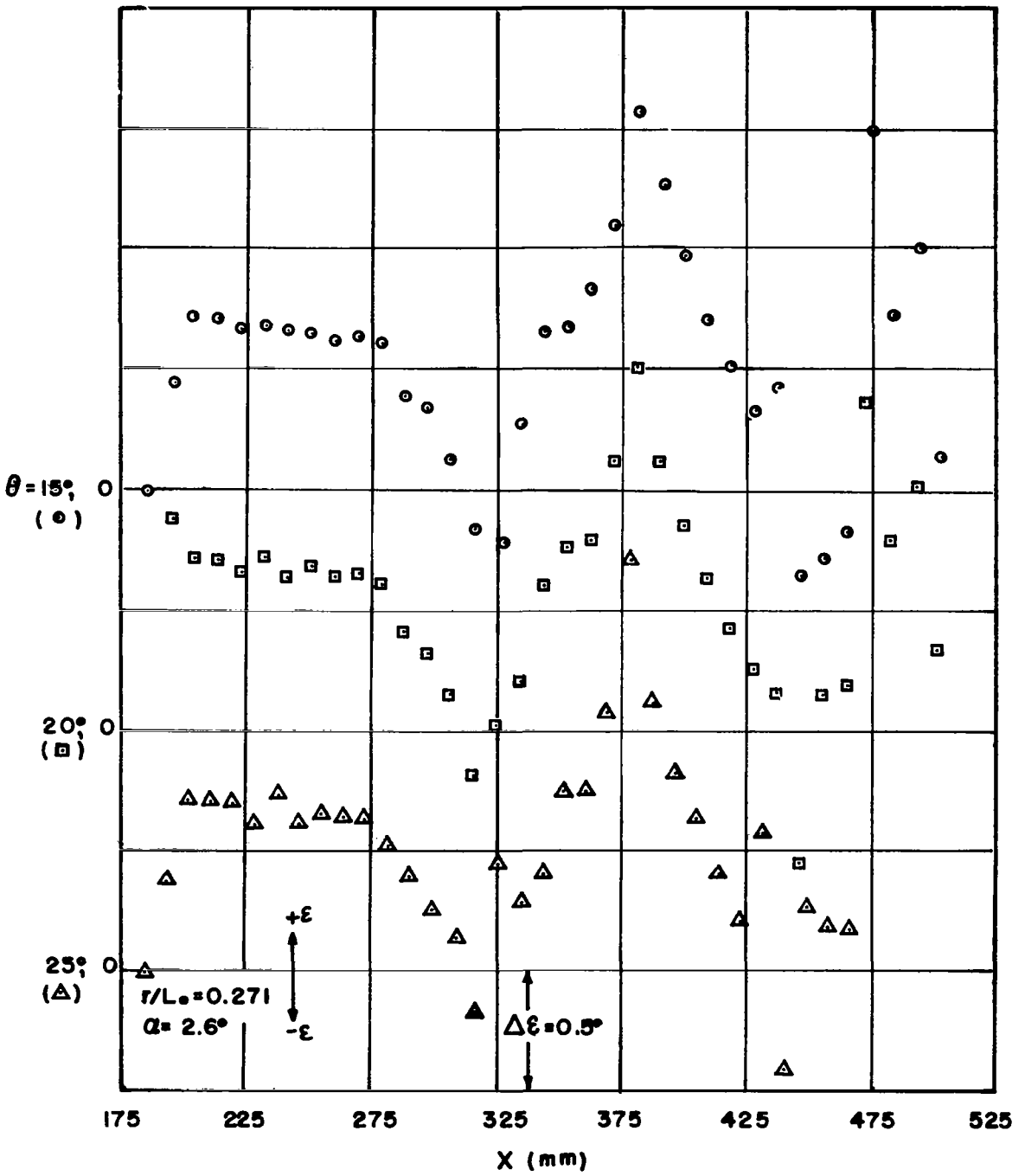

Fig. 14b Continued

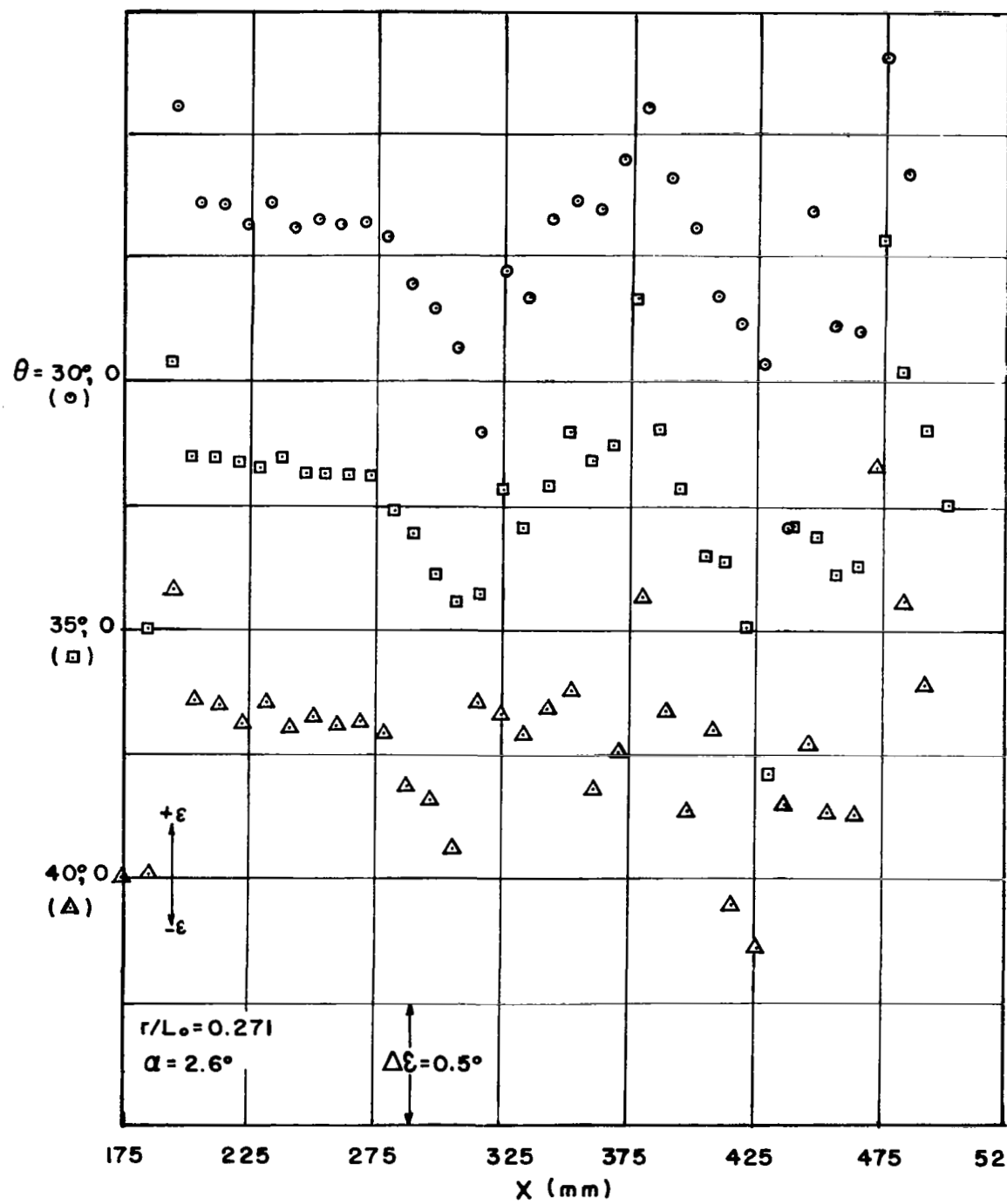

Fig. 14c Continued

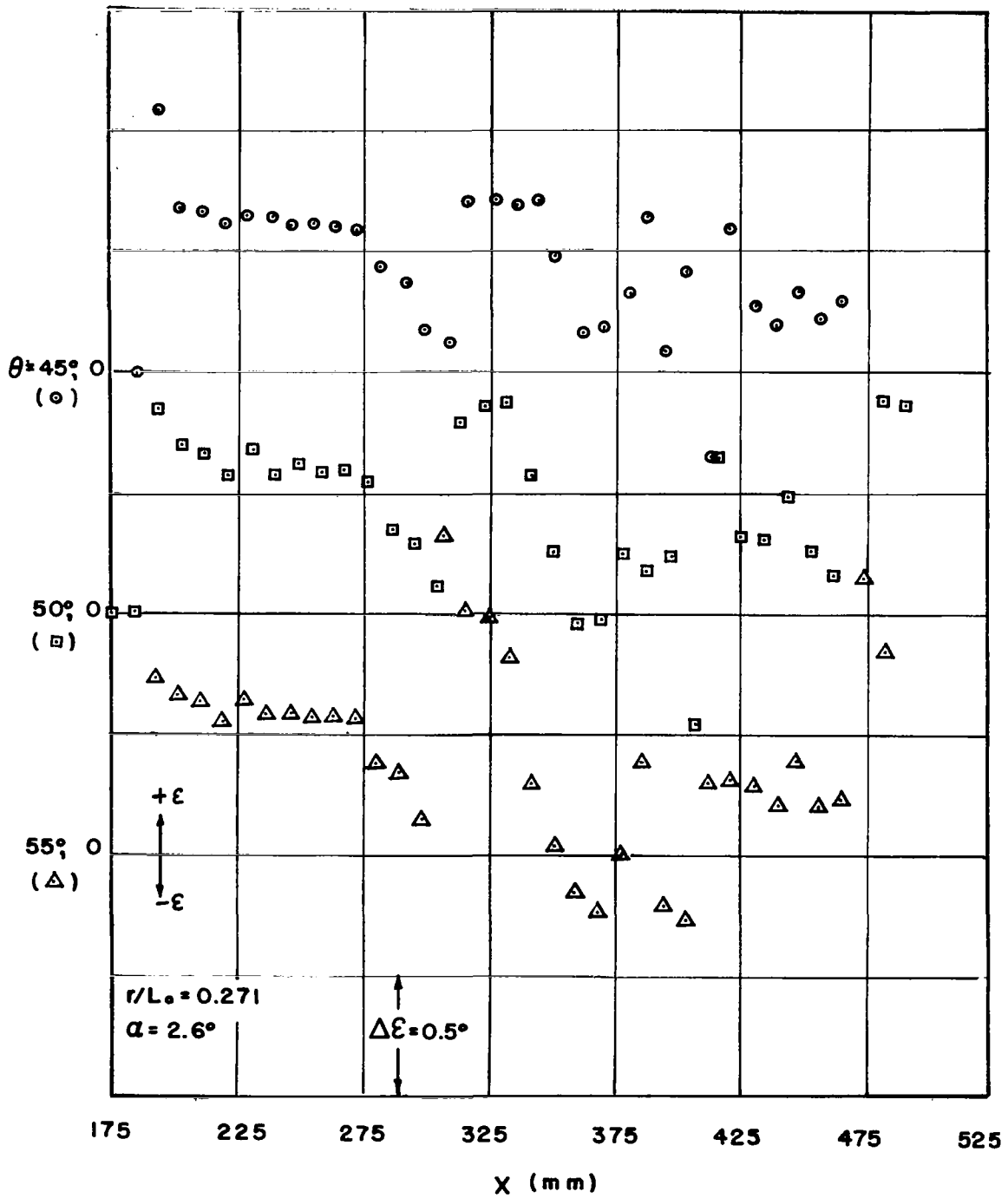

Fig. 14d Continued

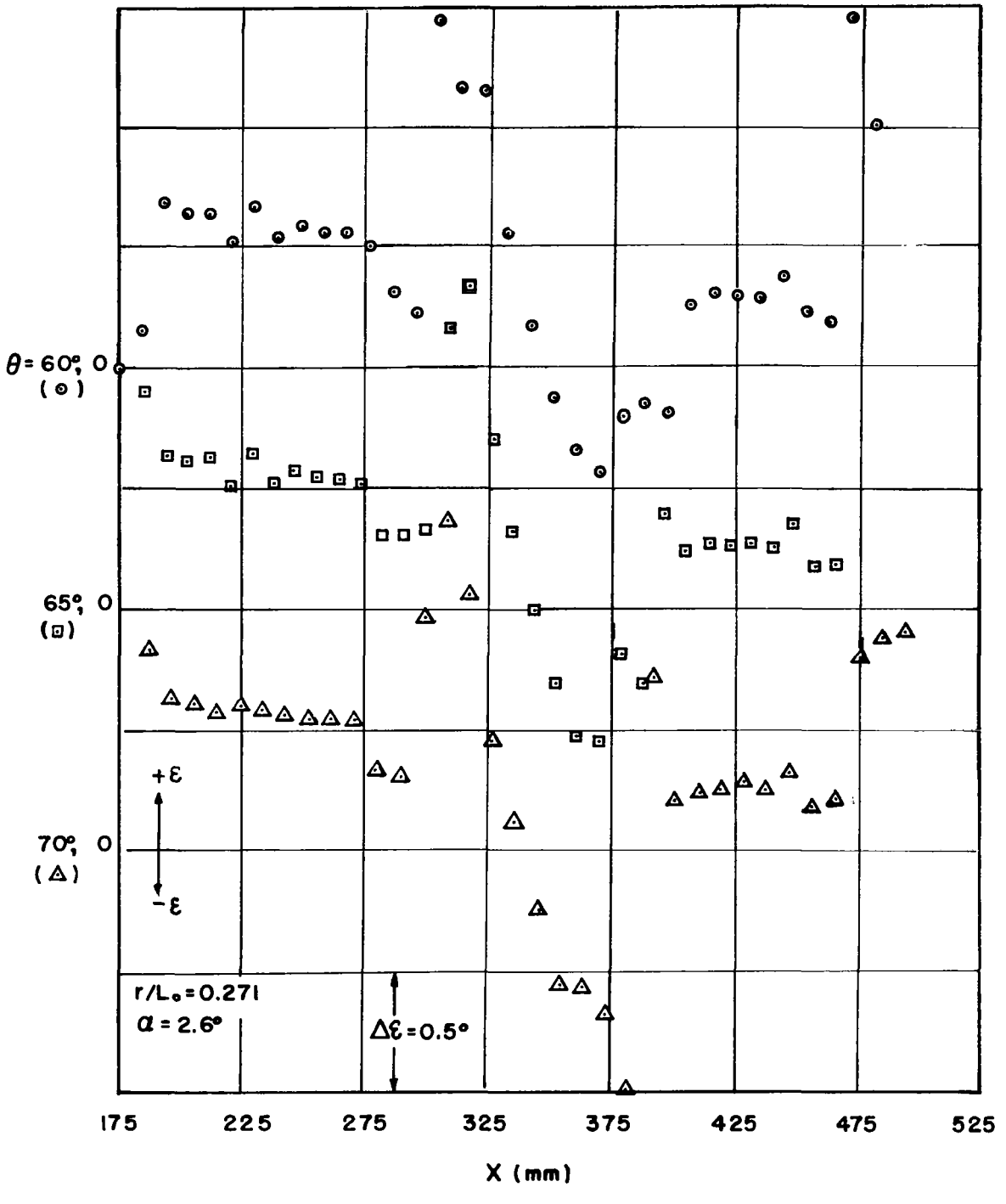

48 Fig. 14e Continued

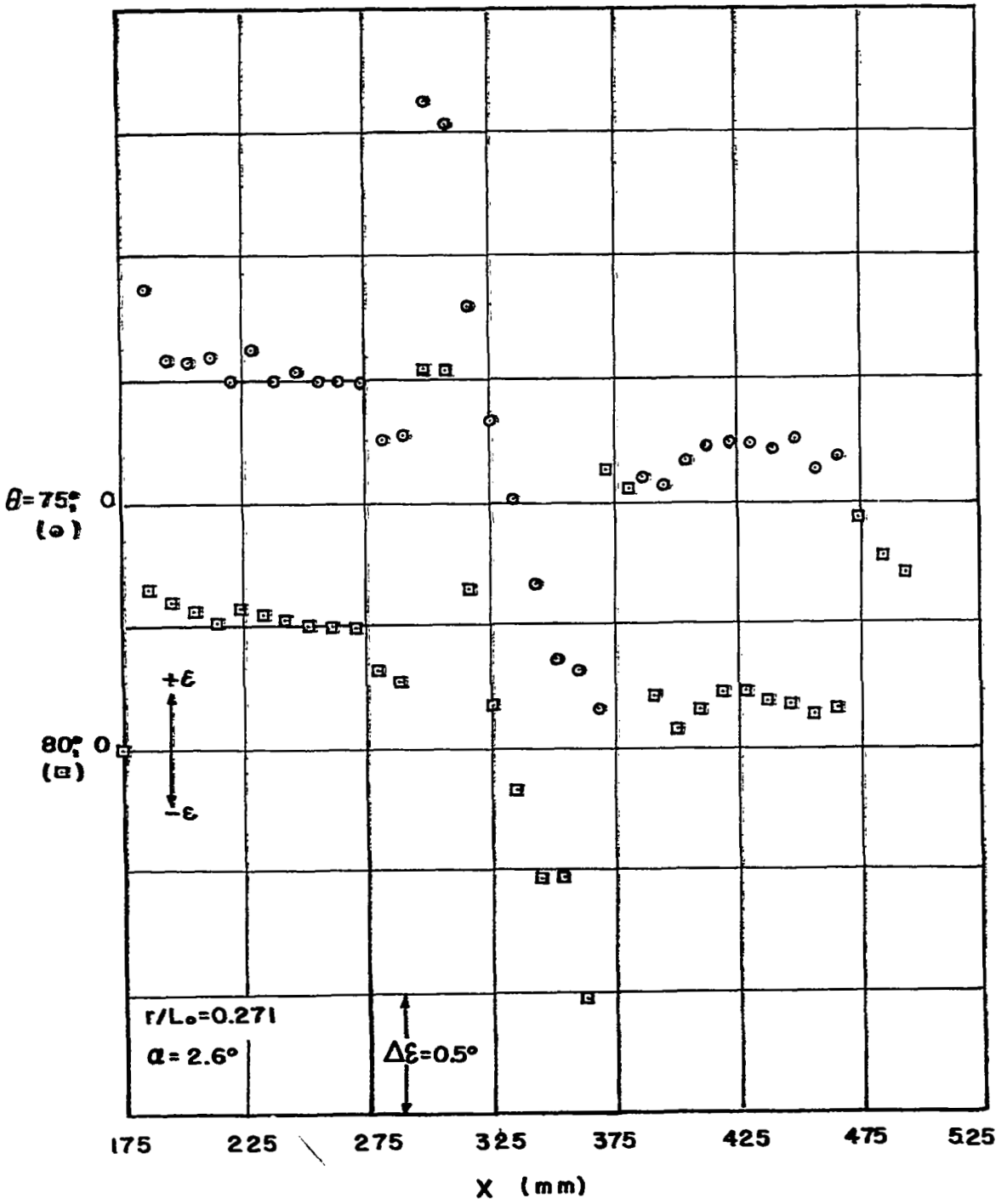

Fig. 14f Continued

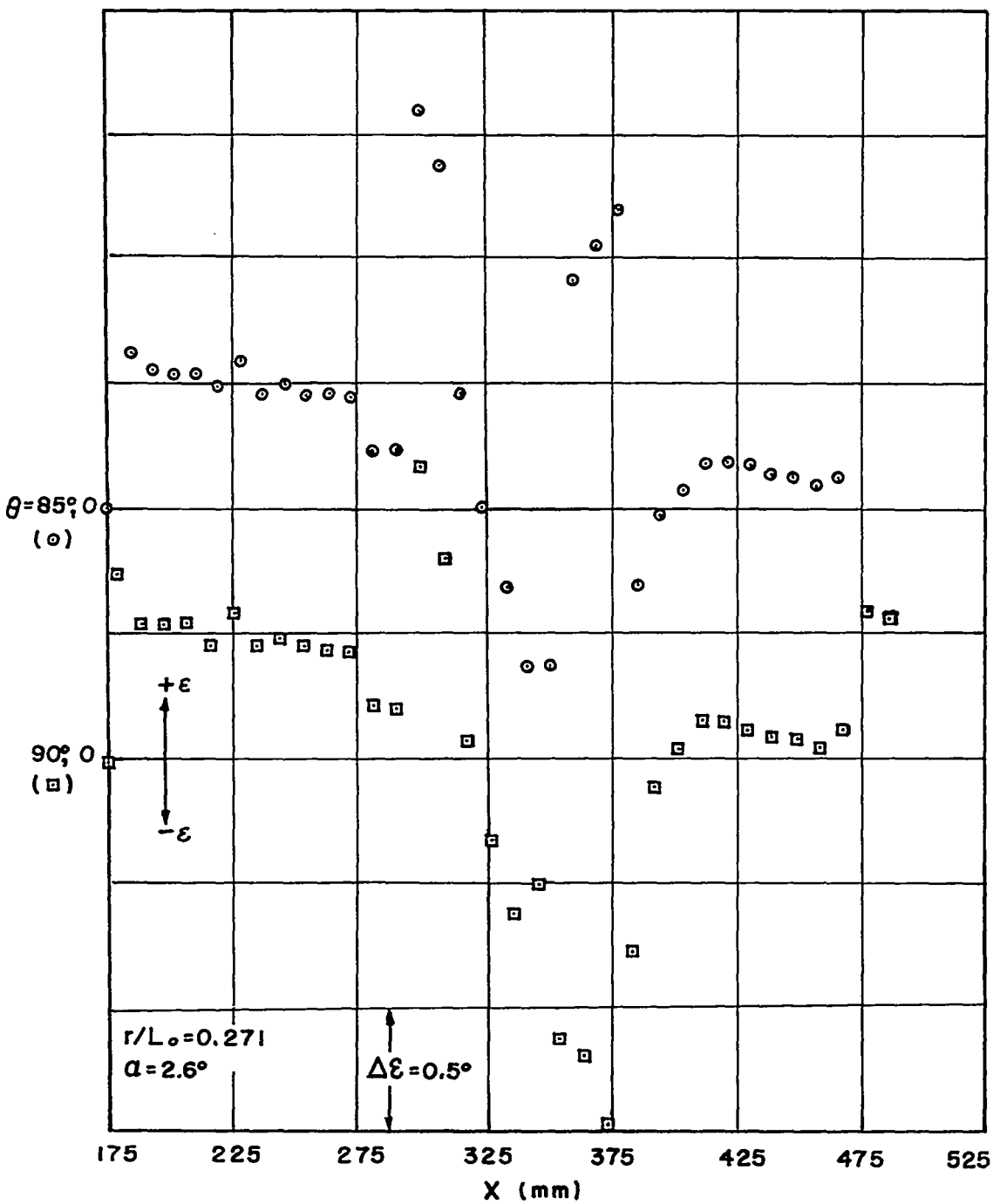

Fig. 14g Continued

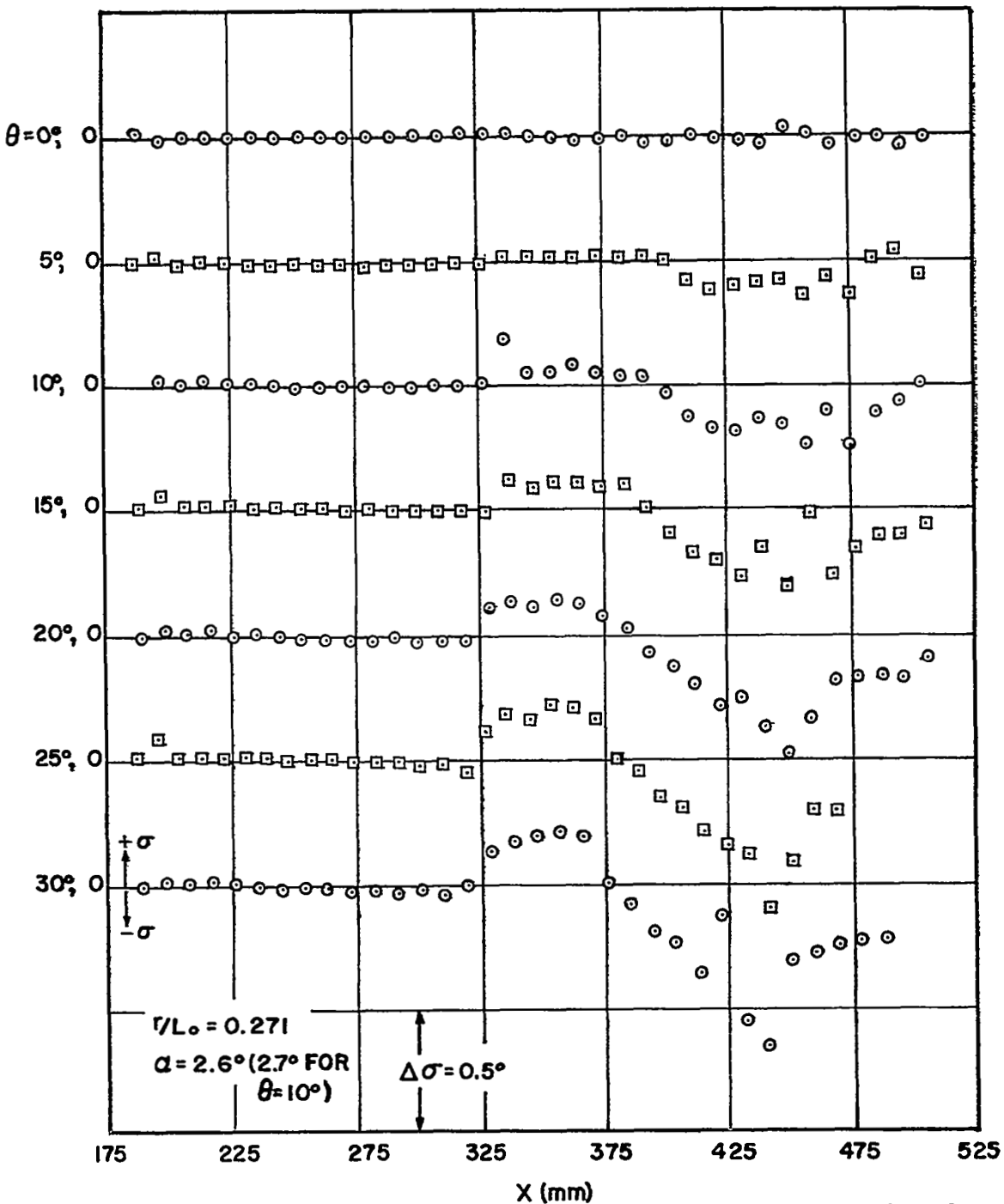

Fig. 15a Experimental values of σ as function of distance at several meridian planes

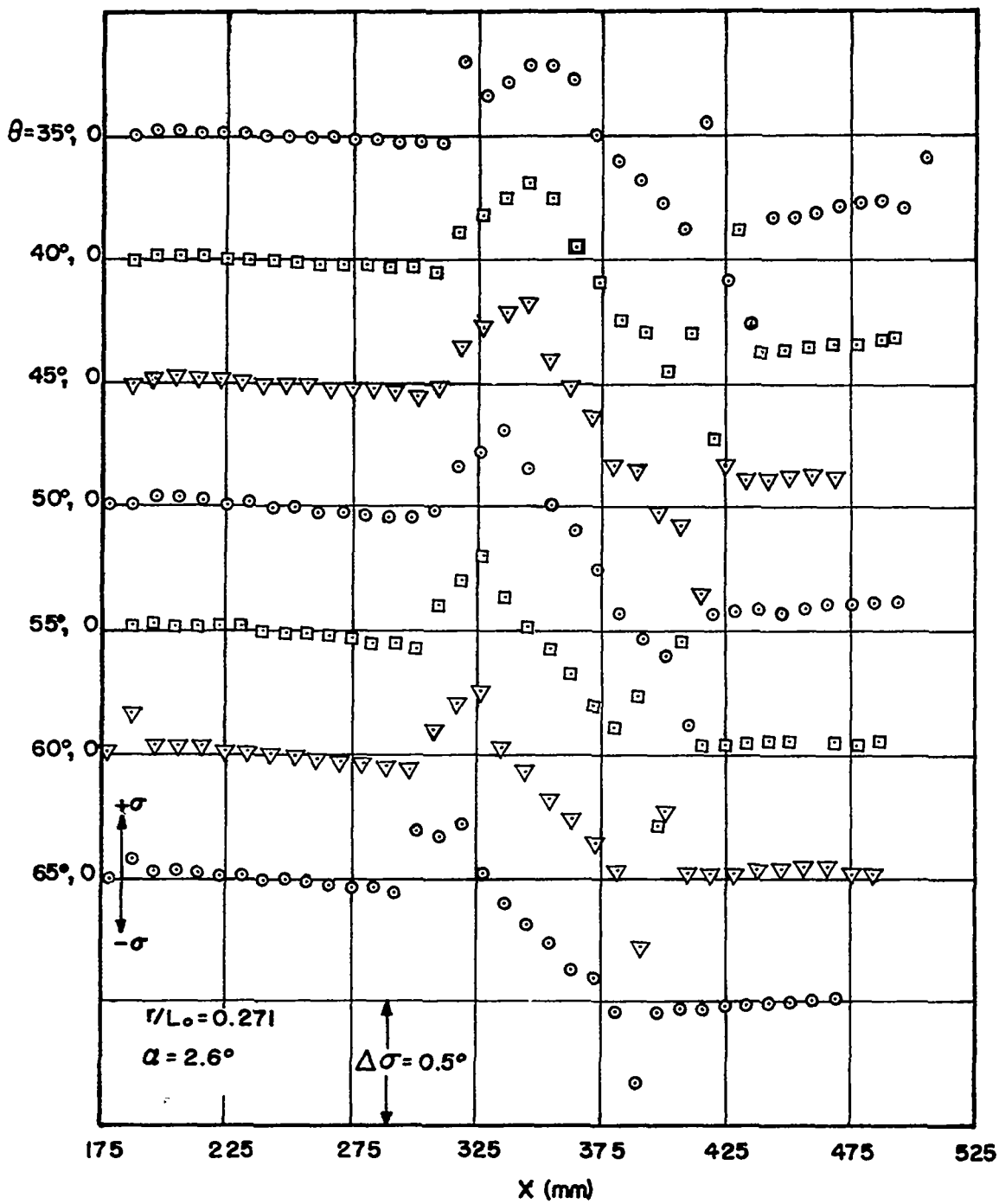

 Fig. 15b Continued

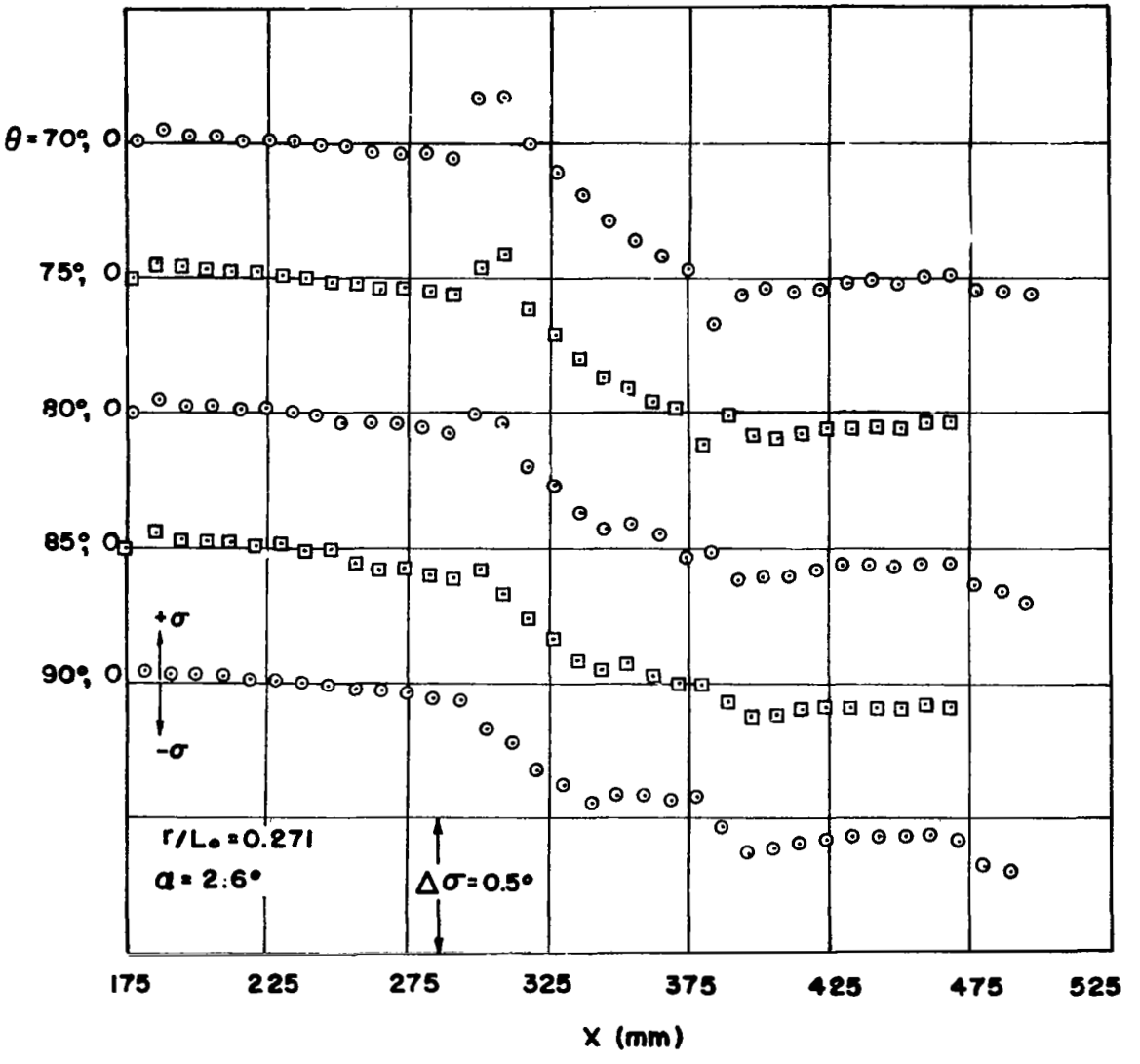

Fig. 15c Continued

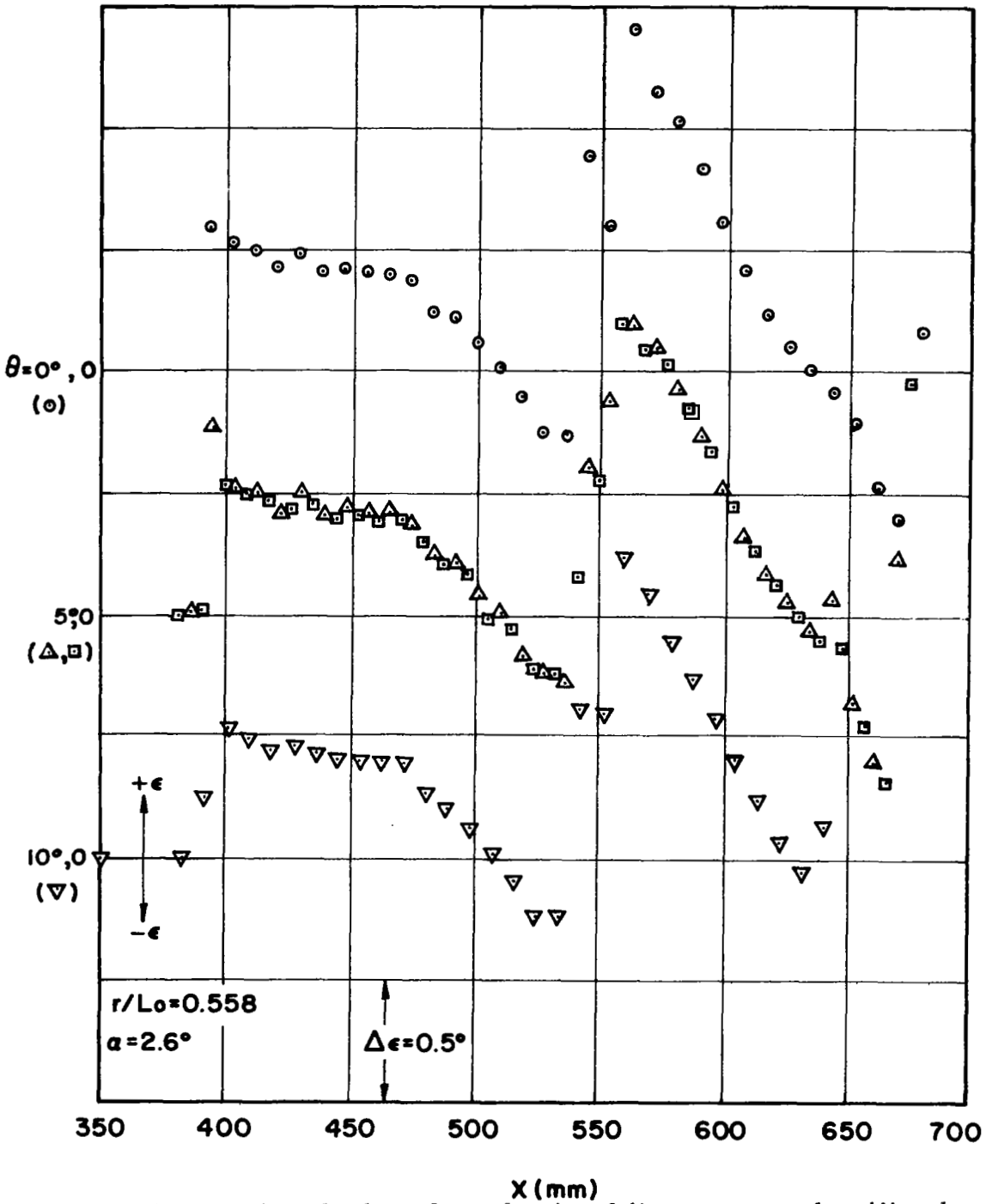

Fig. 16a Experimental values of ϵ as function of distance at several meridian planes $r/L_o = 0.558$, $\alpha = 2.6$

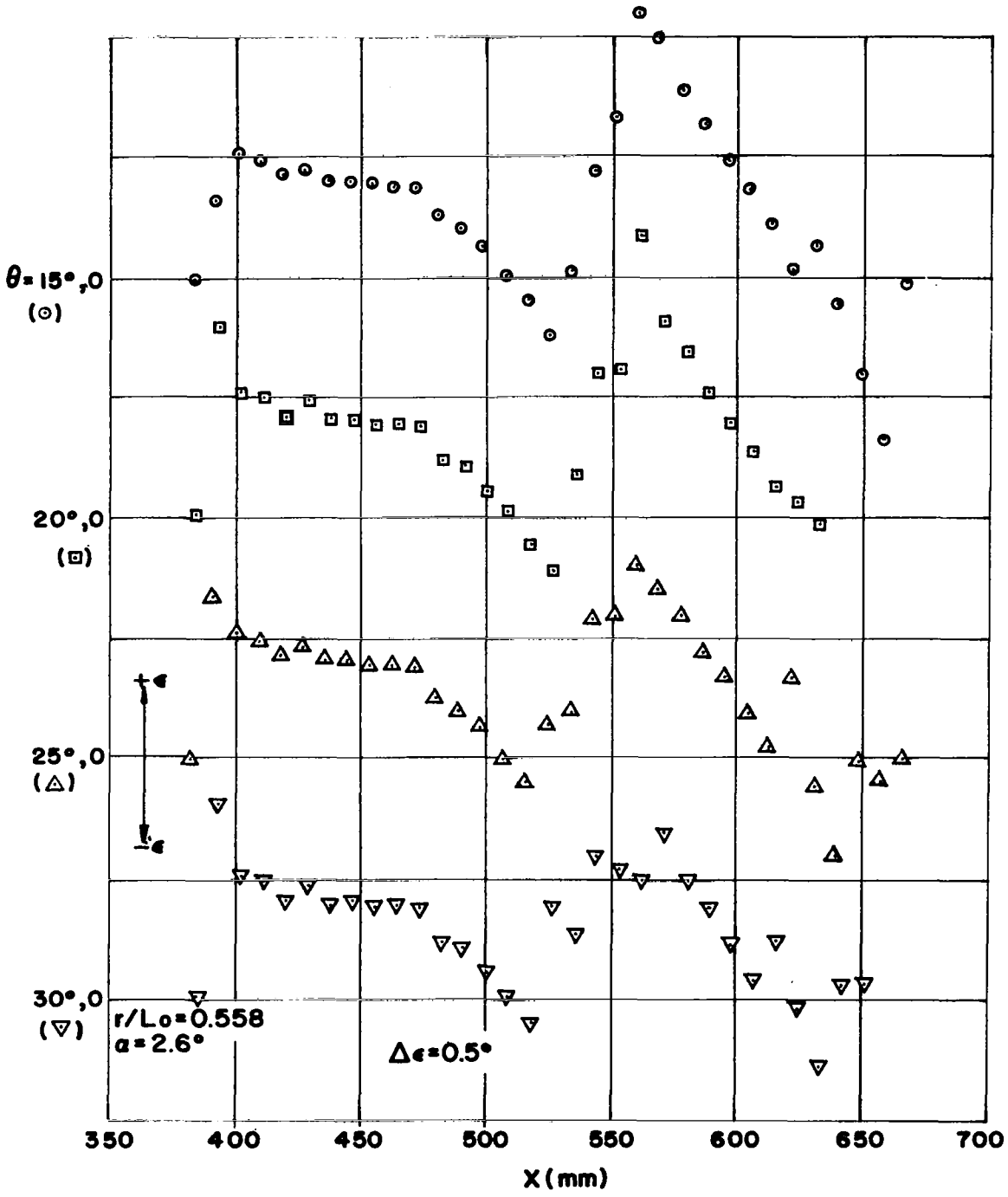

Fig. 16b Continued

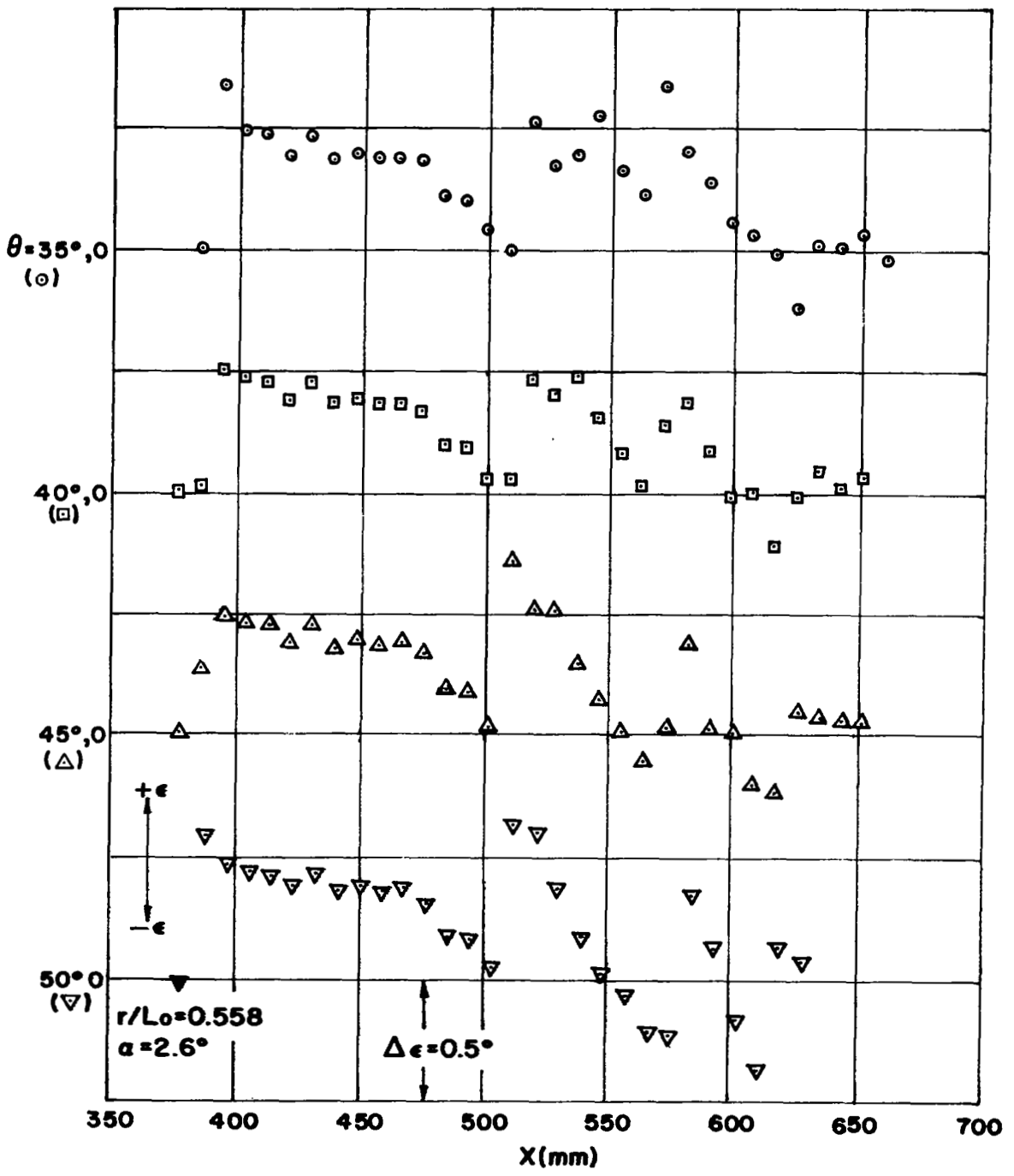

Fig. 16c Continued

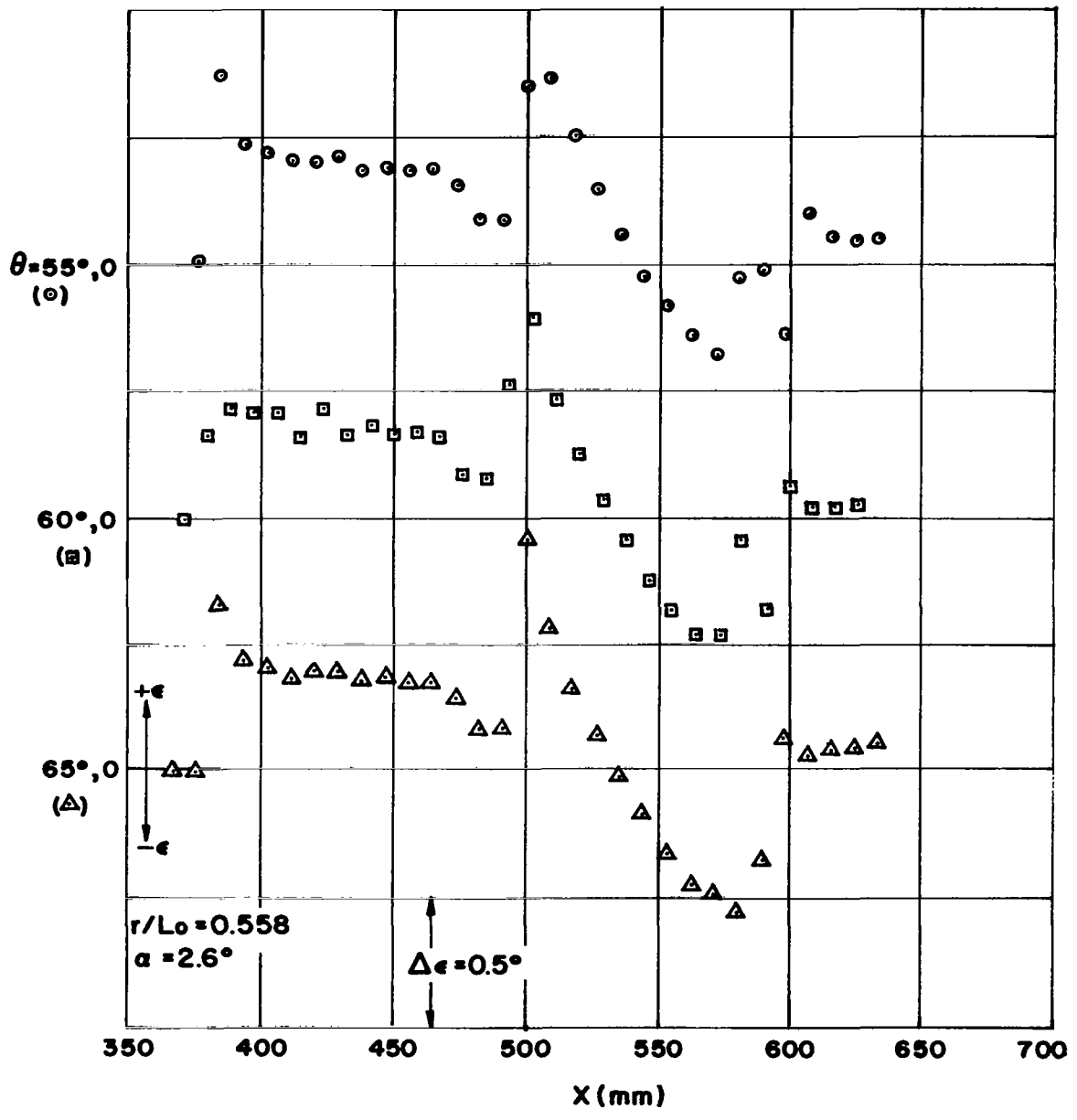

Fig. 16d Continued

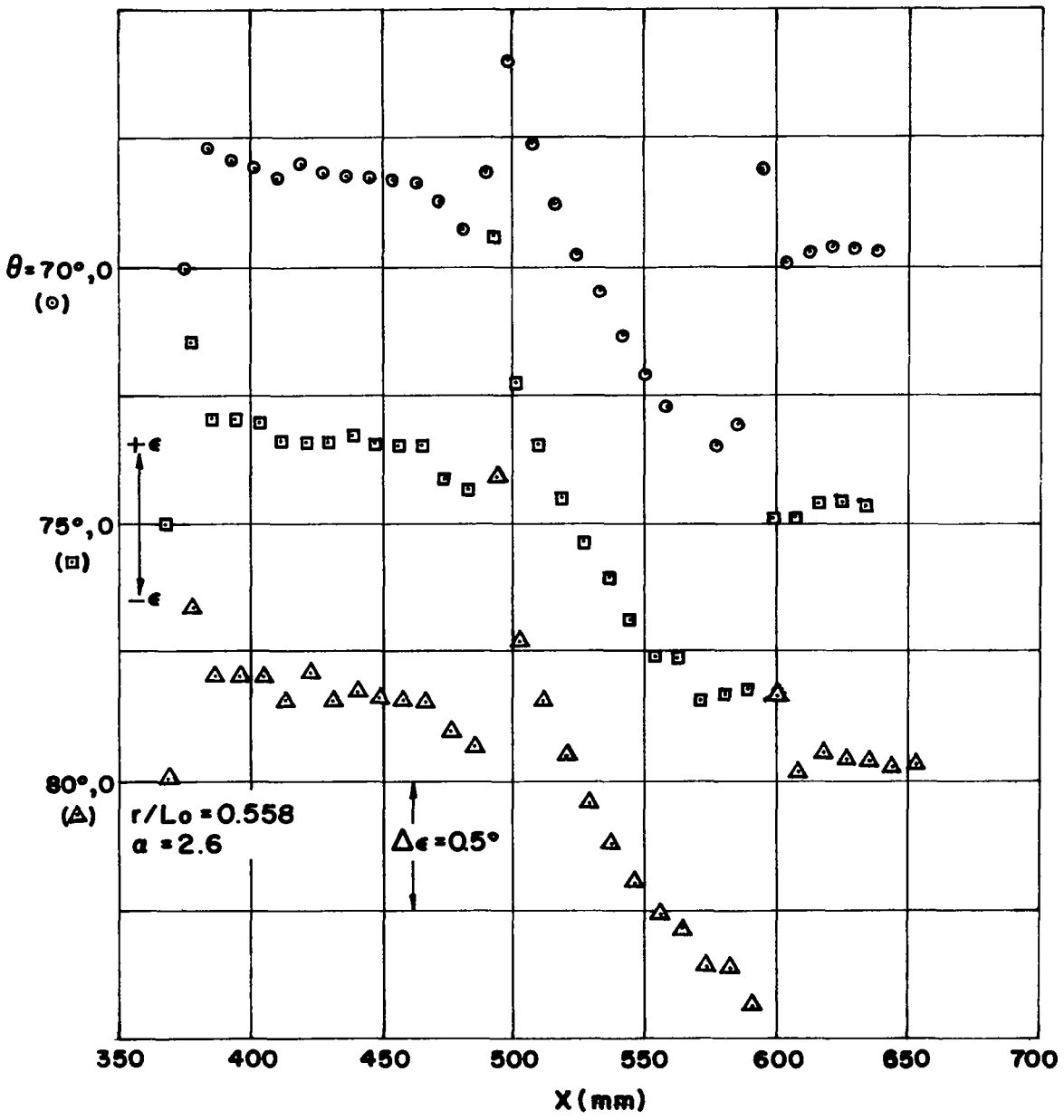

Fig. 16e Continued

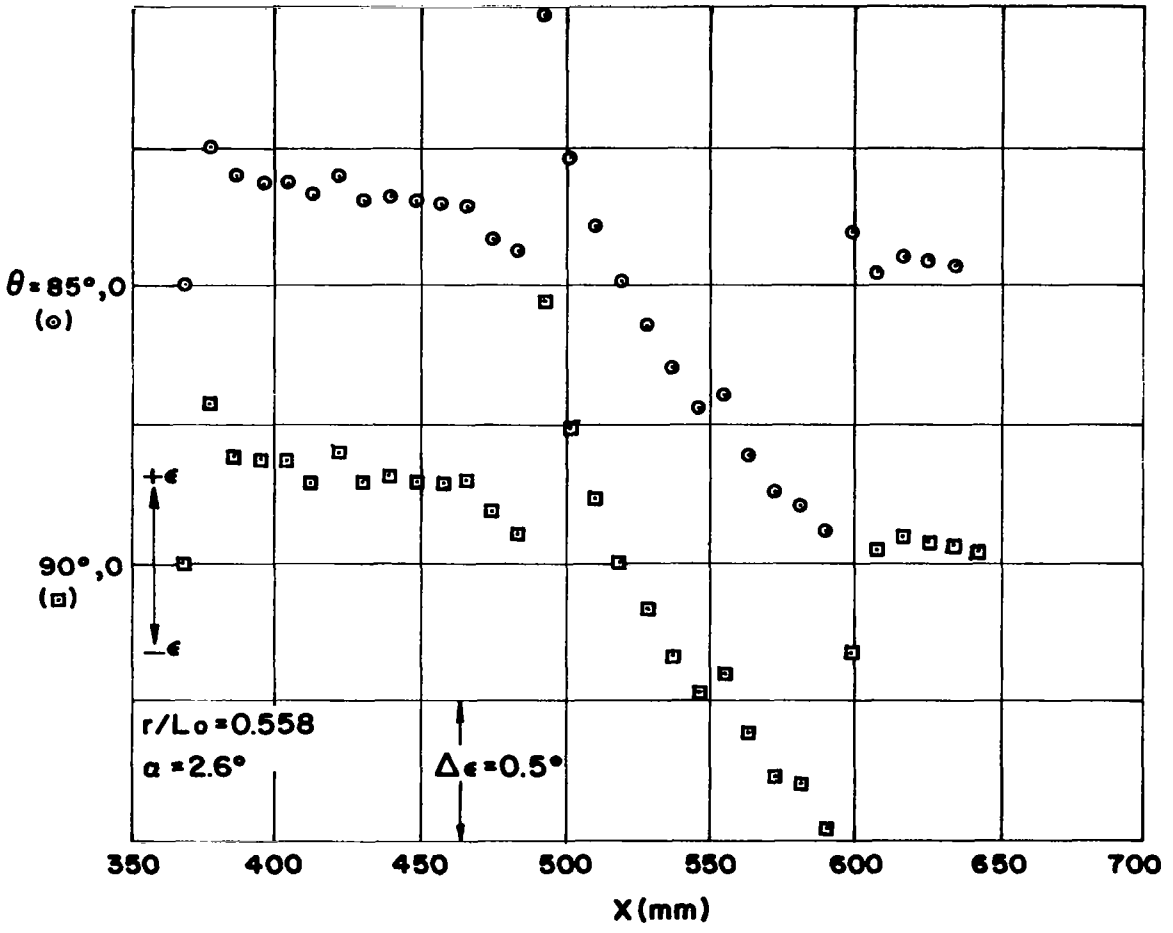

Fig. 16f Continued

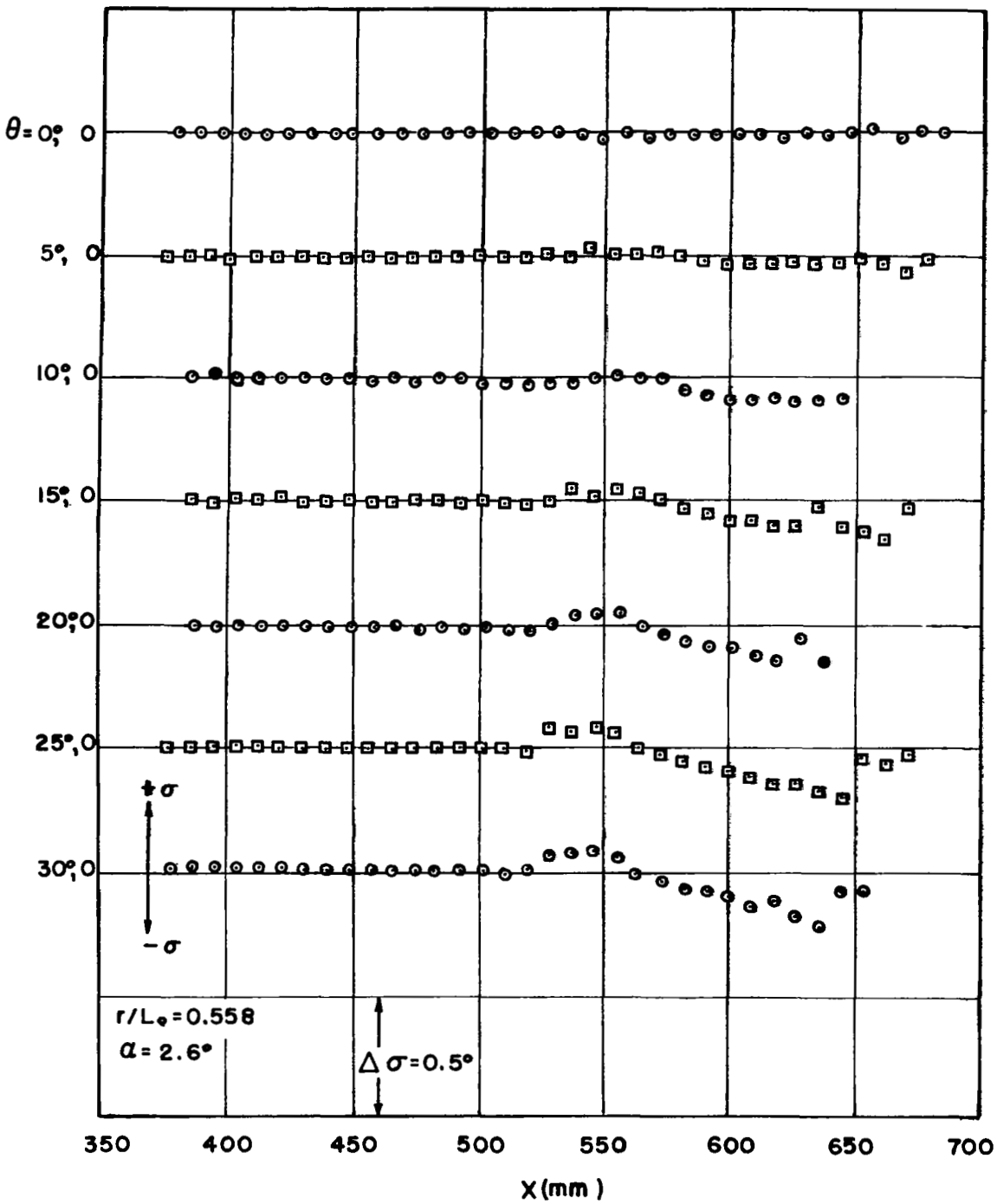

Fig. 17a Experimental values of σ as function of distance at several meridian planes

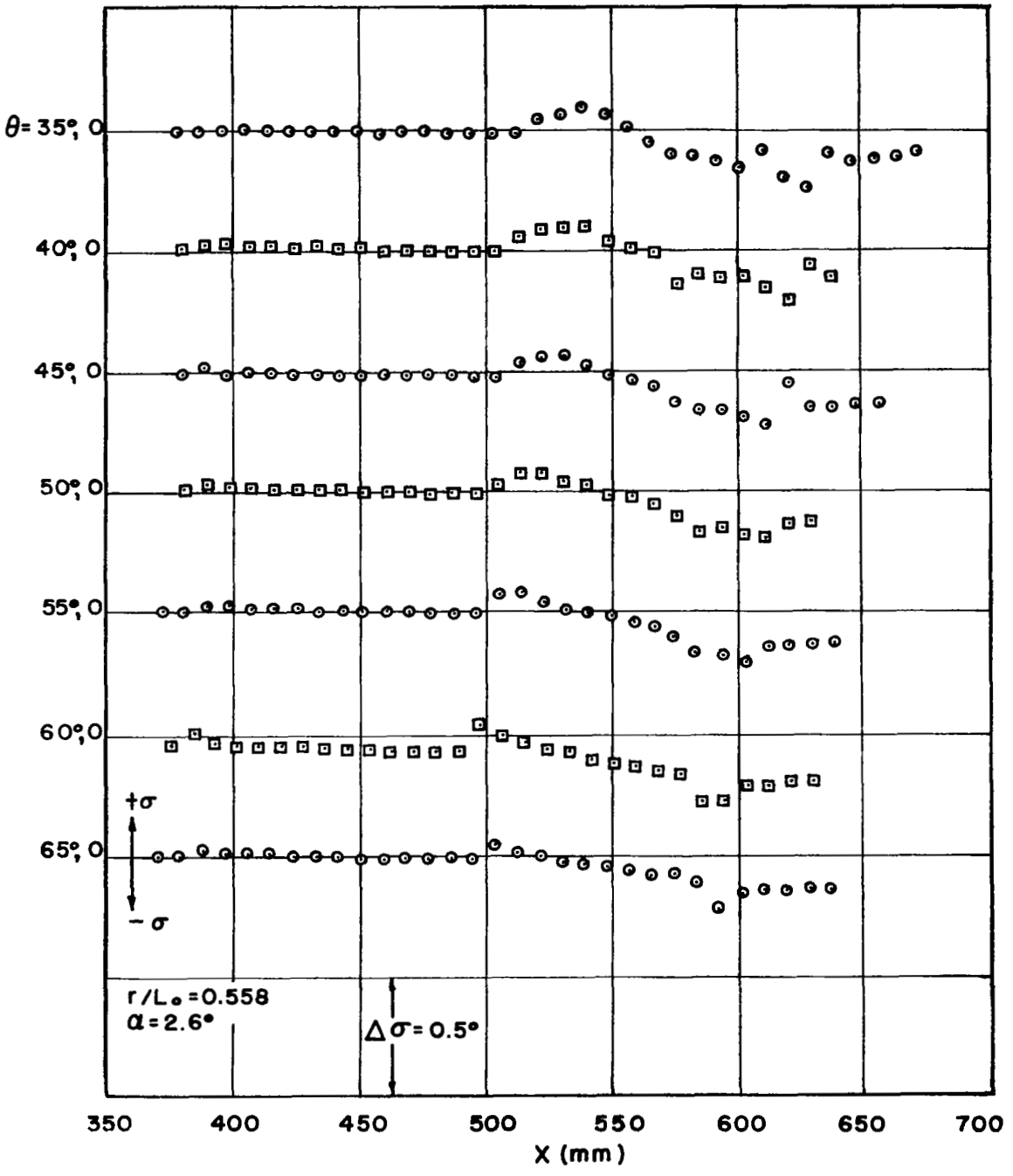

Fig. 17b Continued

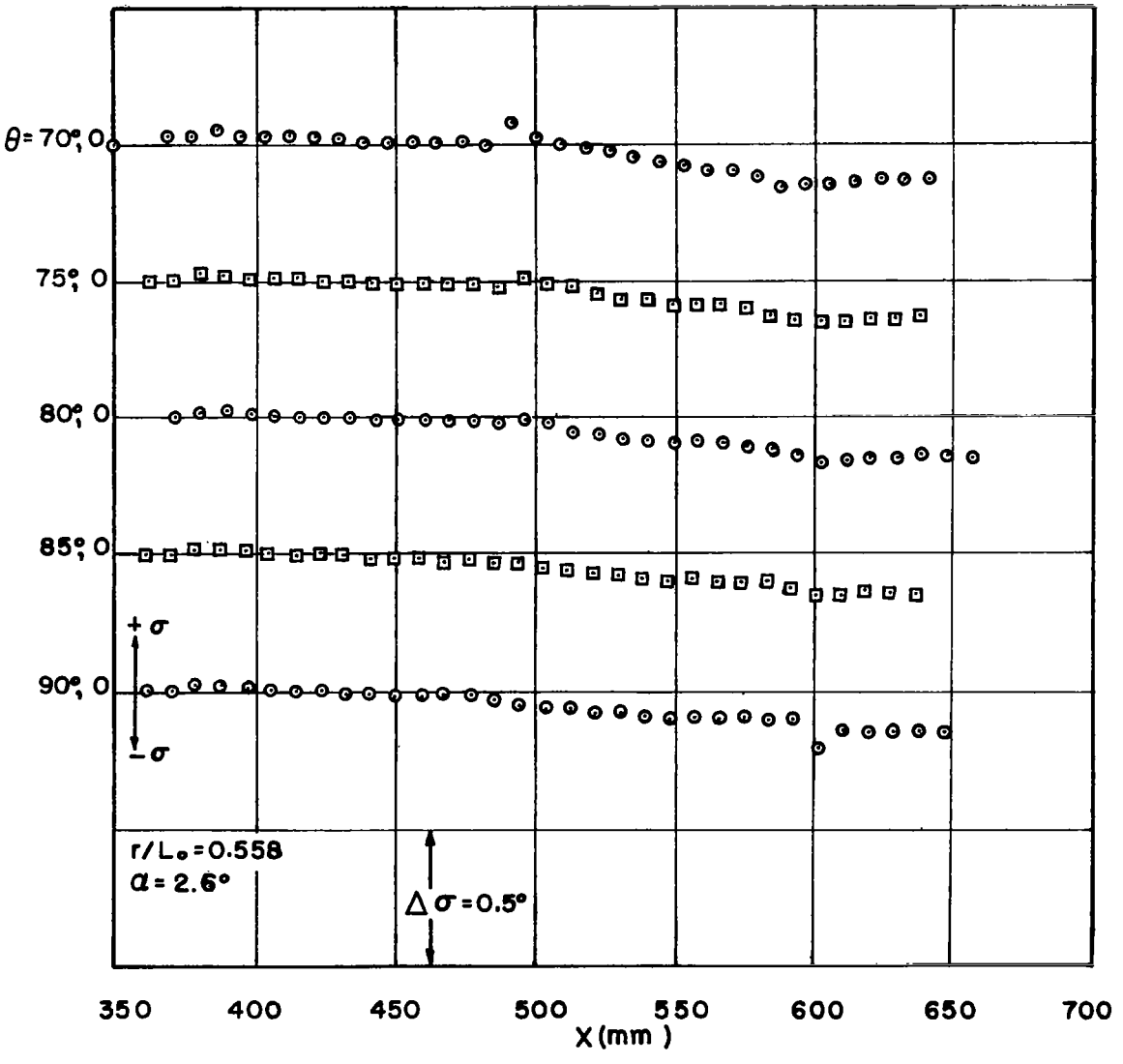

Fig. 17c Continued

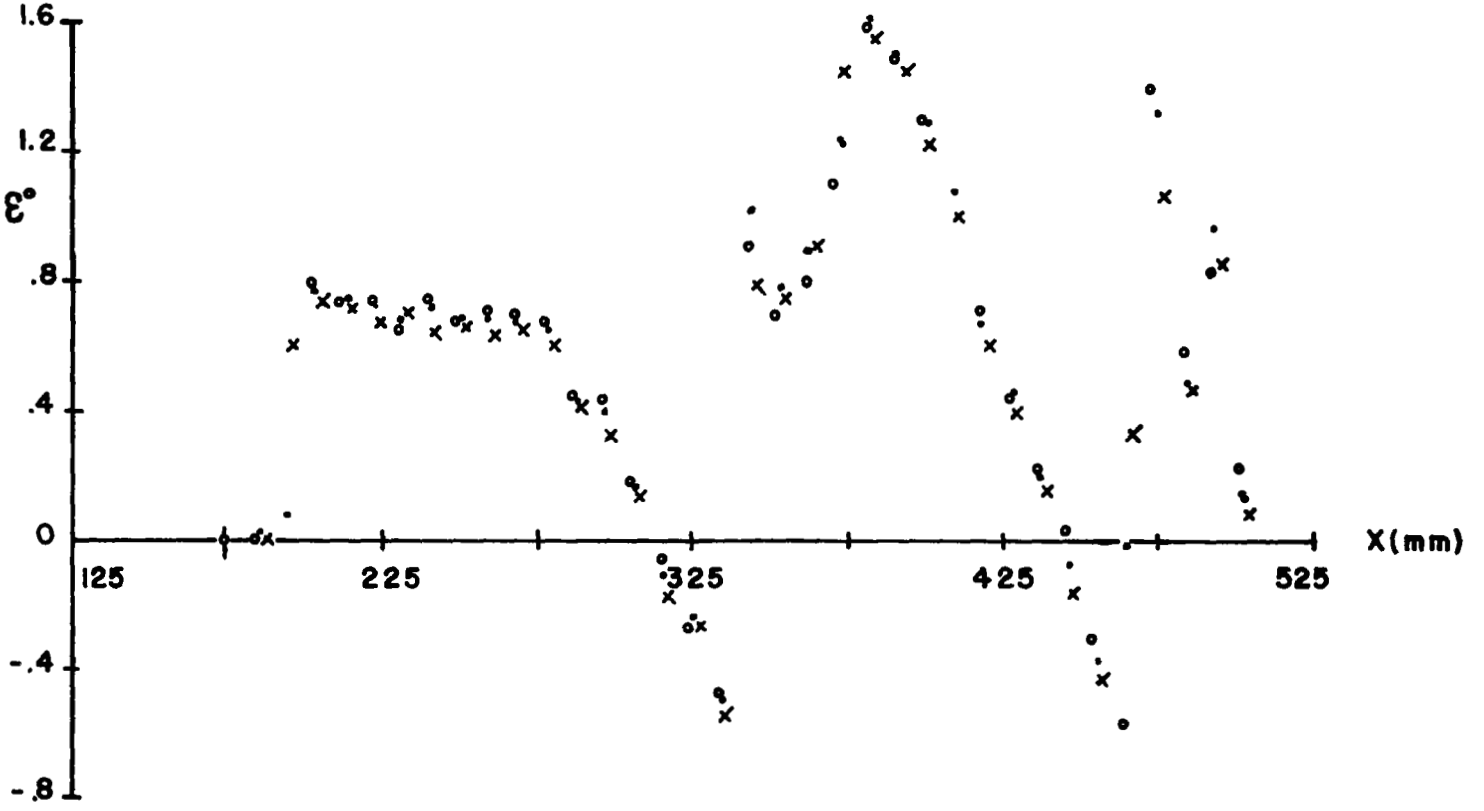

Fig. 18 Distribution of deviation angle ε at $\frac{r}{L_o}$ = 0.271, C_n = 0.055(α = 2.6°), for different longitudinal locations of the model

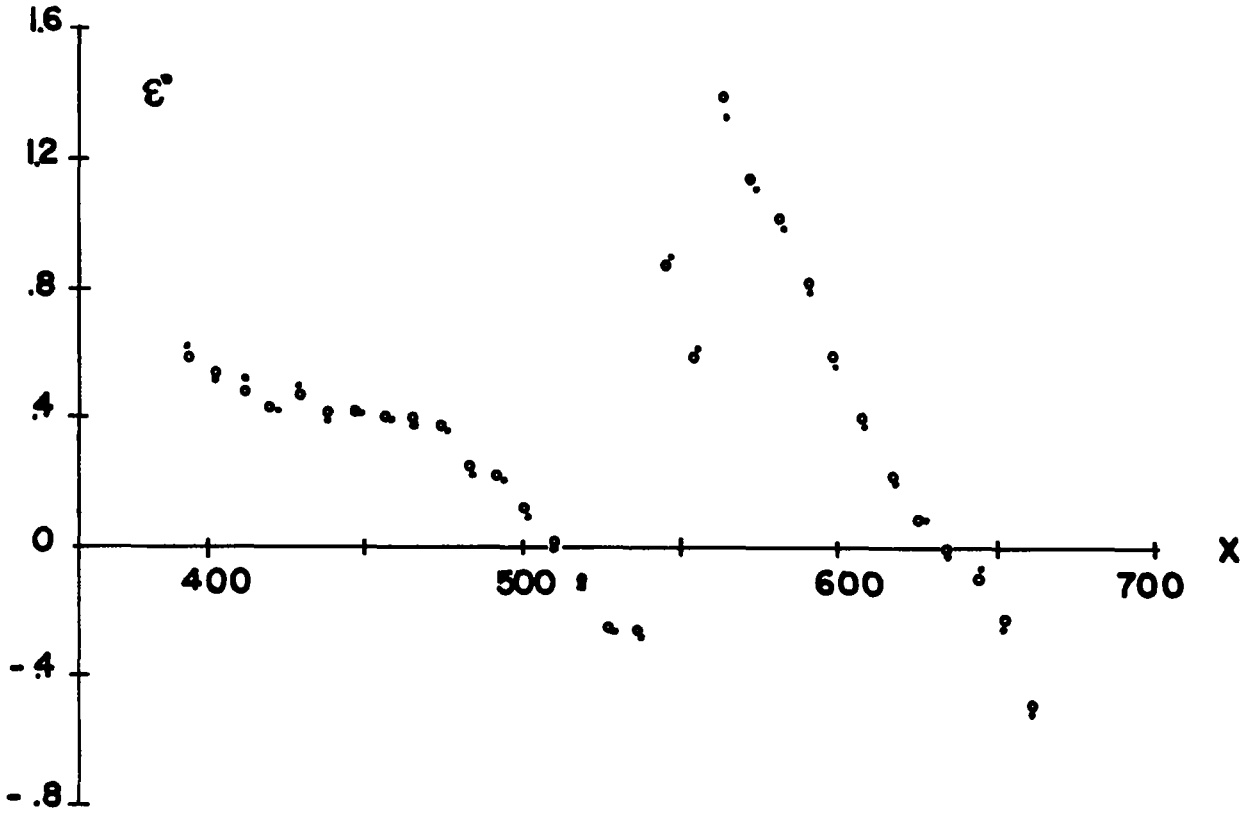

Fig. 19 Distribution of ε for different longitudinal location of the model $\frac{r}{L_o}$ = 0.558 α = 2.6°

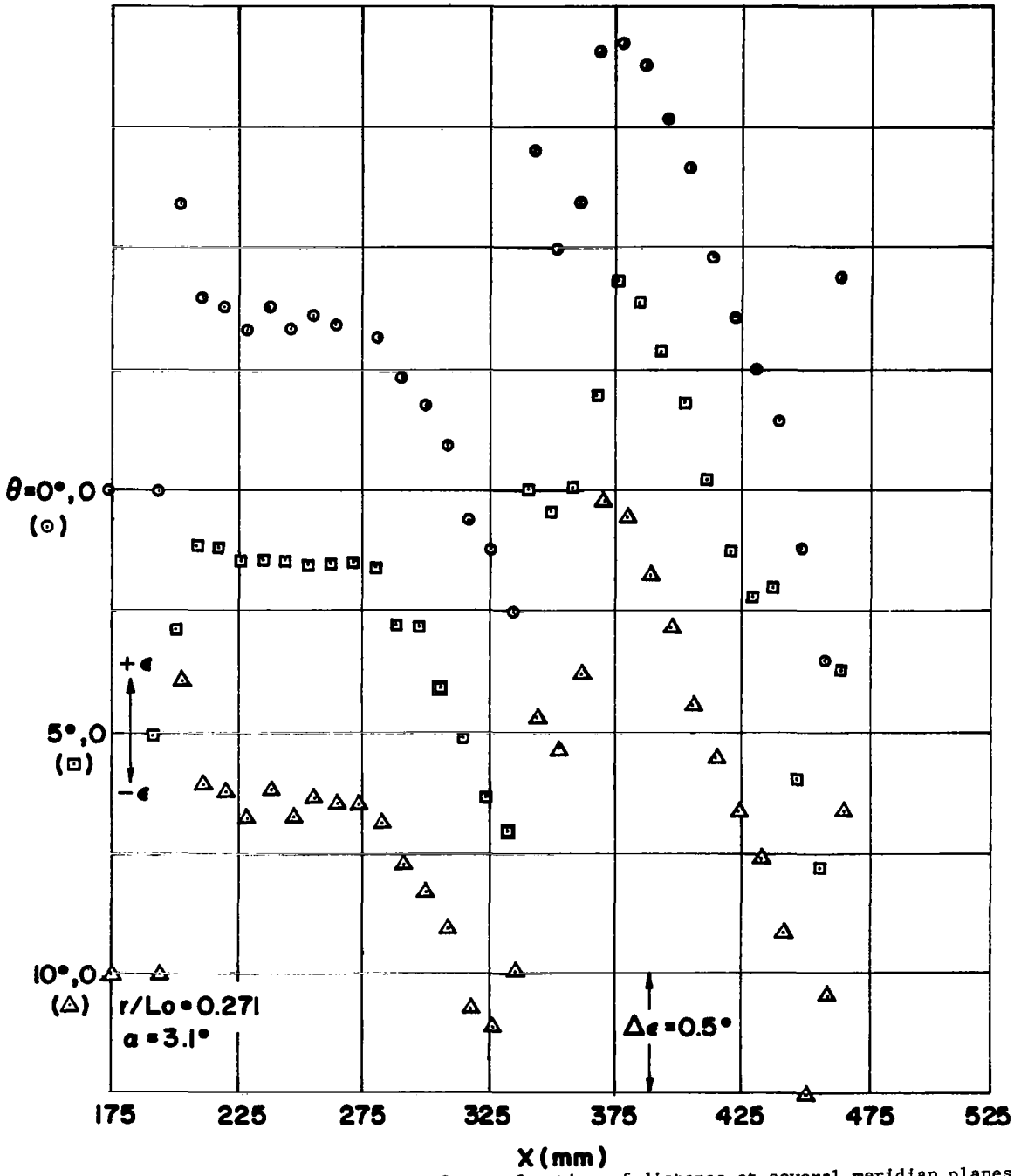

Fig. 20a Experimental values of ε as function of distance at several meridian planes $\alpha = 3.2^{o}$, $r/L_{o} = 0.271$

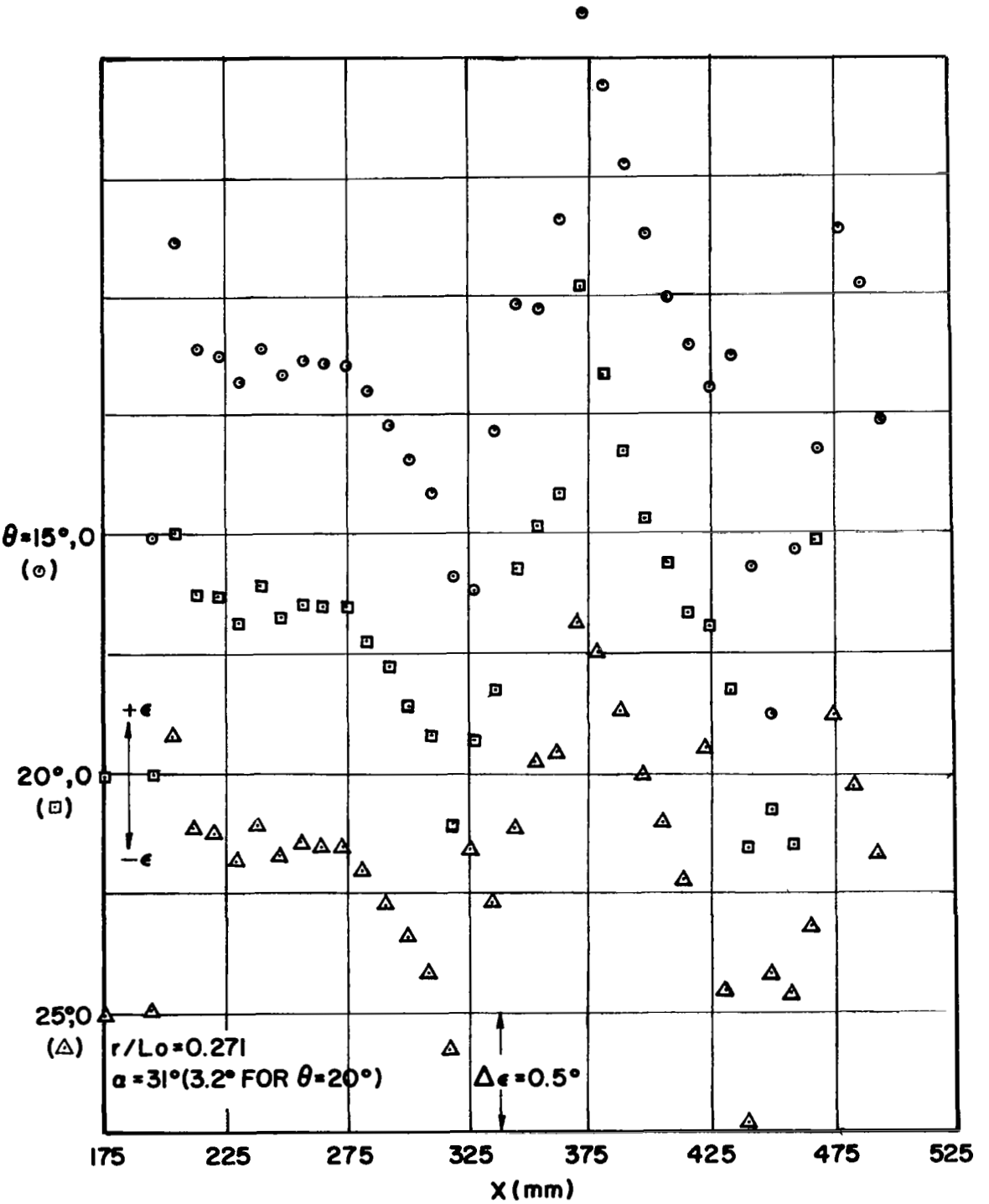

Fig. 20b Continued

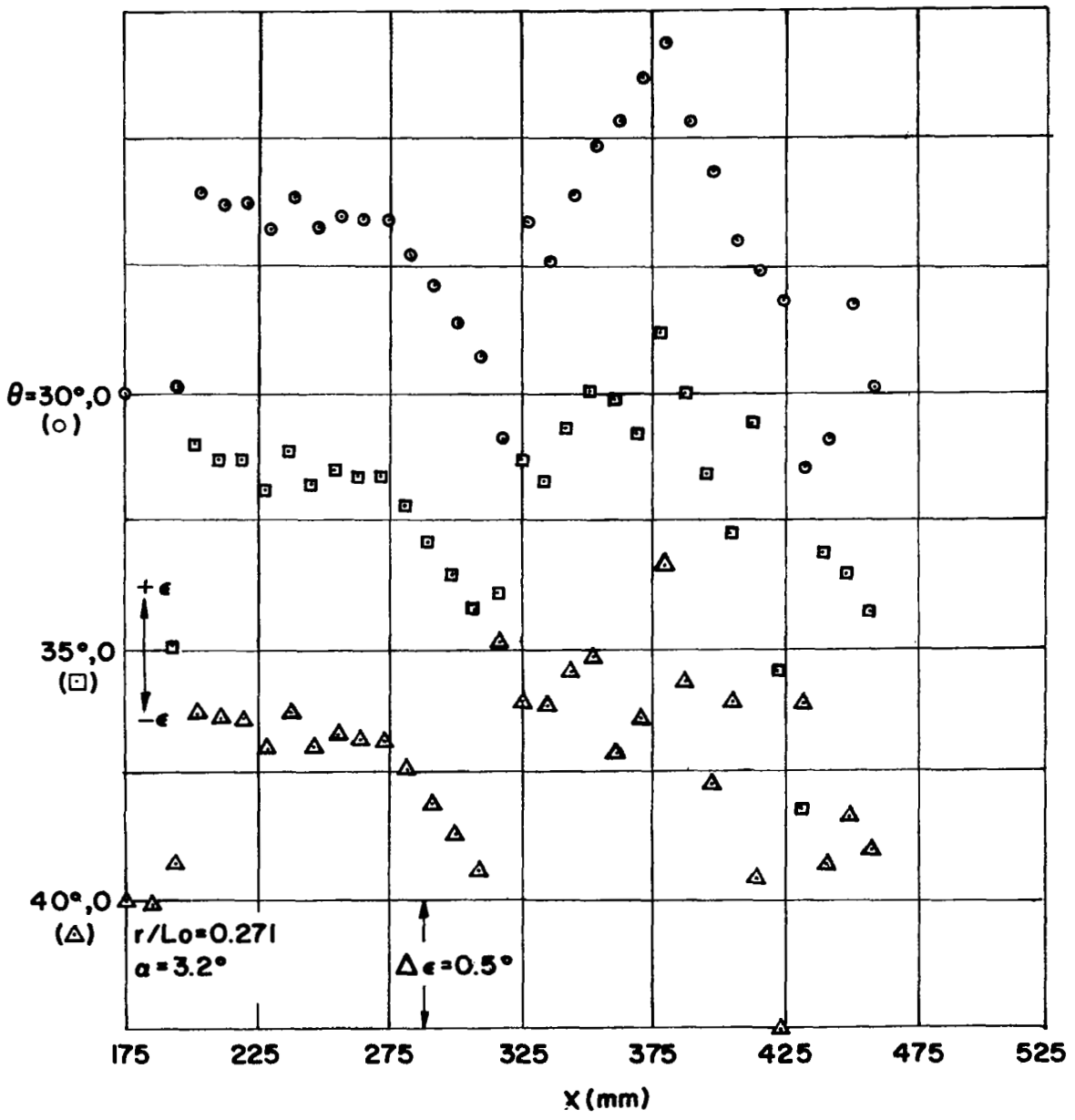

Fig. 20c Continued

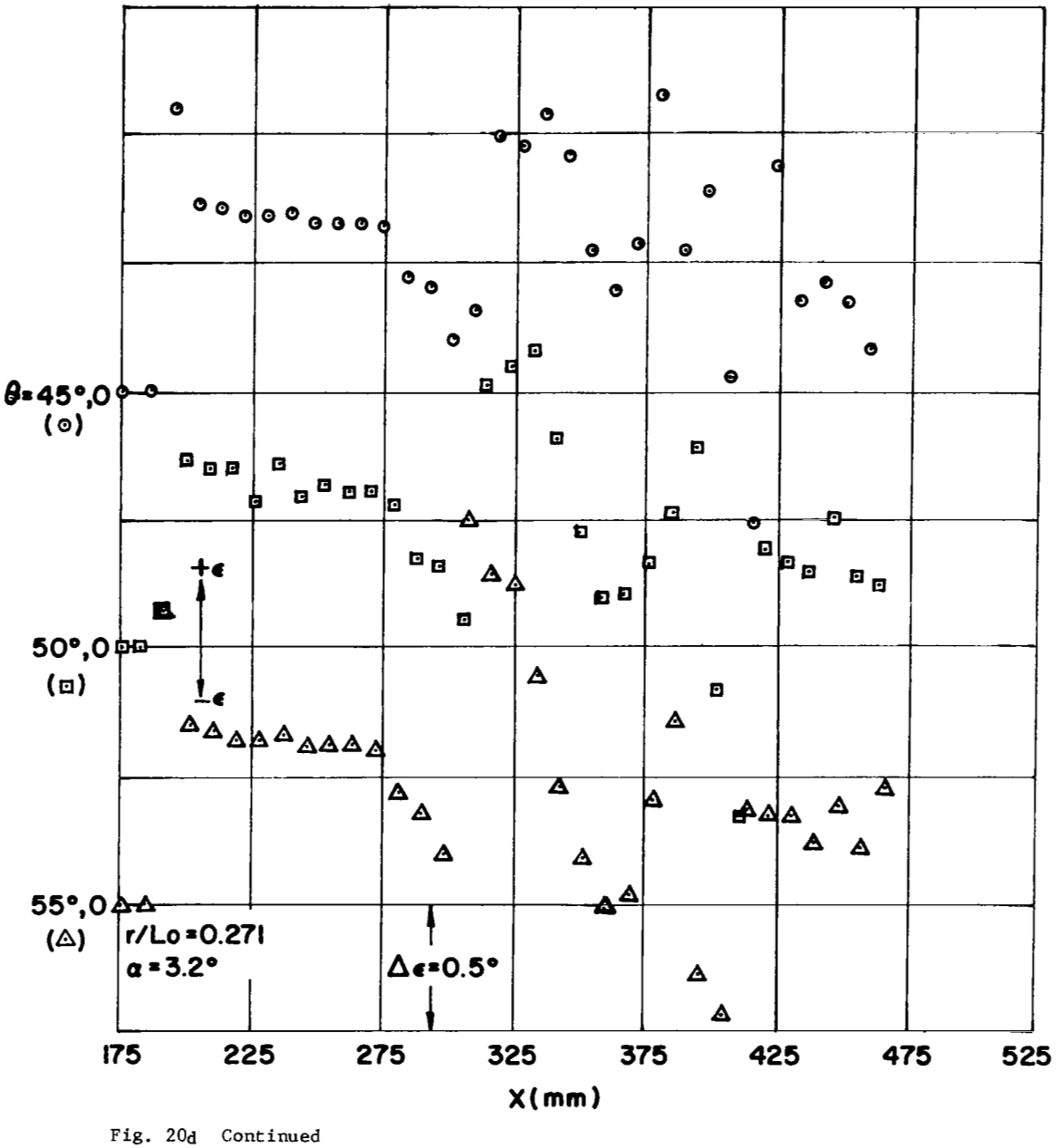

Fig. 20d Continued

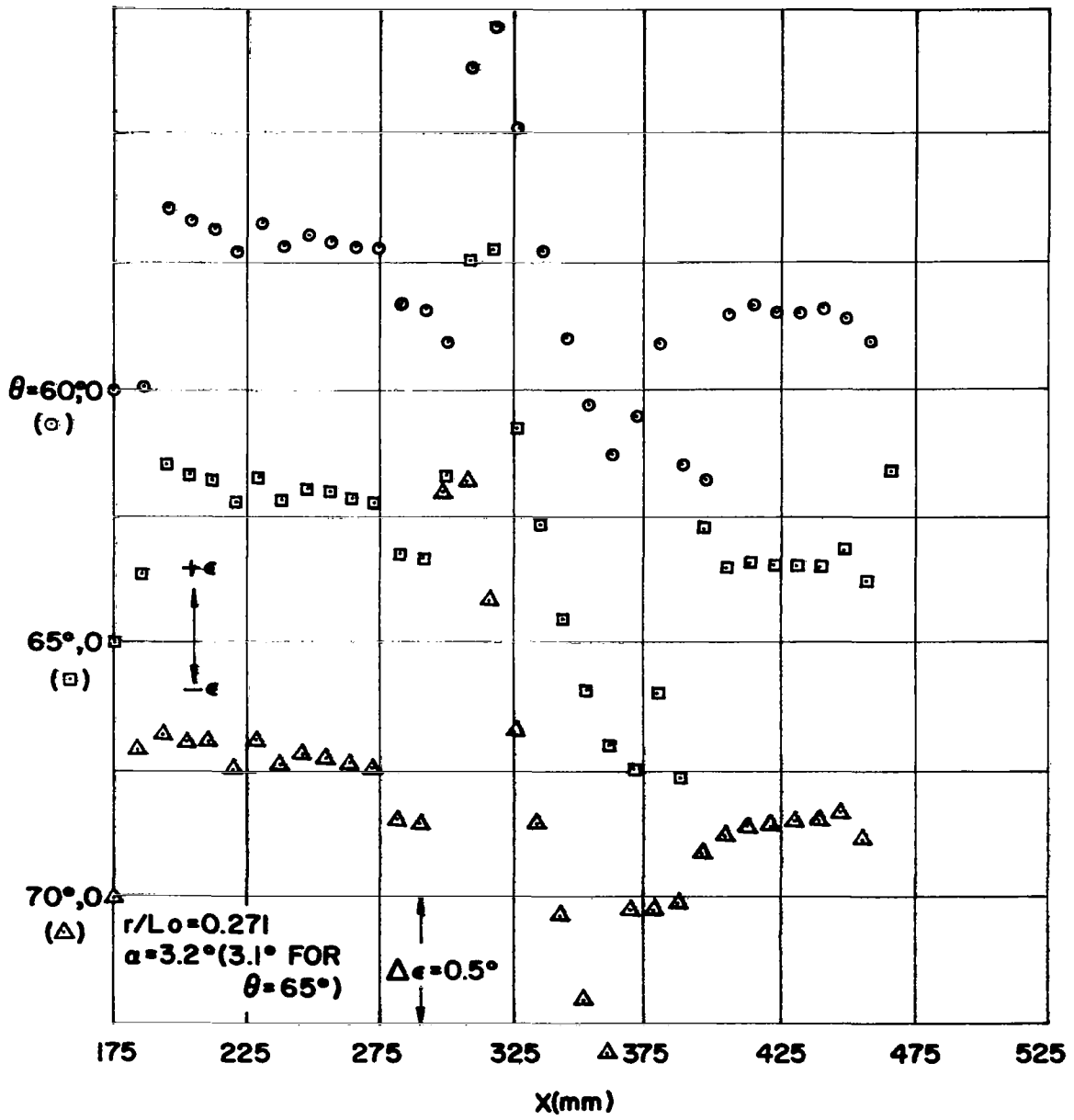

Fig. 20e Continued

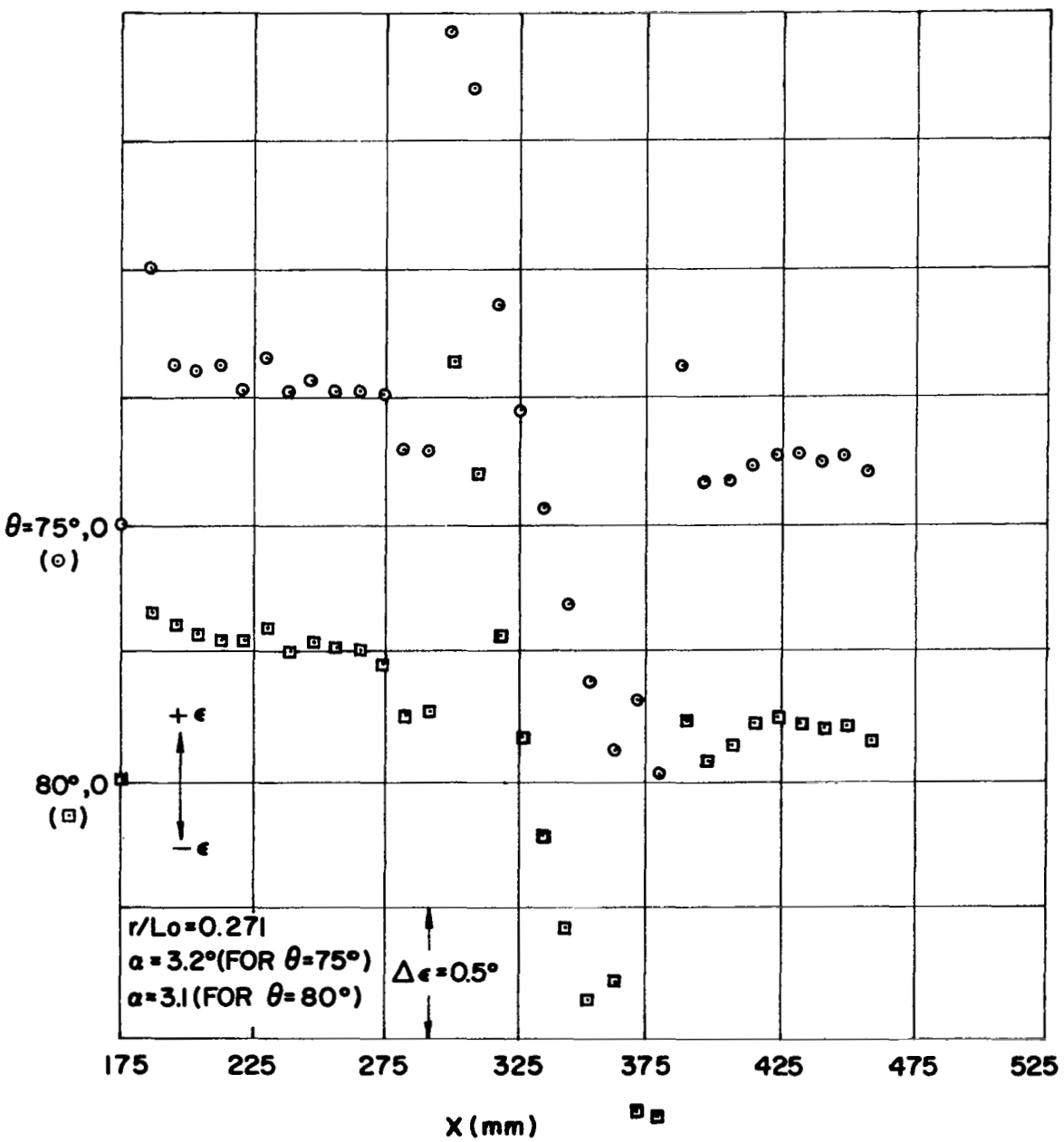

Fig. 20f Continued

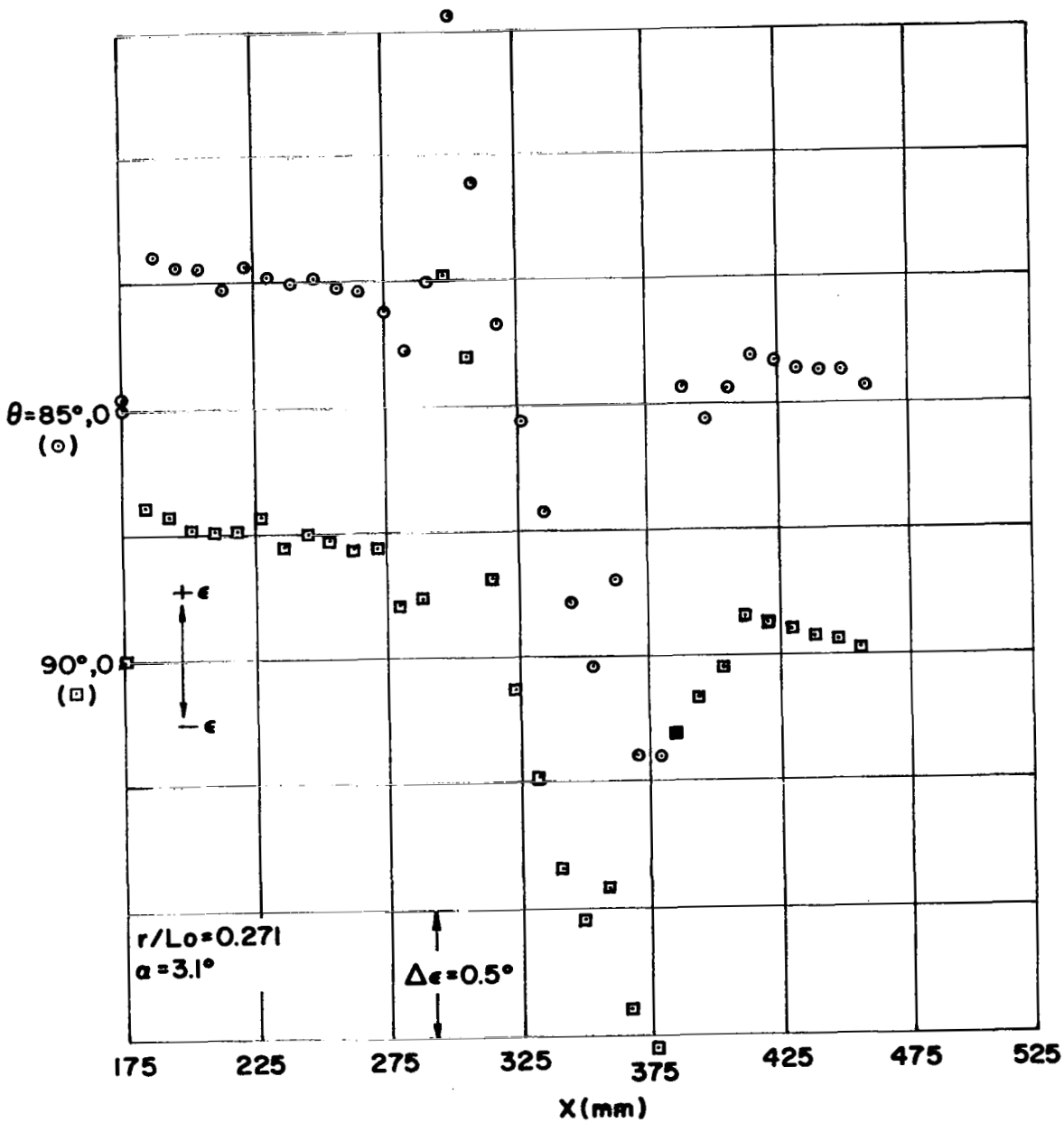

Fig. 20g Continued

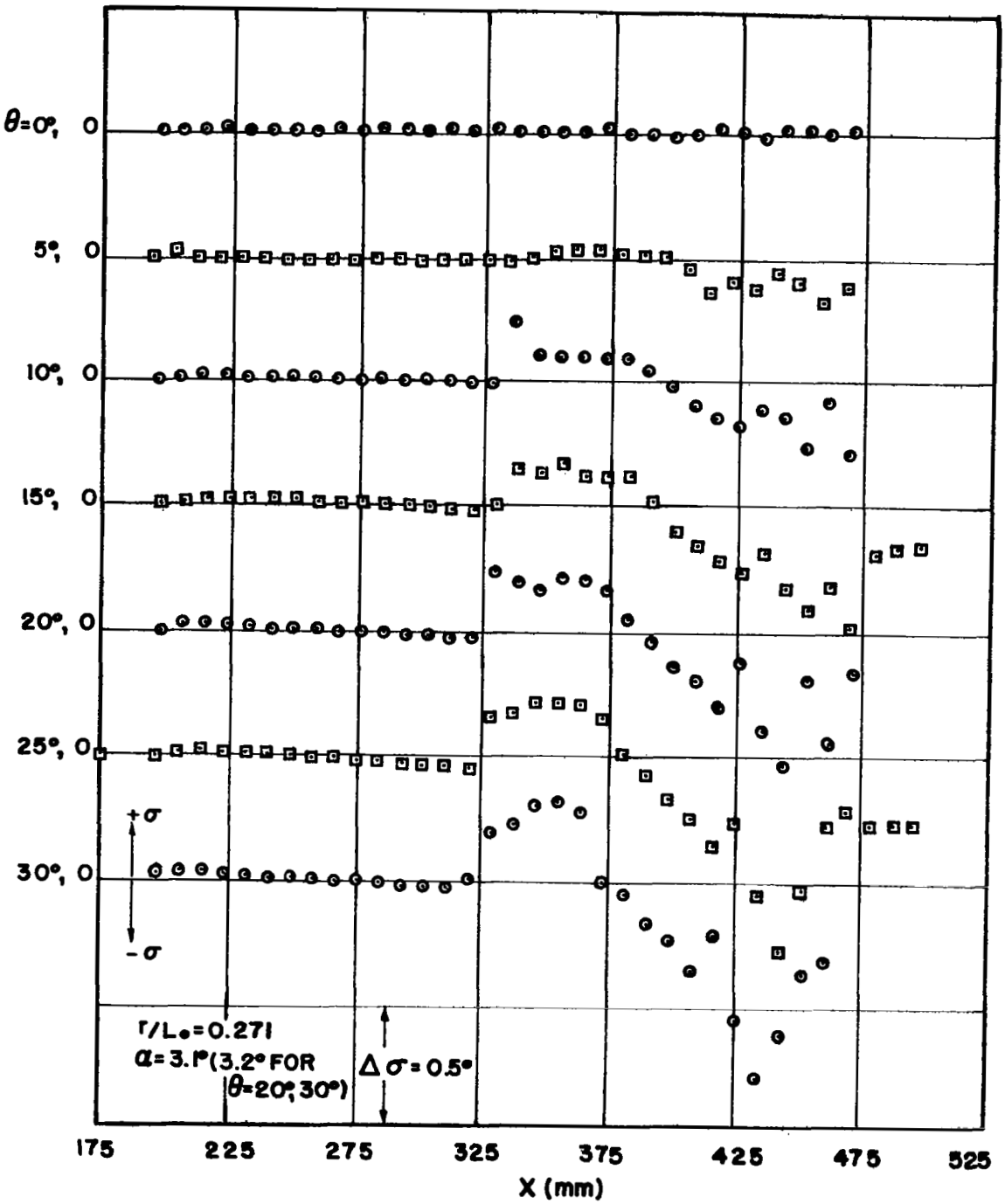

Fig.21a Experimental values of σ as function of distance at several meridian planes

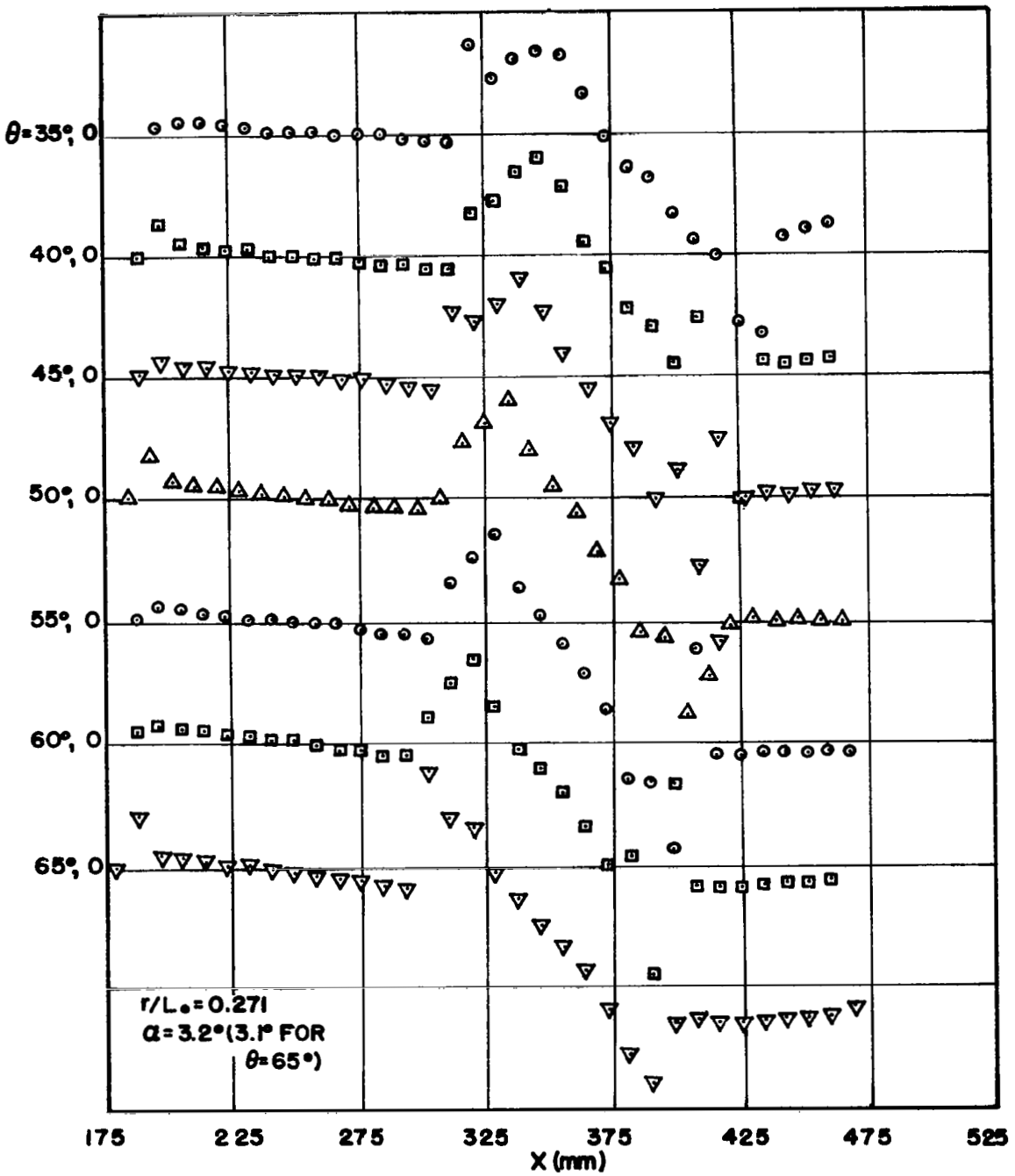

Fig. 21b Continued

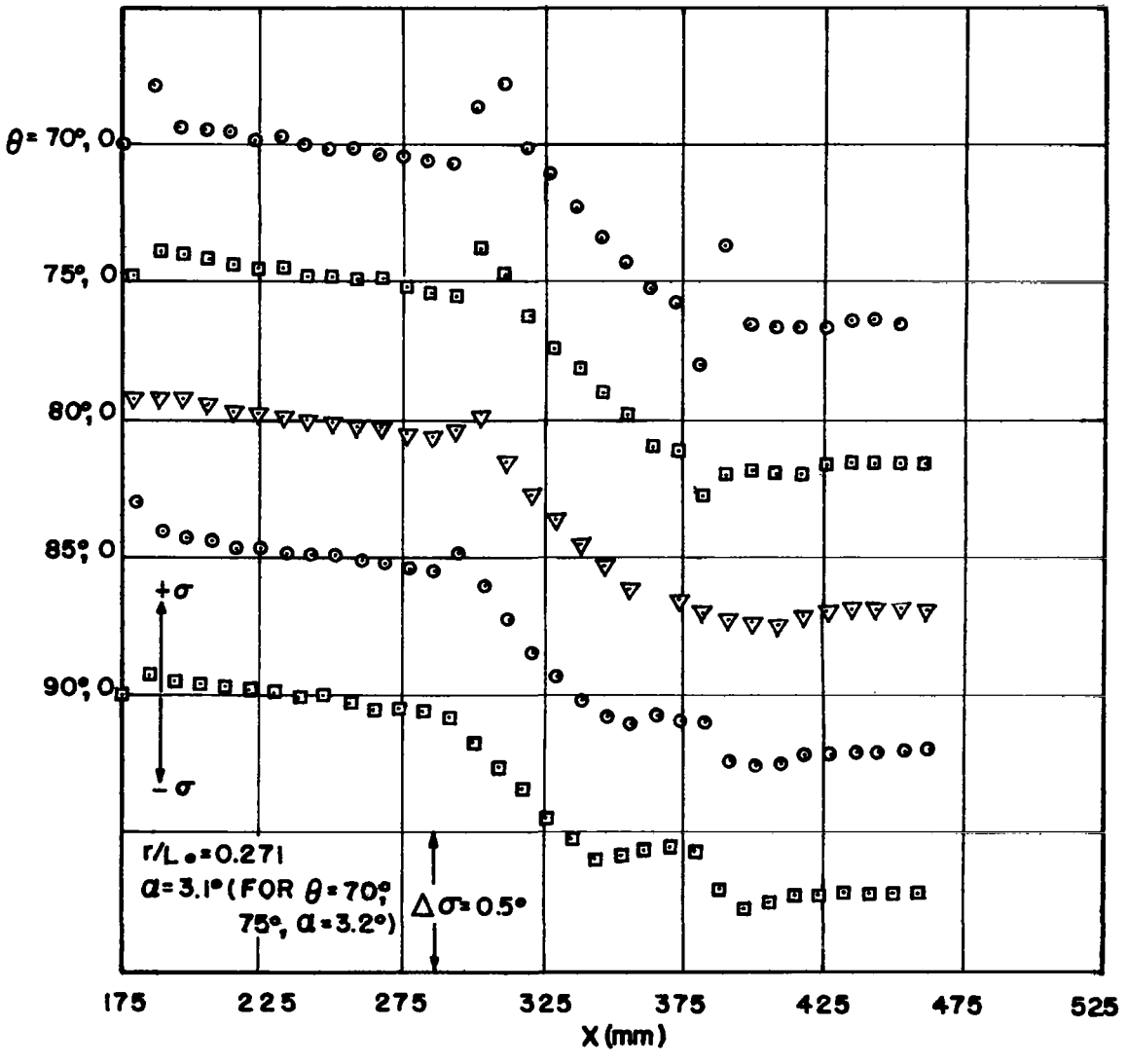

Fig. 21c Continued

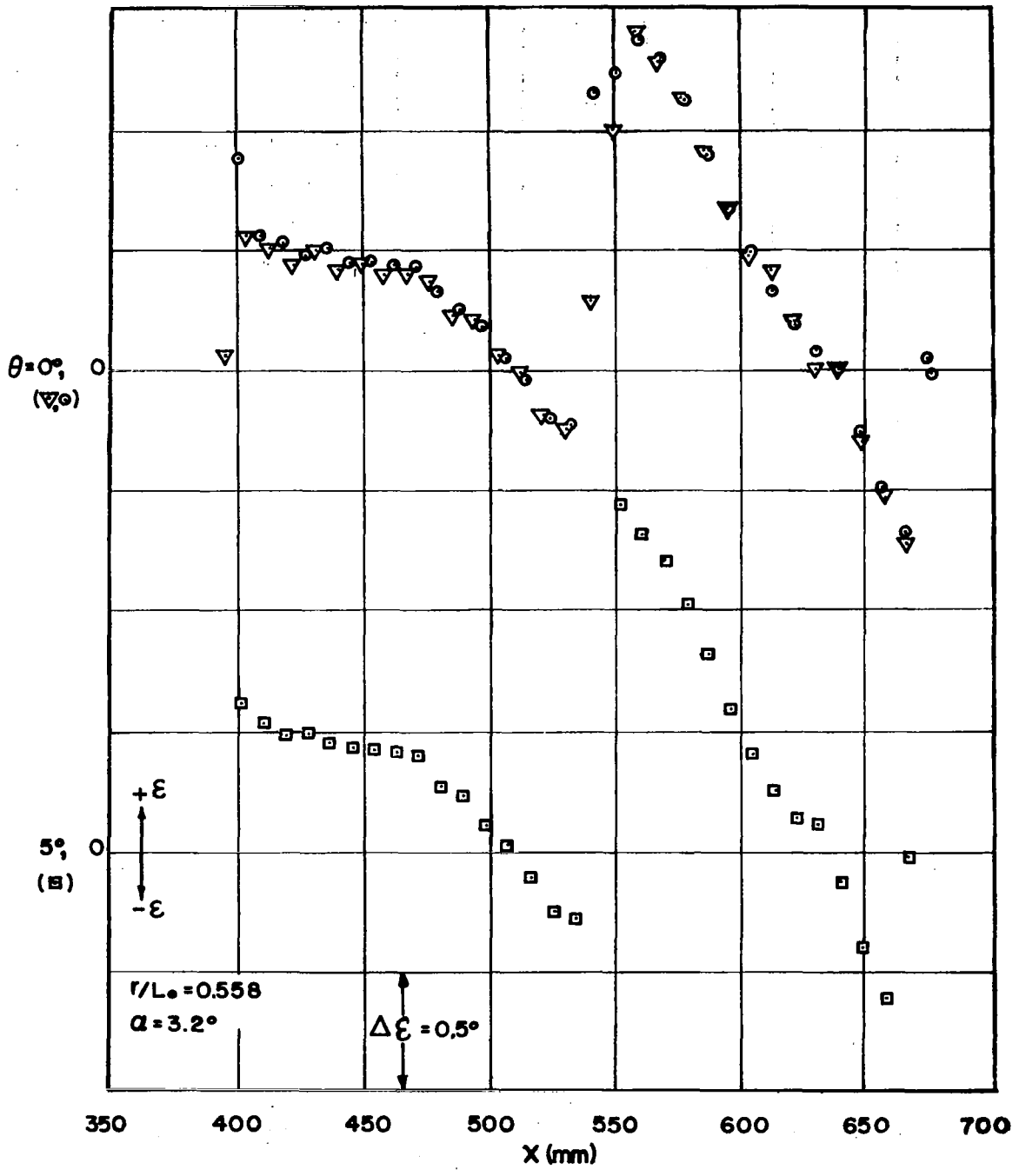

Fig. 22a Experimental values of ε as function of distance at several meridian planes

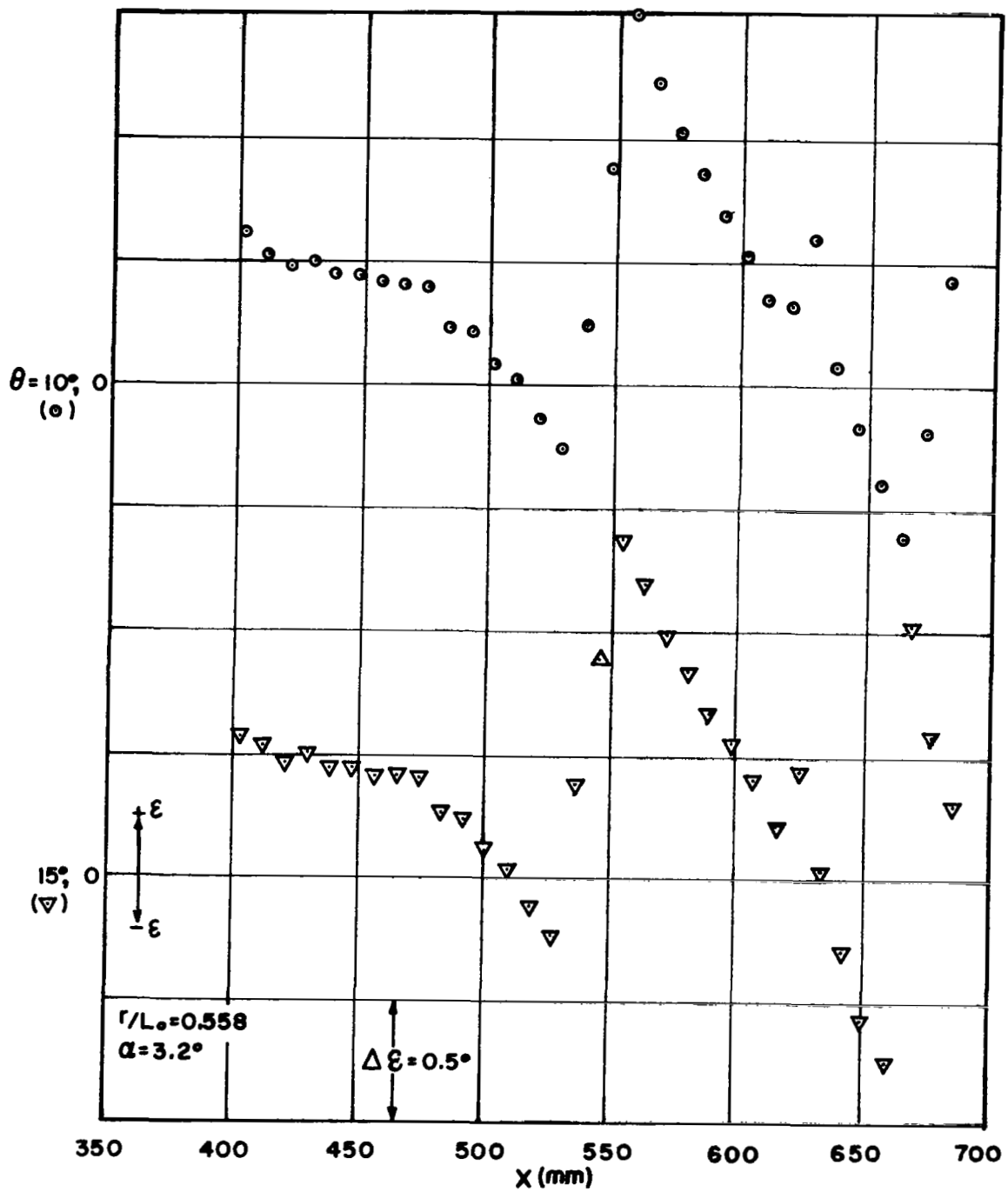

Fig. 22b Continued

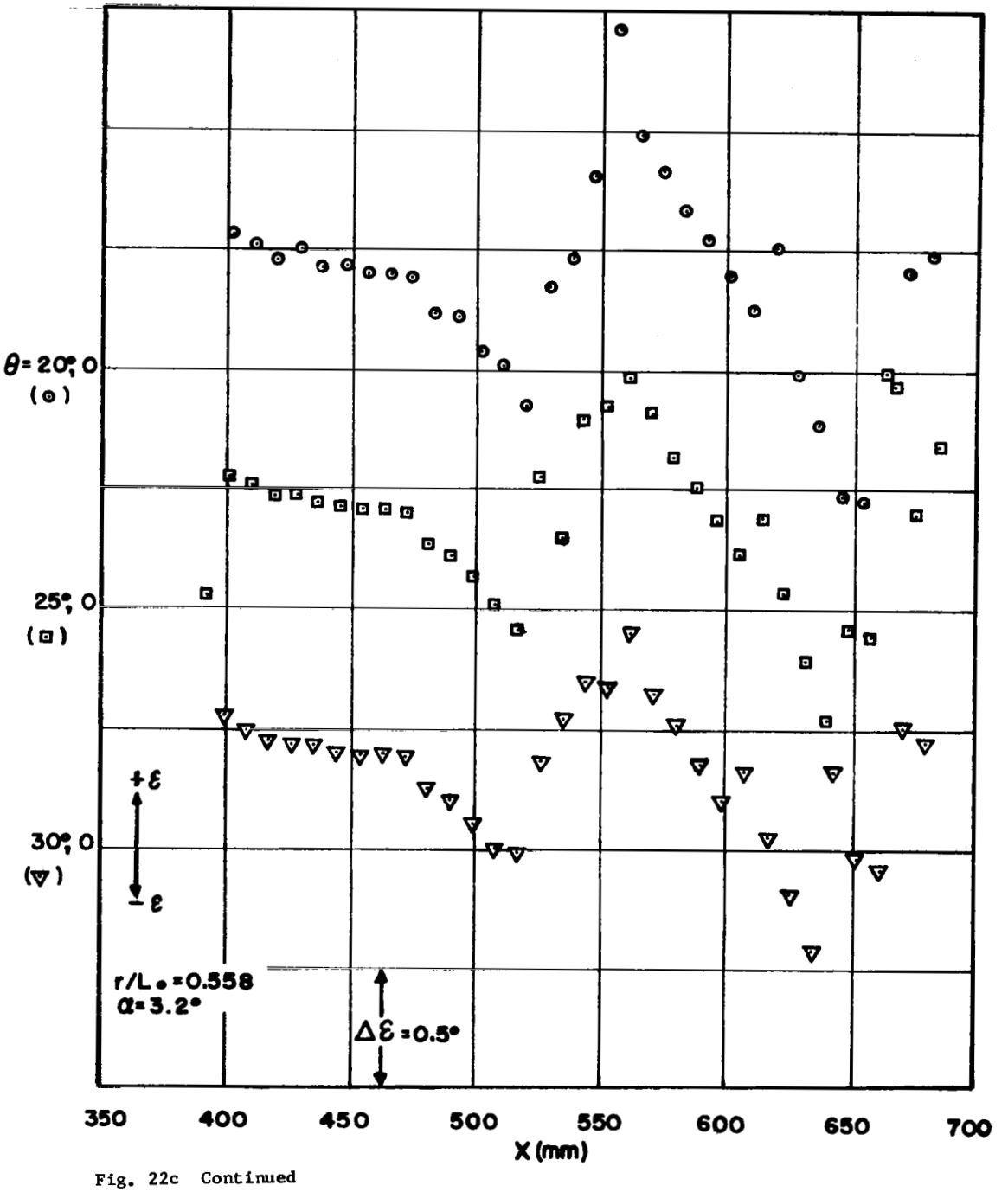

Fig. 22c Continued

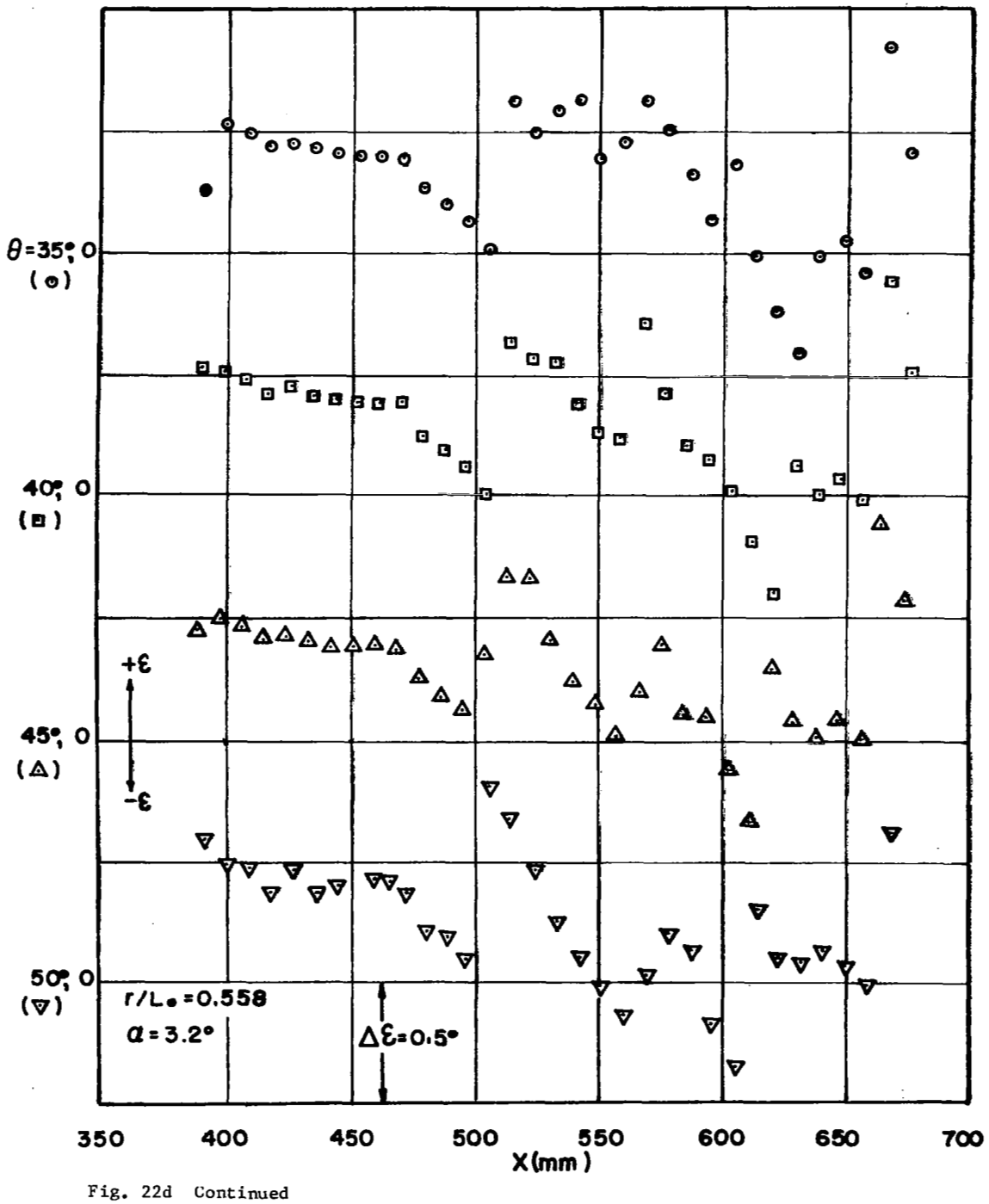

Fig. 22d Continued

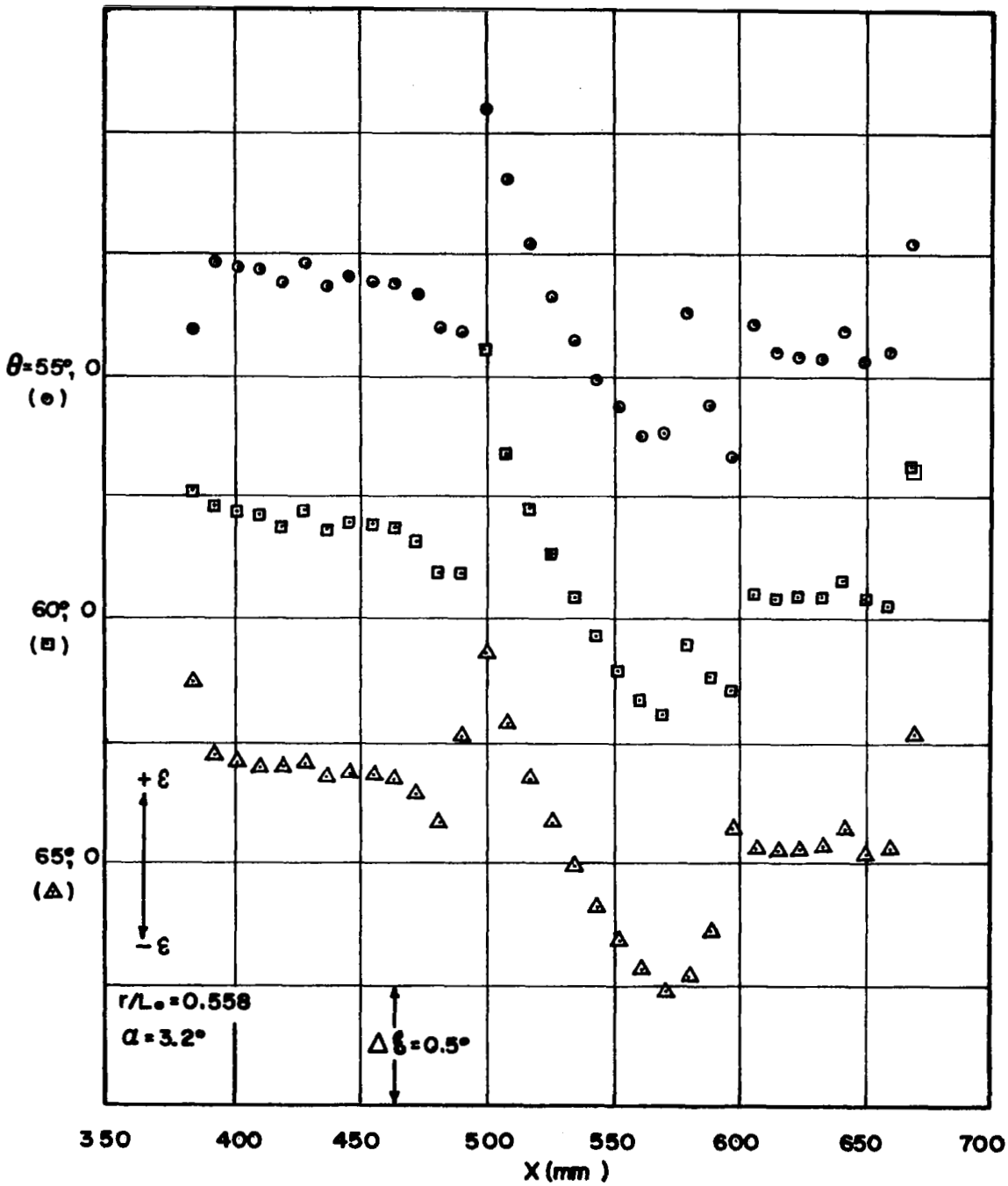

Fig. 22e Continued

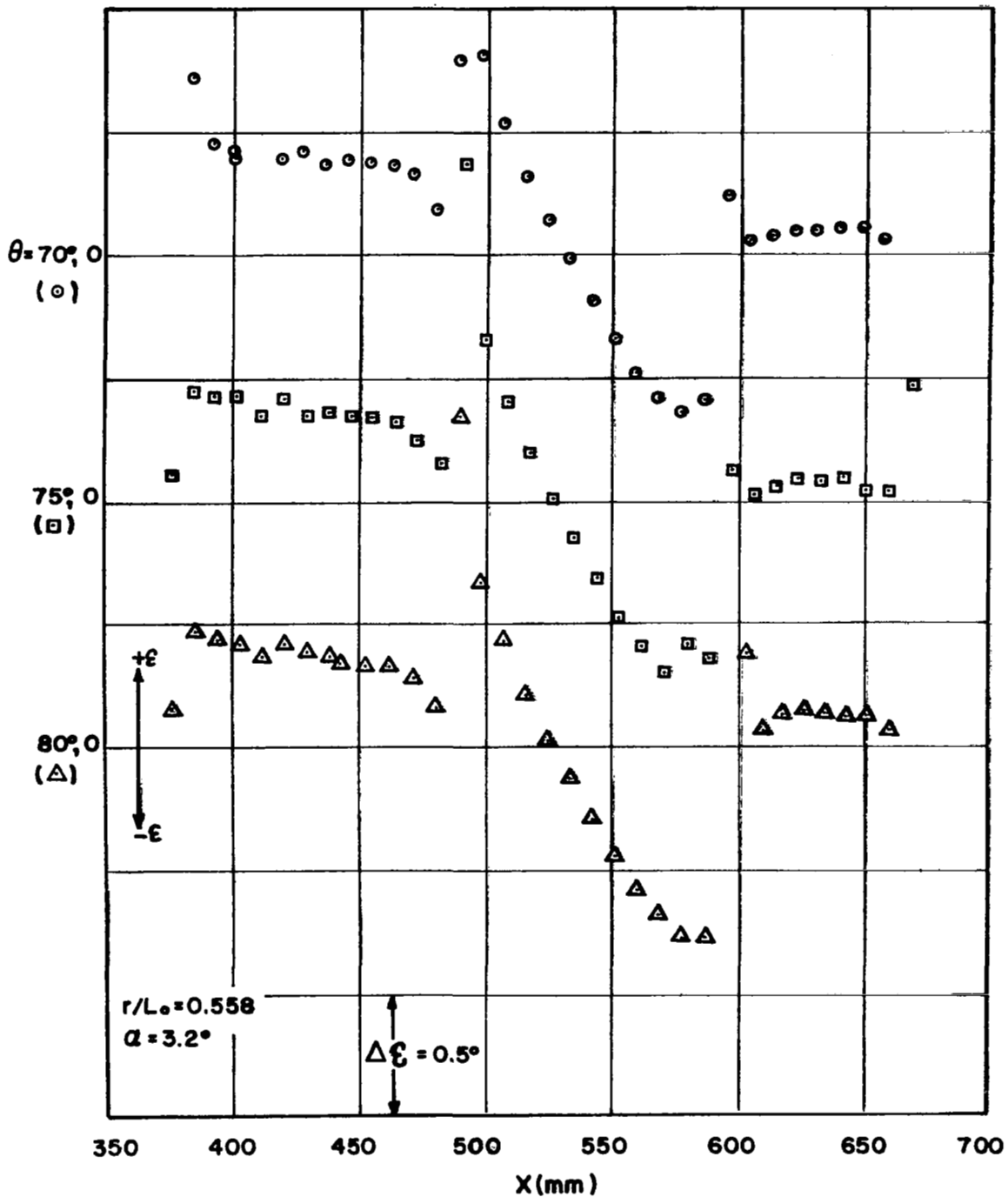

Fig. 22f Continued

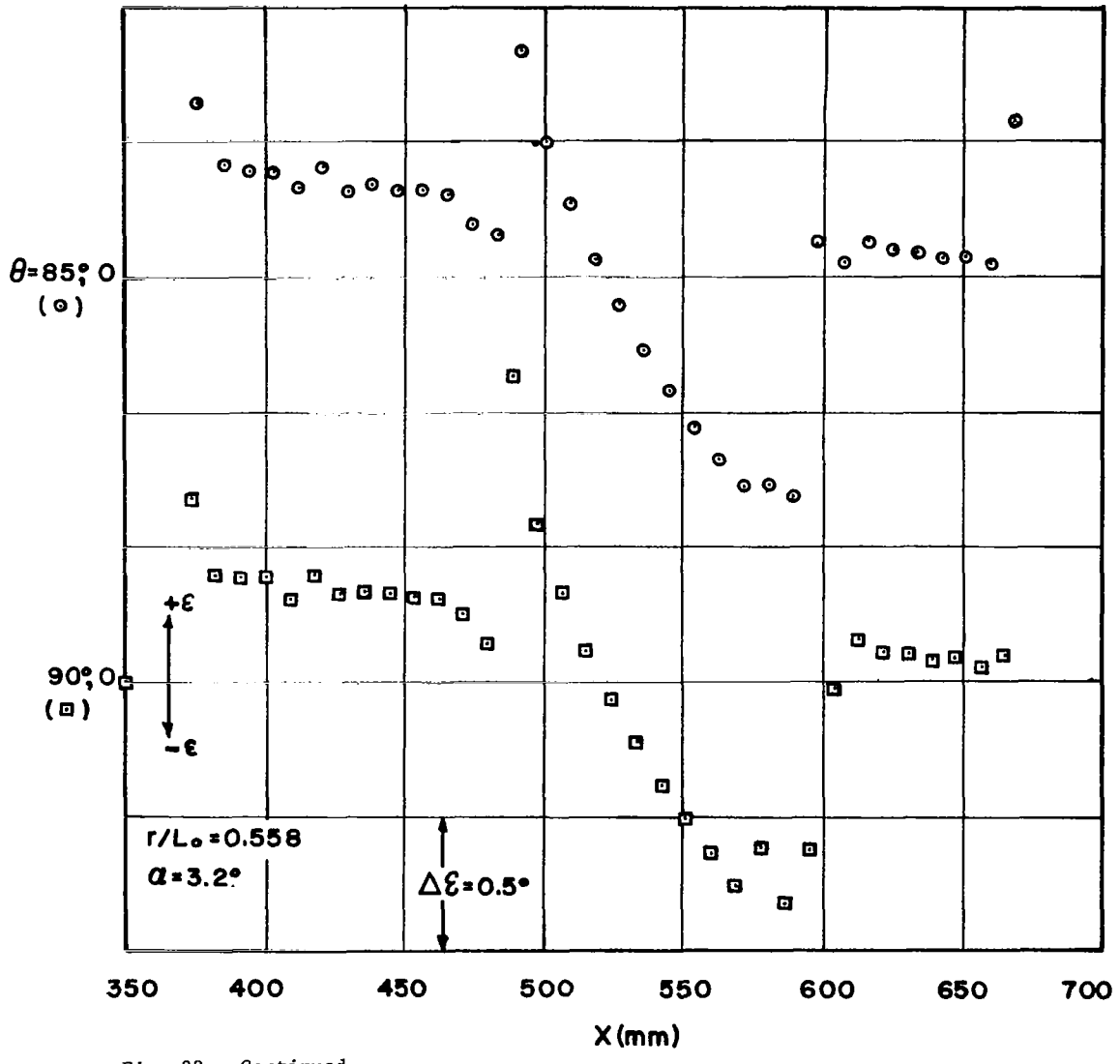

Fig. 22g Continued

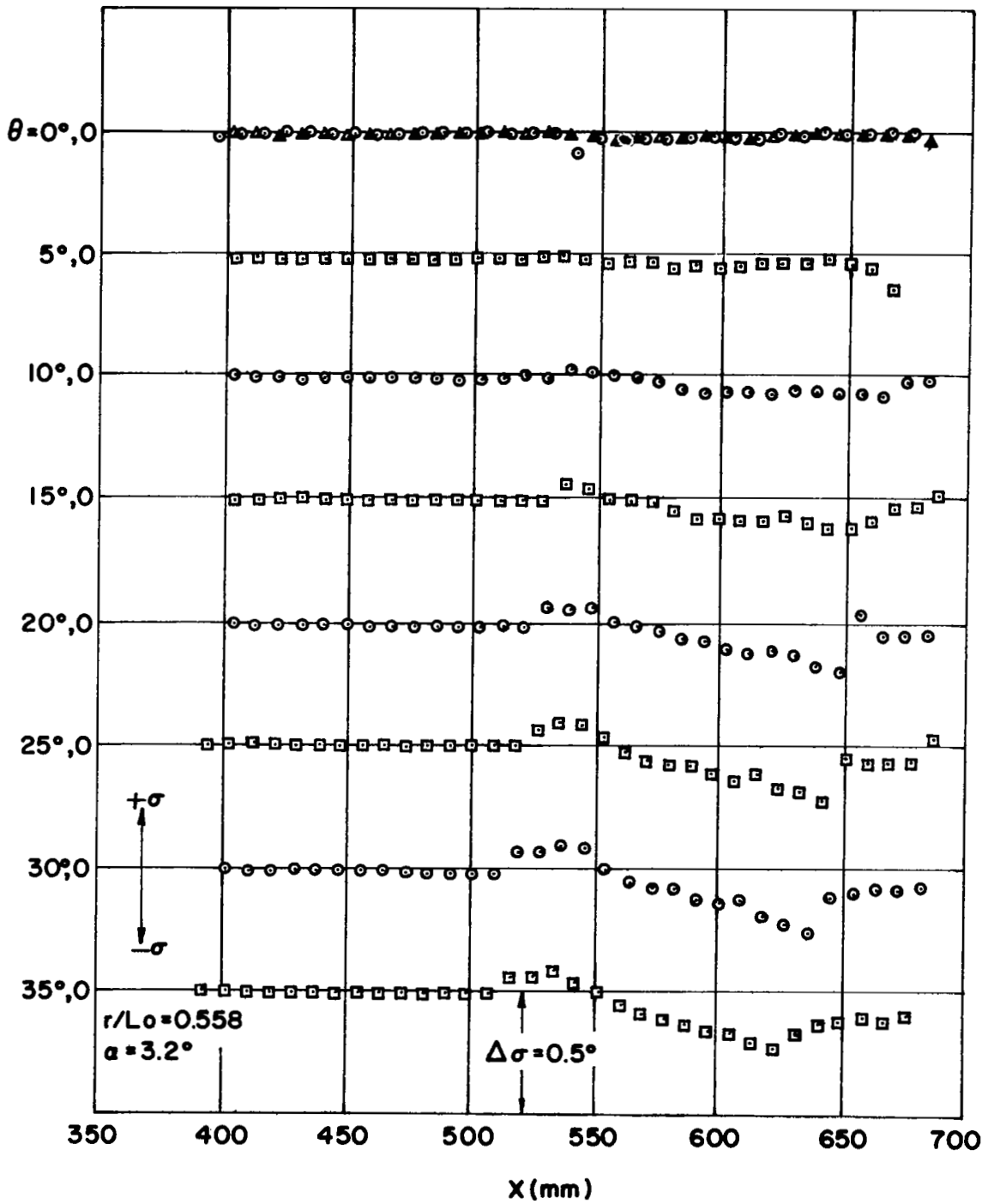

Fig. 23a Experimental values of σ as function of distance at several meridian planes , $\alpha = 3.2^{o}$, $r/L_{o} = 0.558$

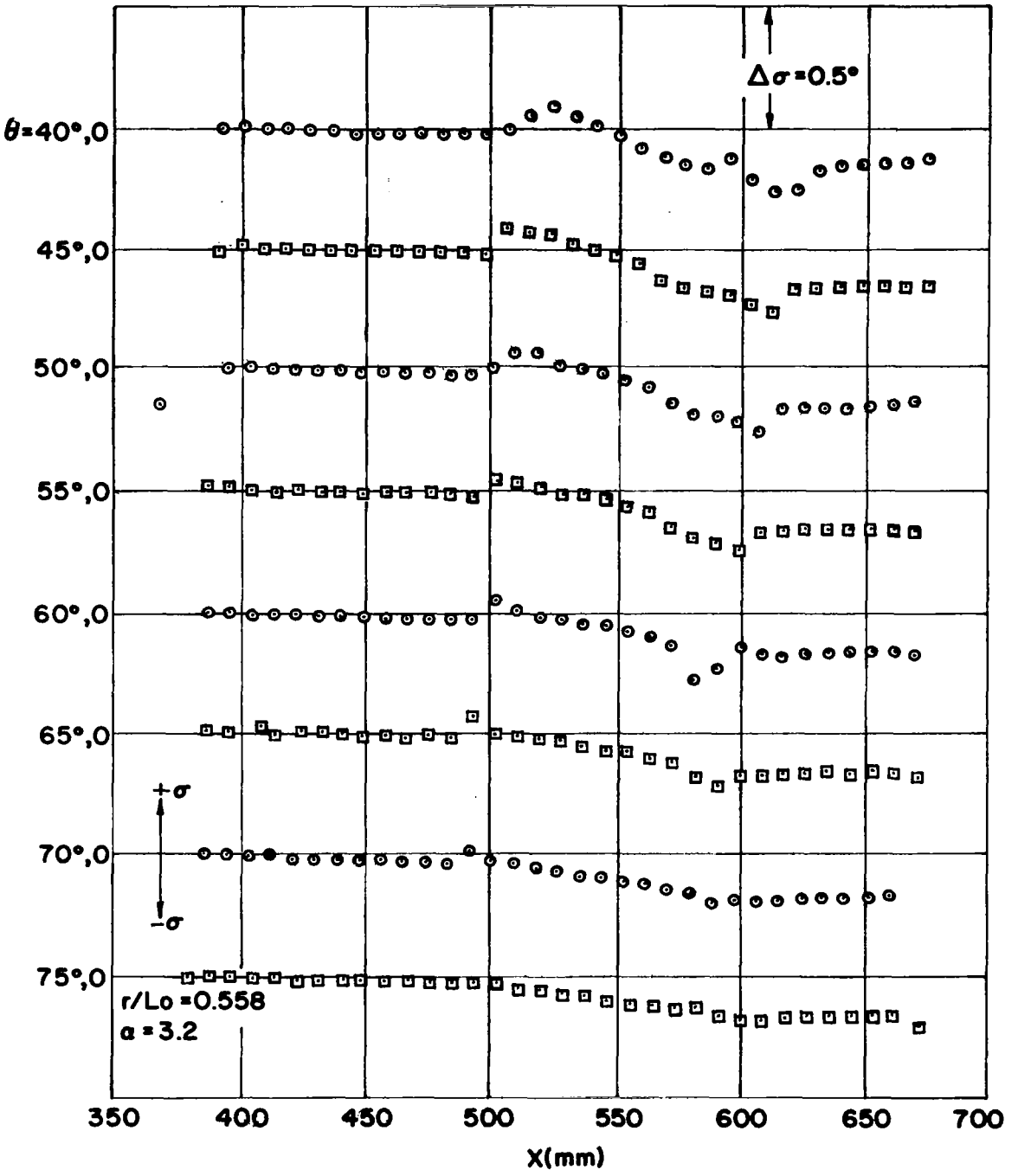

Fig. 23b Continued

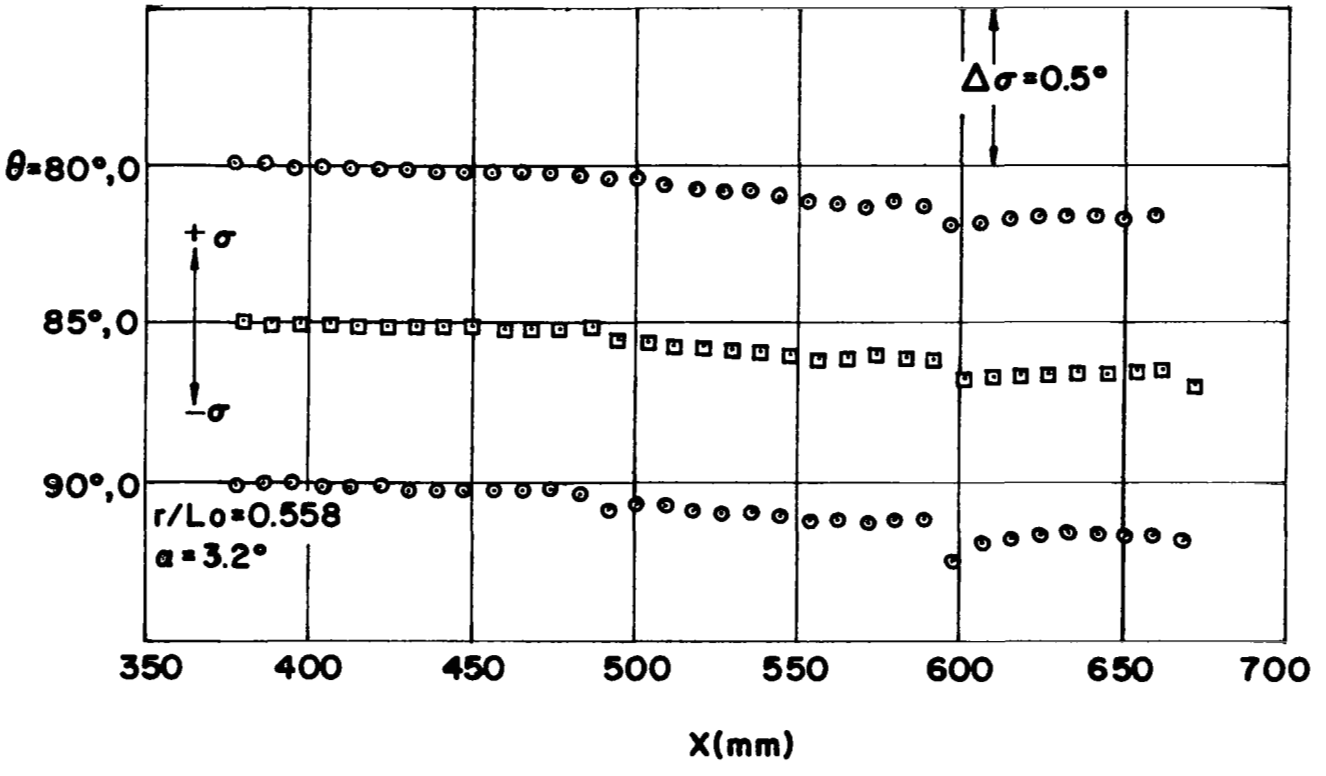

Fig. 23c Continued

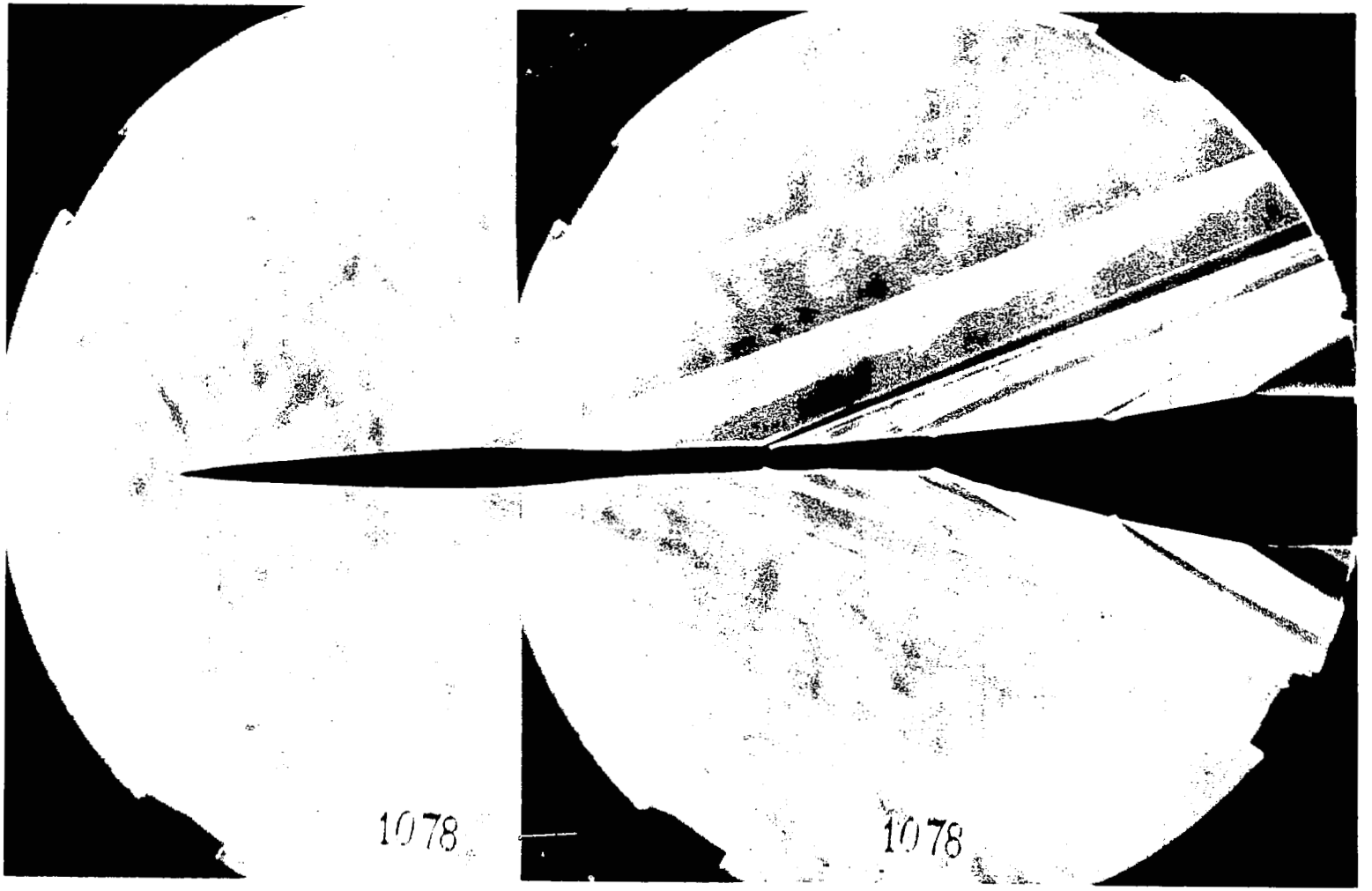

Fig. 24a Schlieren Photographs at $\alpha = 2.6^{\circ}$, $\theta = 0^{\circ}$

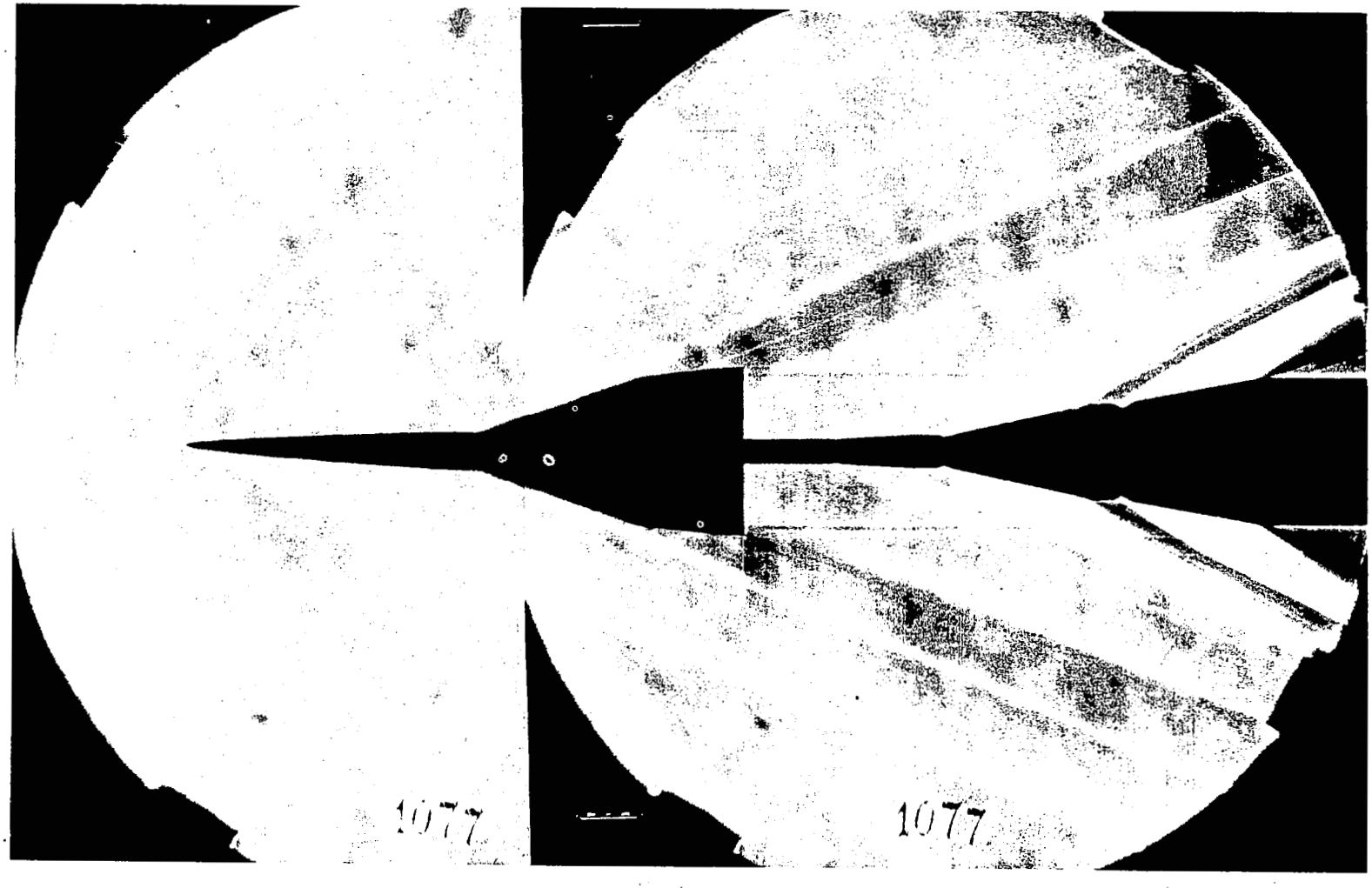

Fig. 24b Schlieren photographs at $\alpha = 2.6^{o}$, $\theta = 90^{o}$

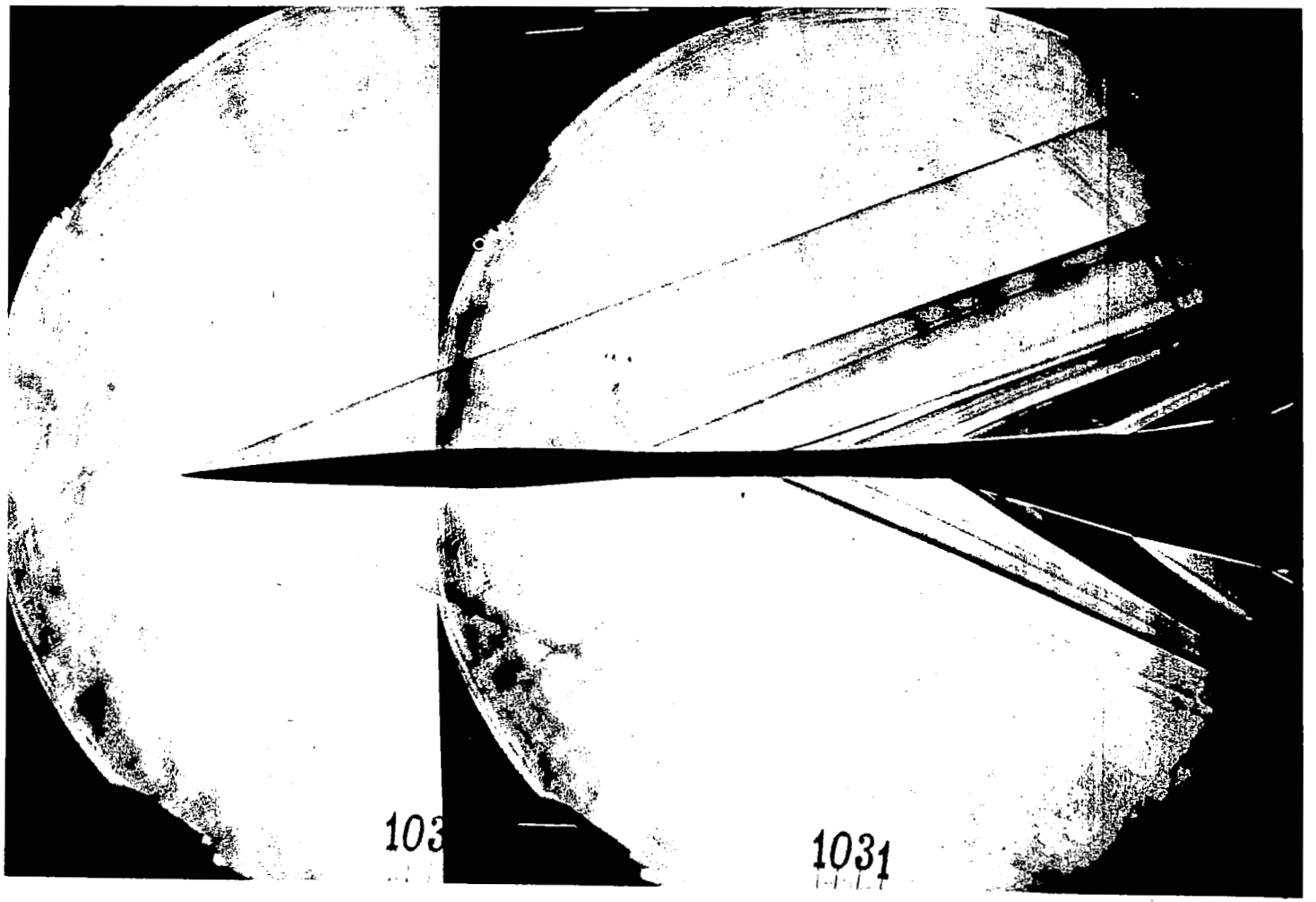

Fig. 25a Schlieren Photographs at $\alpha = 3.2^{\circ}$, $\theta = 0^{\circ}$

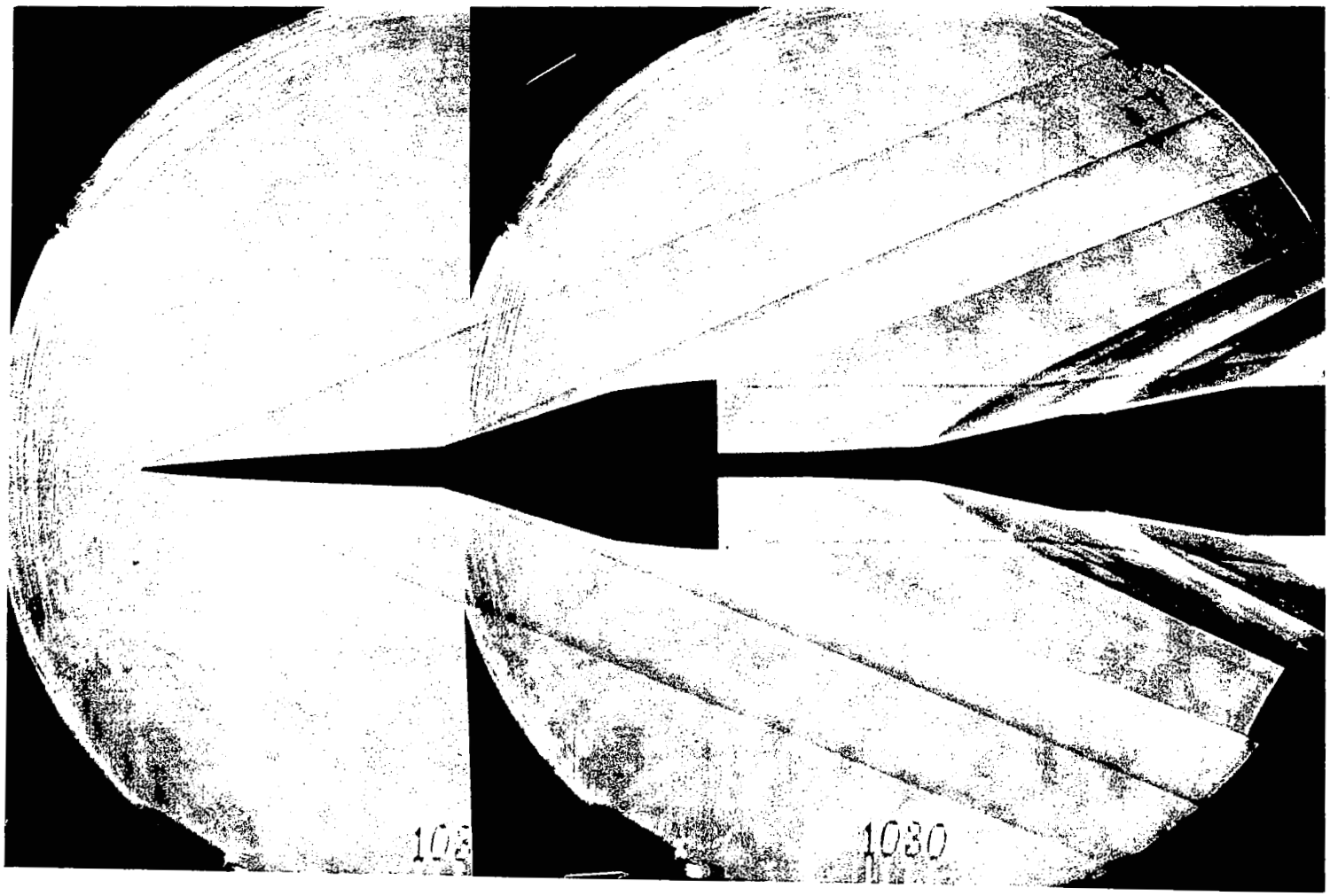

Fig. 25b Schlieren photographs $\alpha = 3.2^{\circ}$, $\theta = 90^{\circ}$

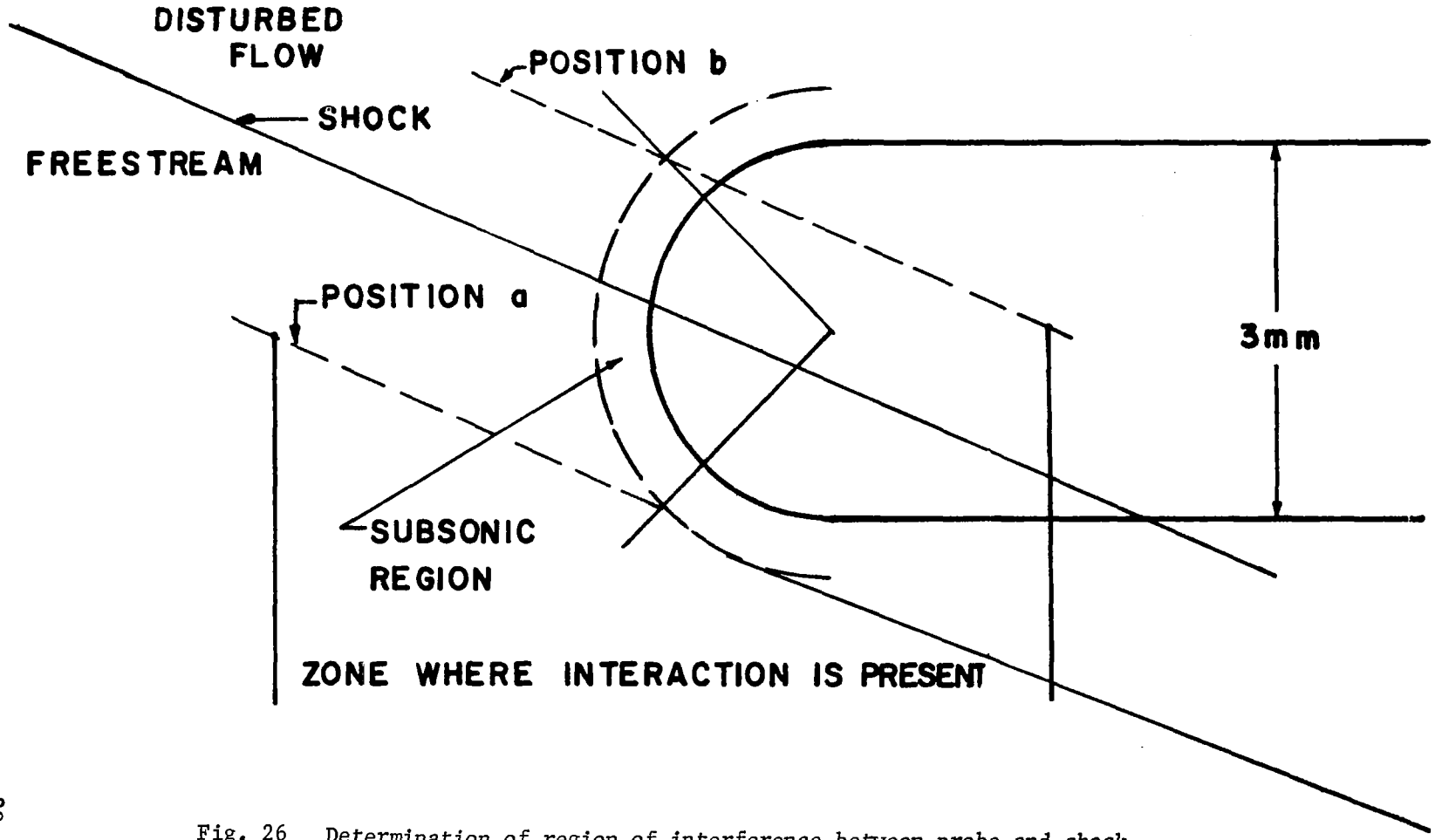

Fig. 26 Determination of region of interference between probe and shock

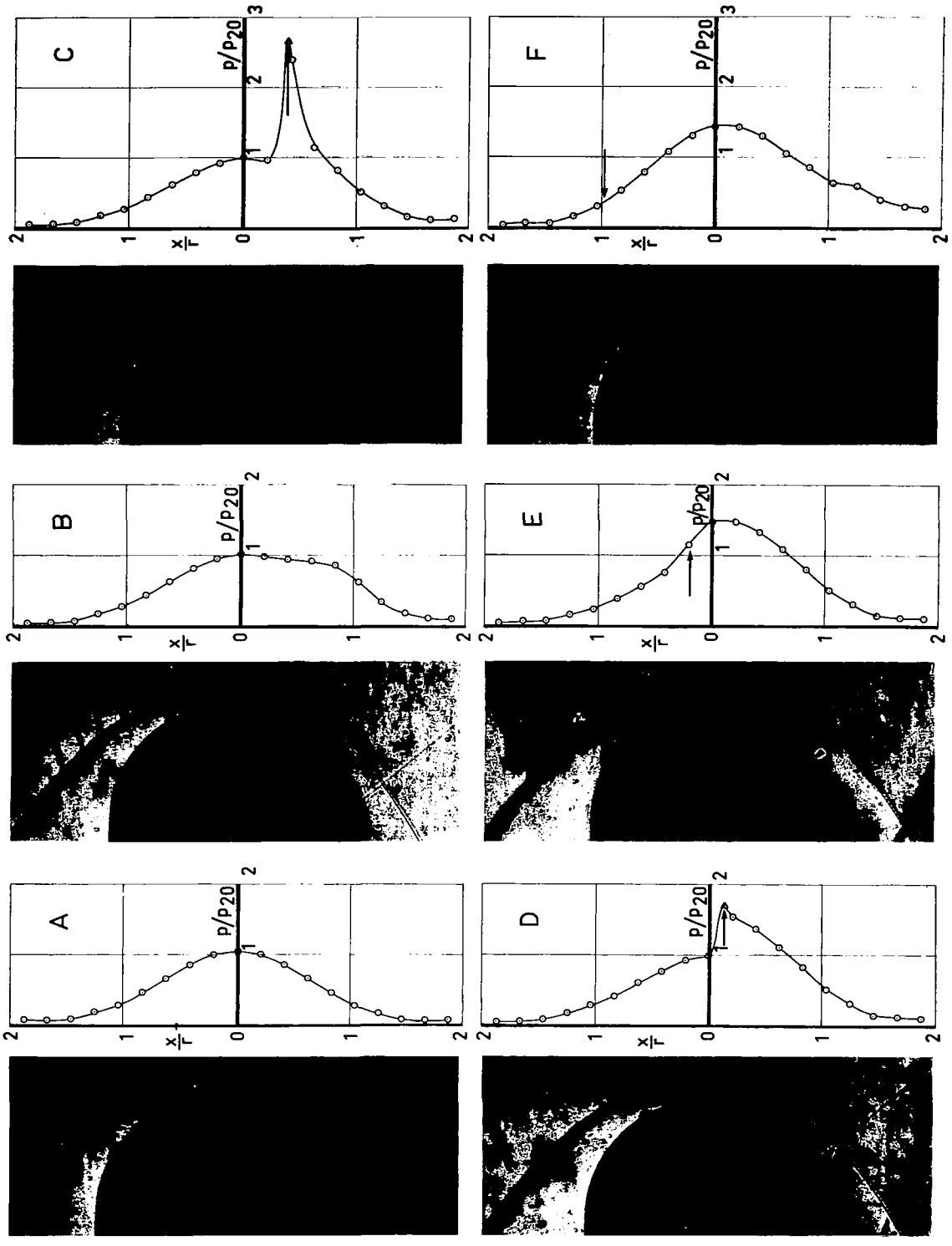

Fig. 27 Pressure distribution on a hemisphere, $M_\infty = 4.6$ interacting with a shock that deflects the flow of 5^o. Arrow indicates point at which disturbance meets model surface.

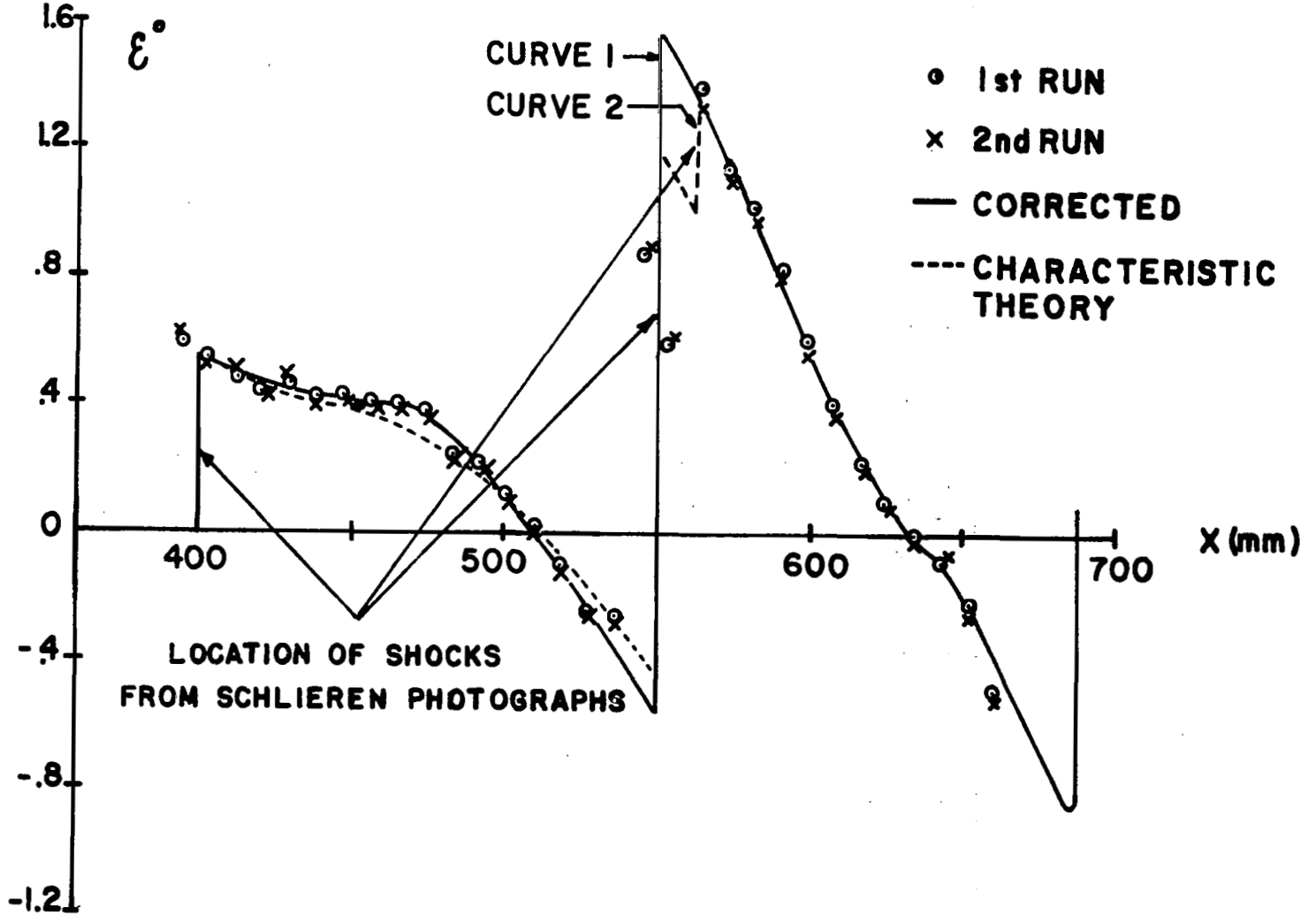

Fig. 28 Distribution of ε at r/L = 0.558, $\alpha = 2.6^{\circ}$, $\theta = 0$

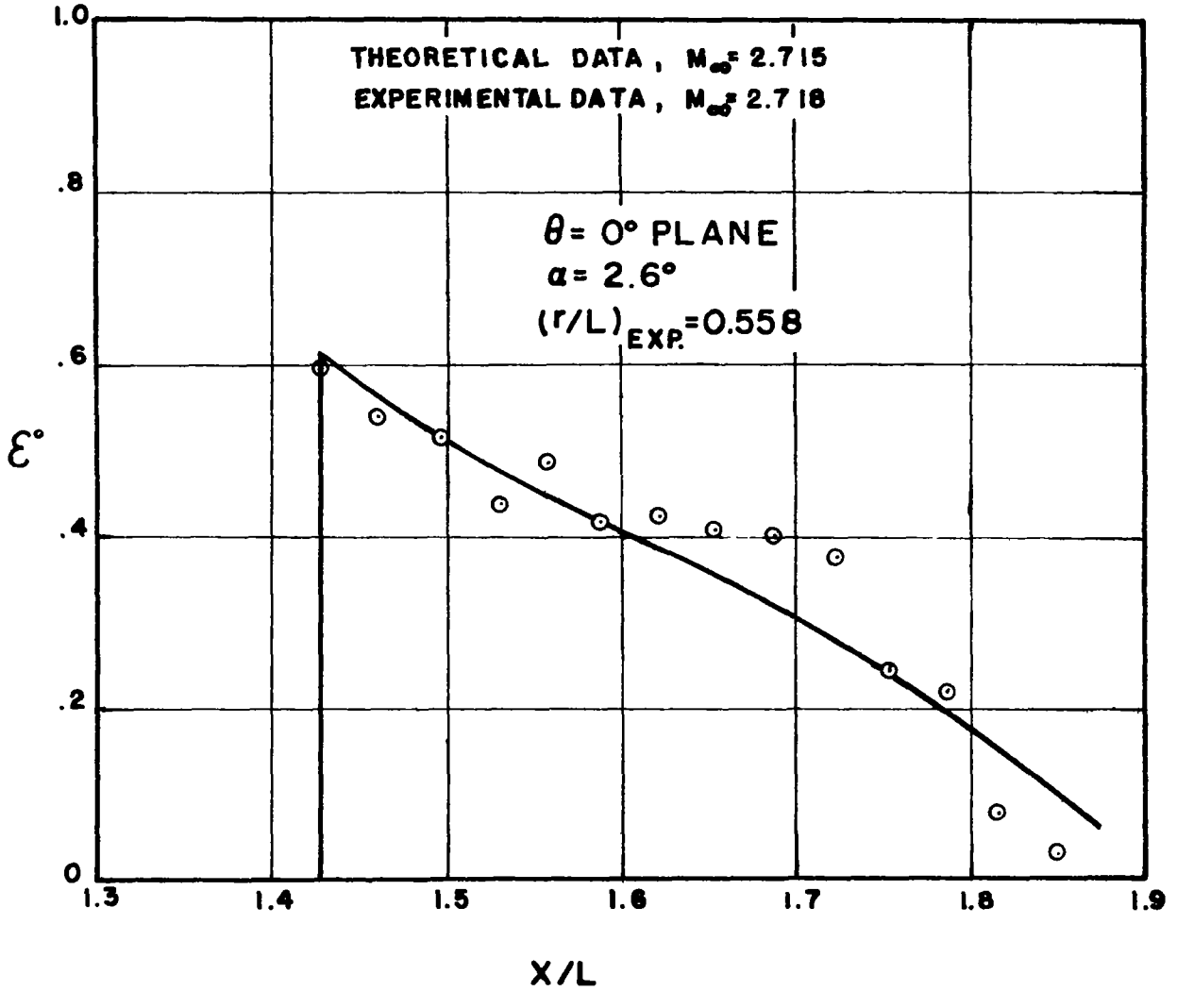

Fig. 29 Comparison between experimental and calculated values

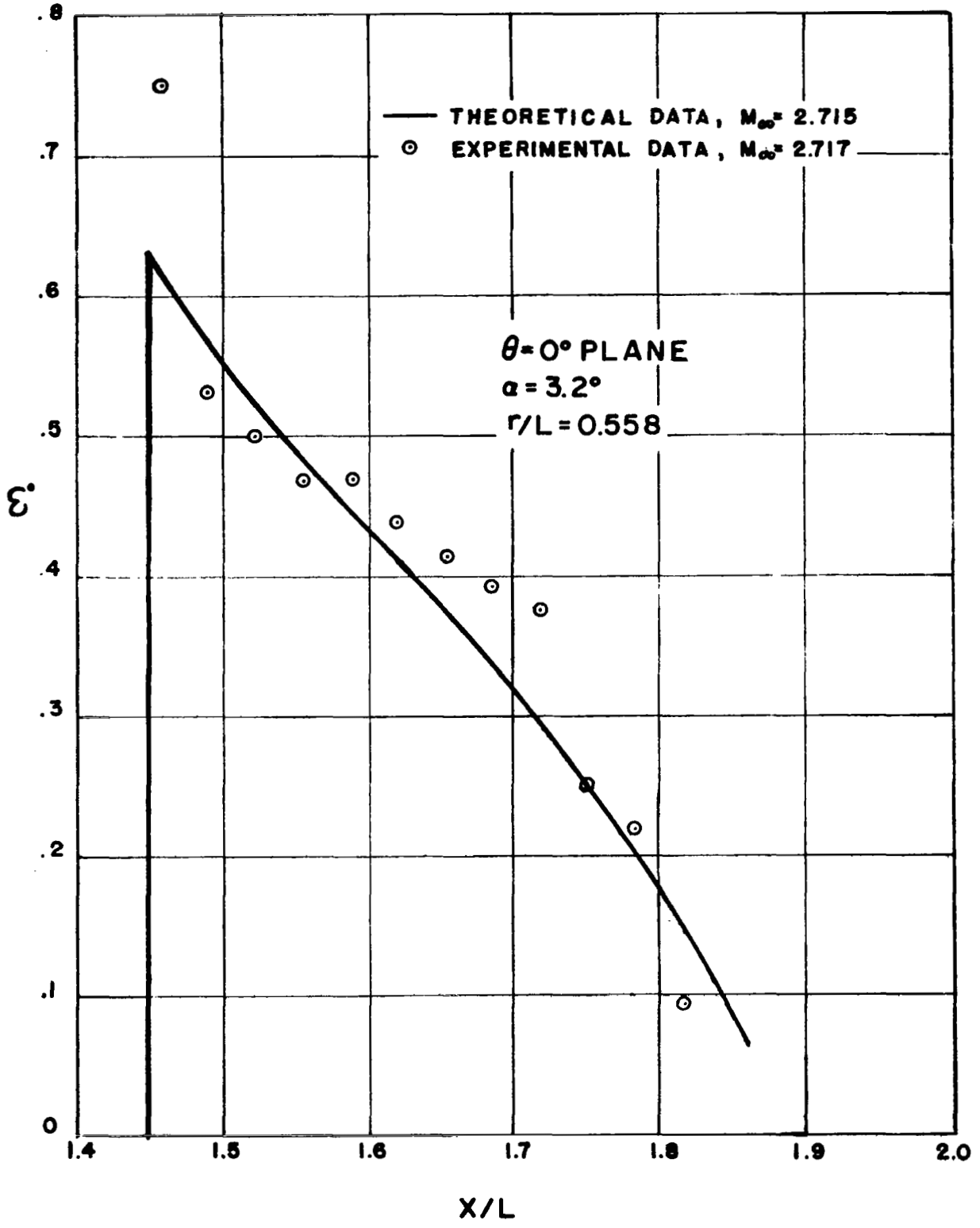

Fig. 30 Comparison between experimental and calculated values

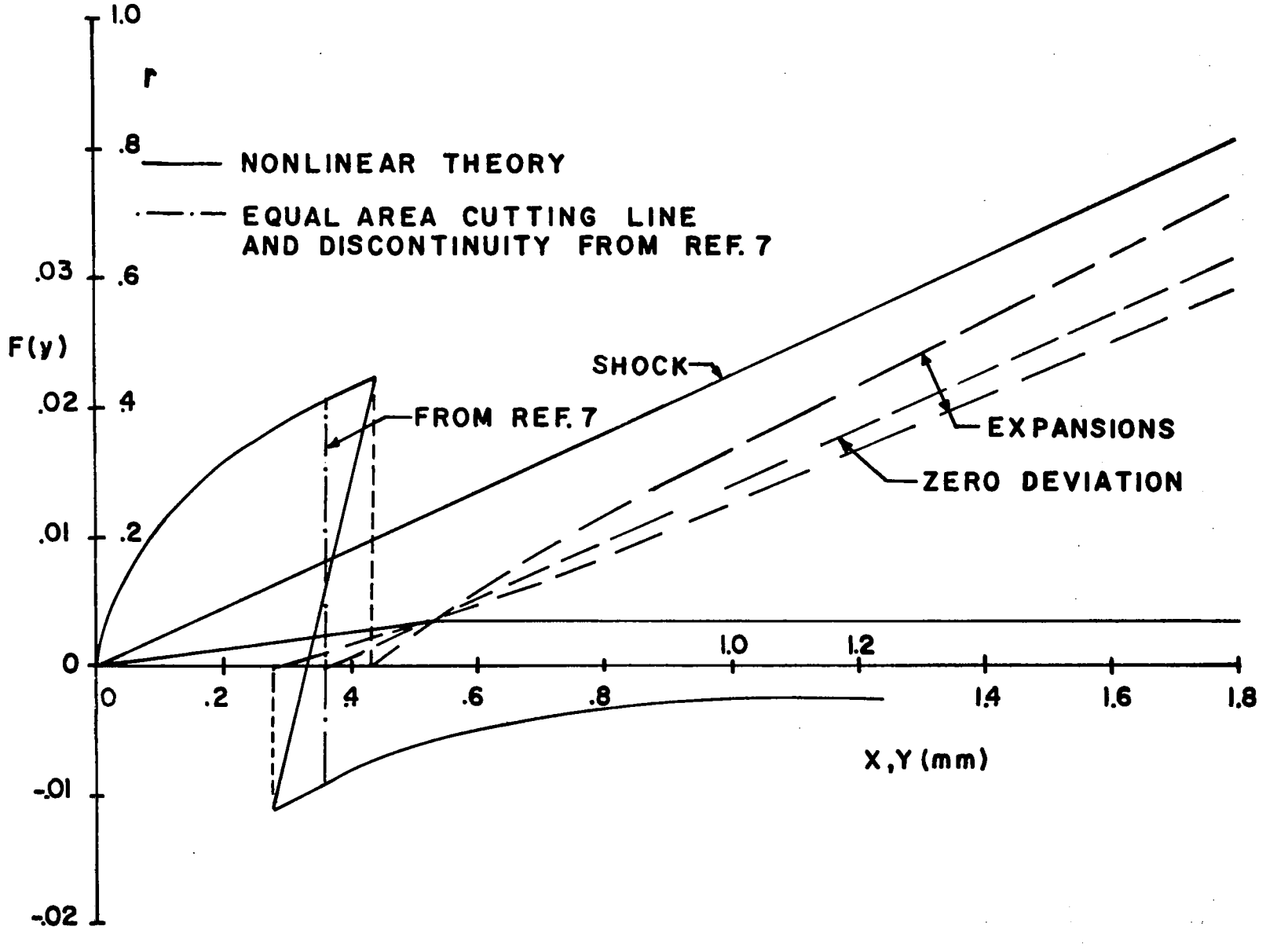

Fig. 31 Double values of F (y) for cone cylinder

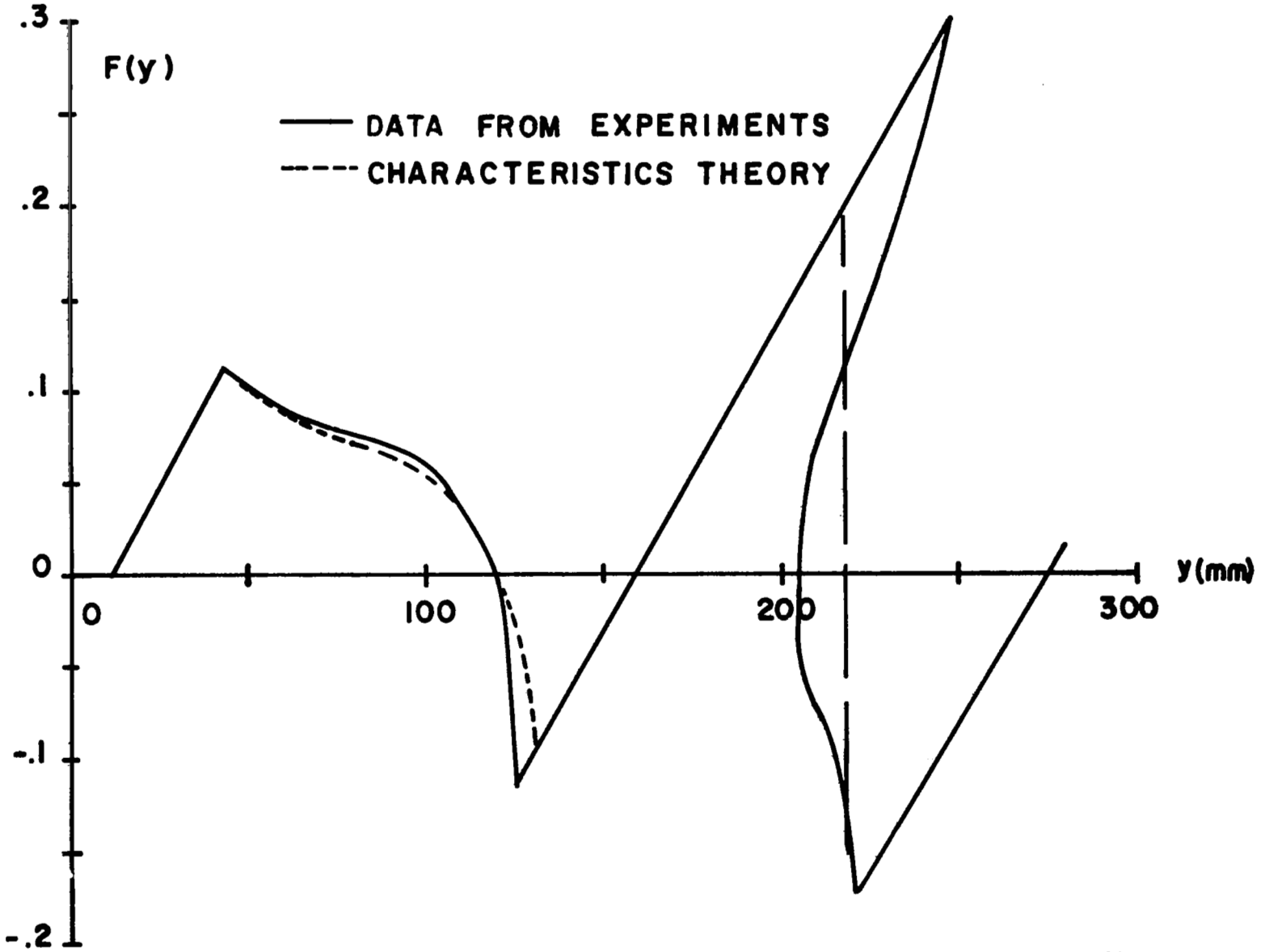

Fig. 32 Distribution of F function as function of y corresponding to curve 1 of Fig. 28

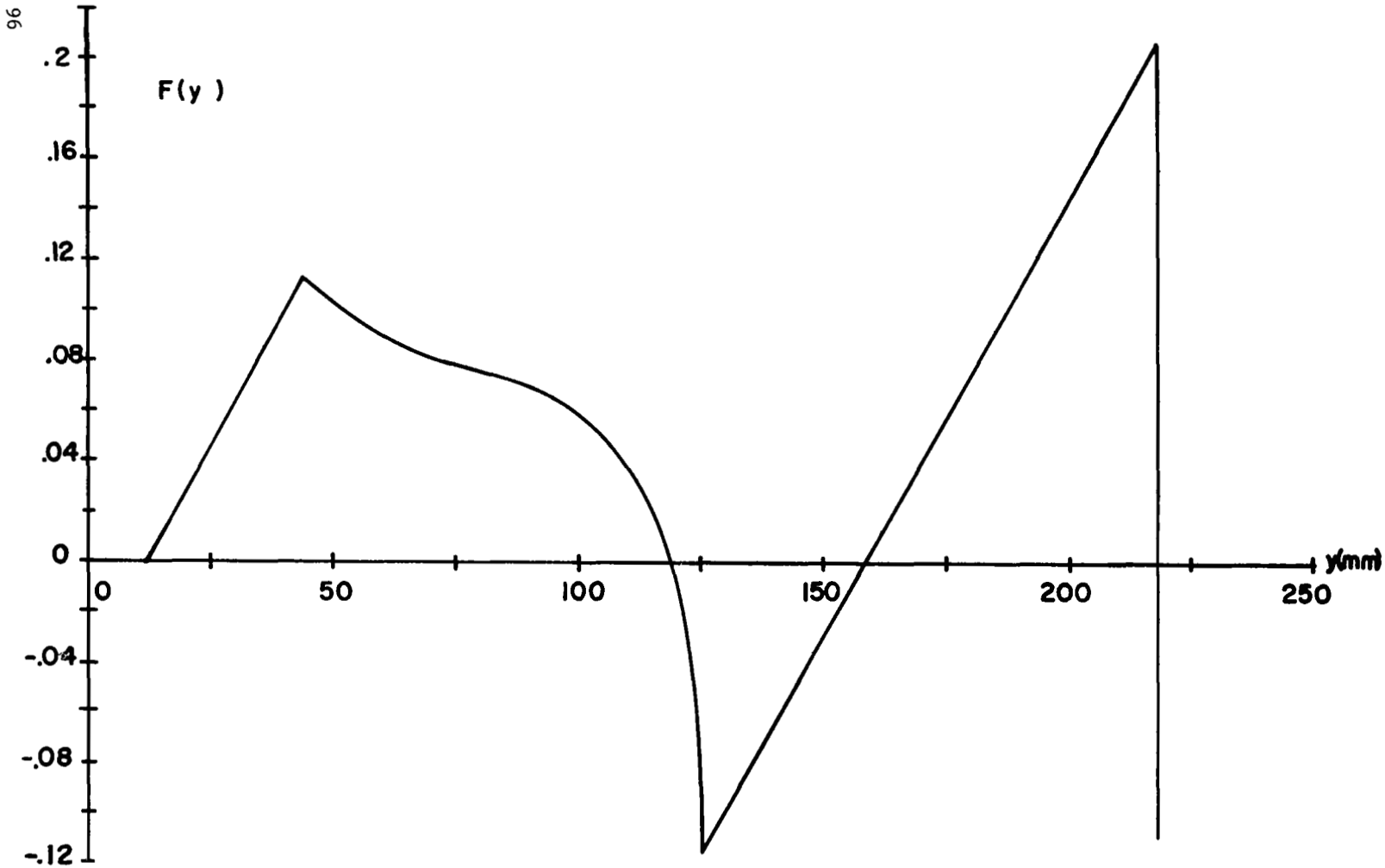

Fig. 33 F (y) used in the analysis corresponding to curve 1 of Fig. 28, $\alpha = 2.6^{\circ}$, r/L = 0.558

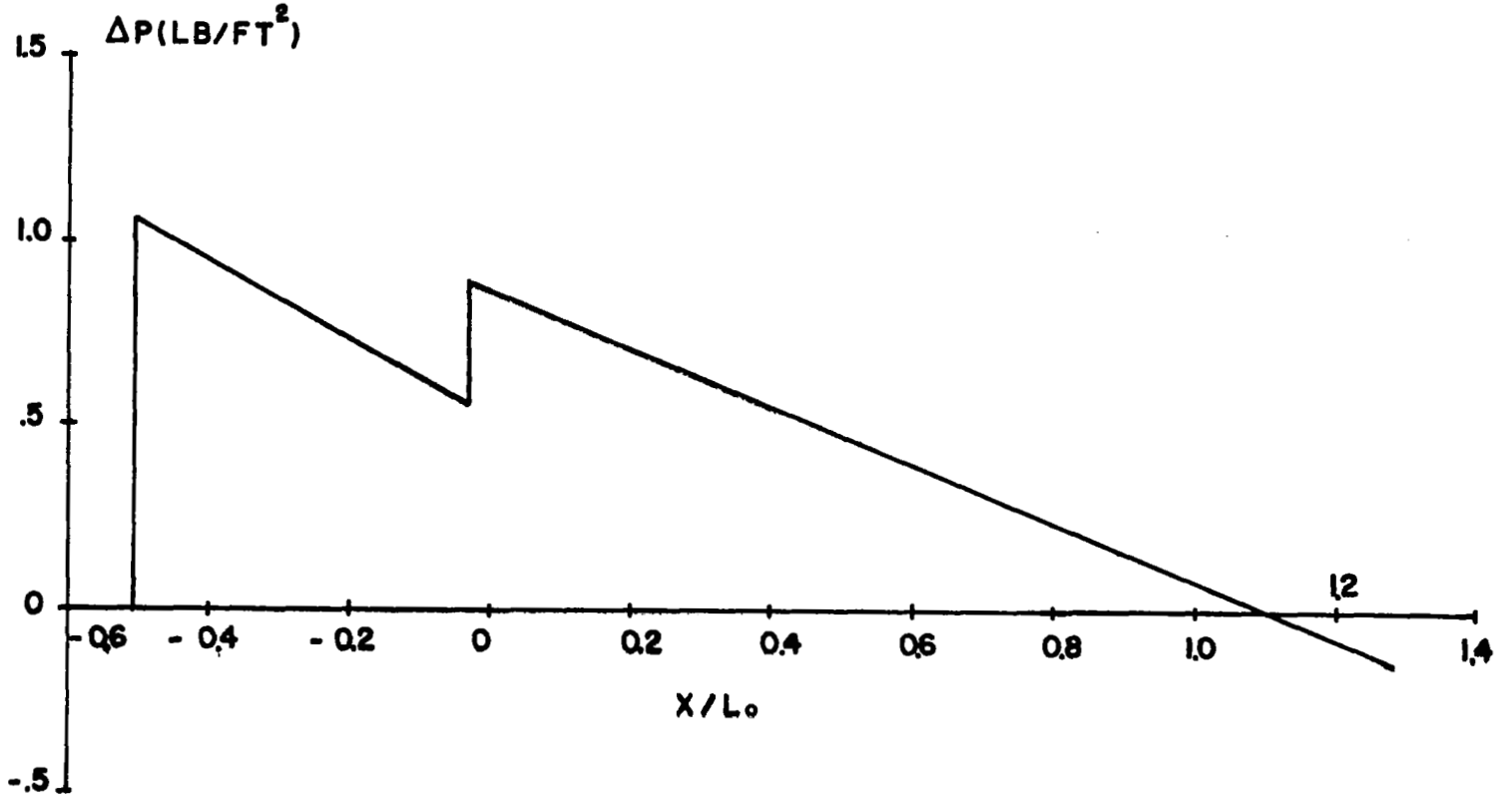

Fig. 34 Sonic boom signature at $r/L_o = 200$, for $L_o = 300$ ft and $L_o = 0.555$, variable density program (Curve 2 of Fig. 28)

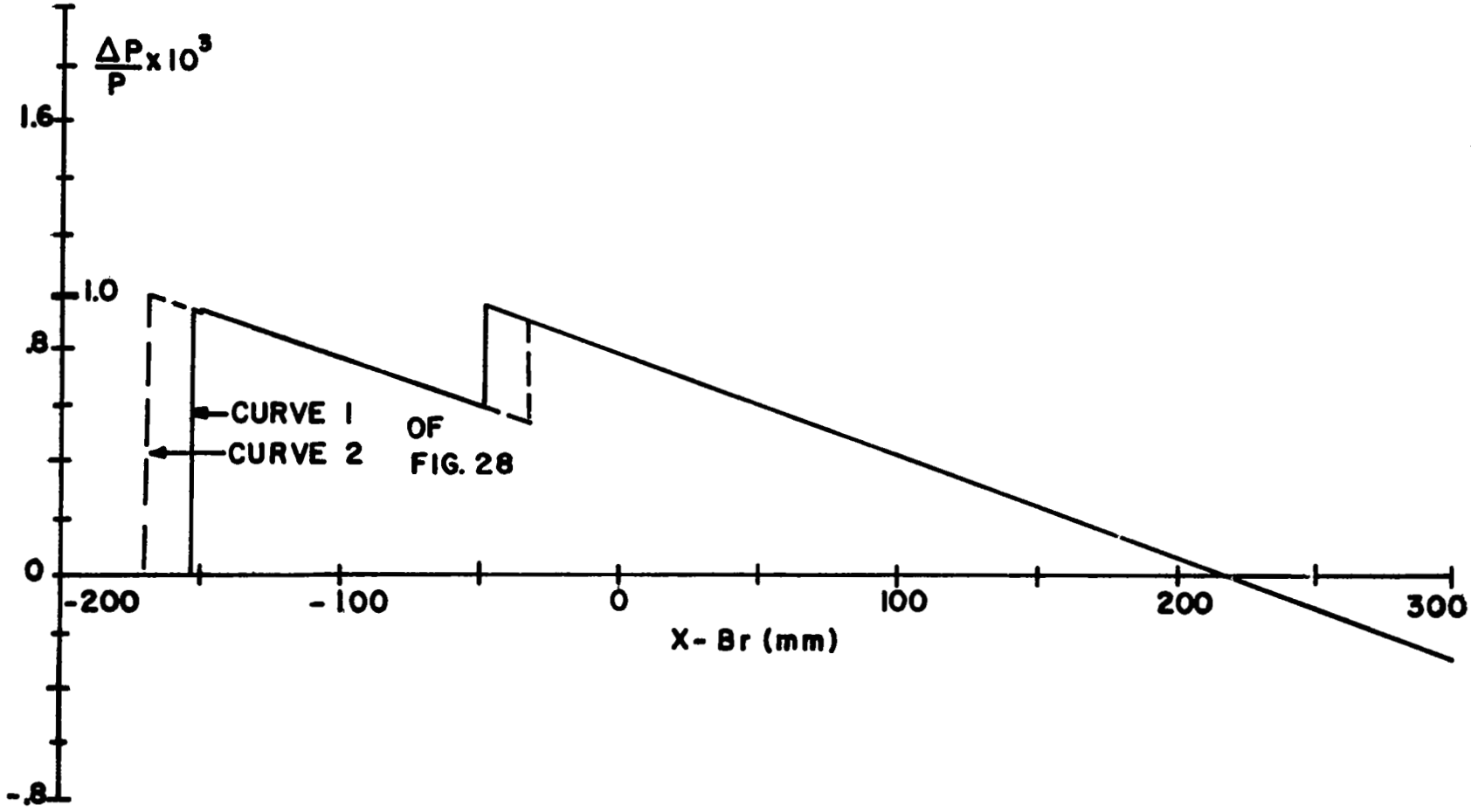

Fig. 35 Sonic Boom Signature (constant pressure) at r/L = 200 Kp = 1017 lb/ft^2

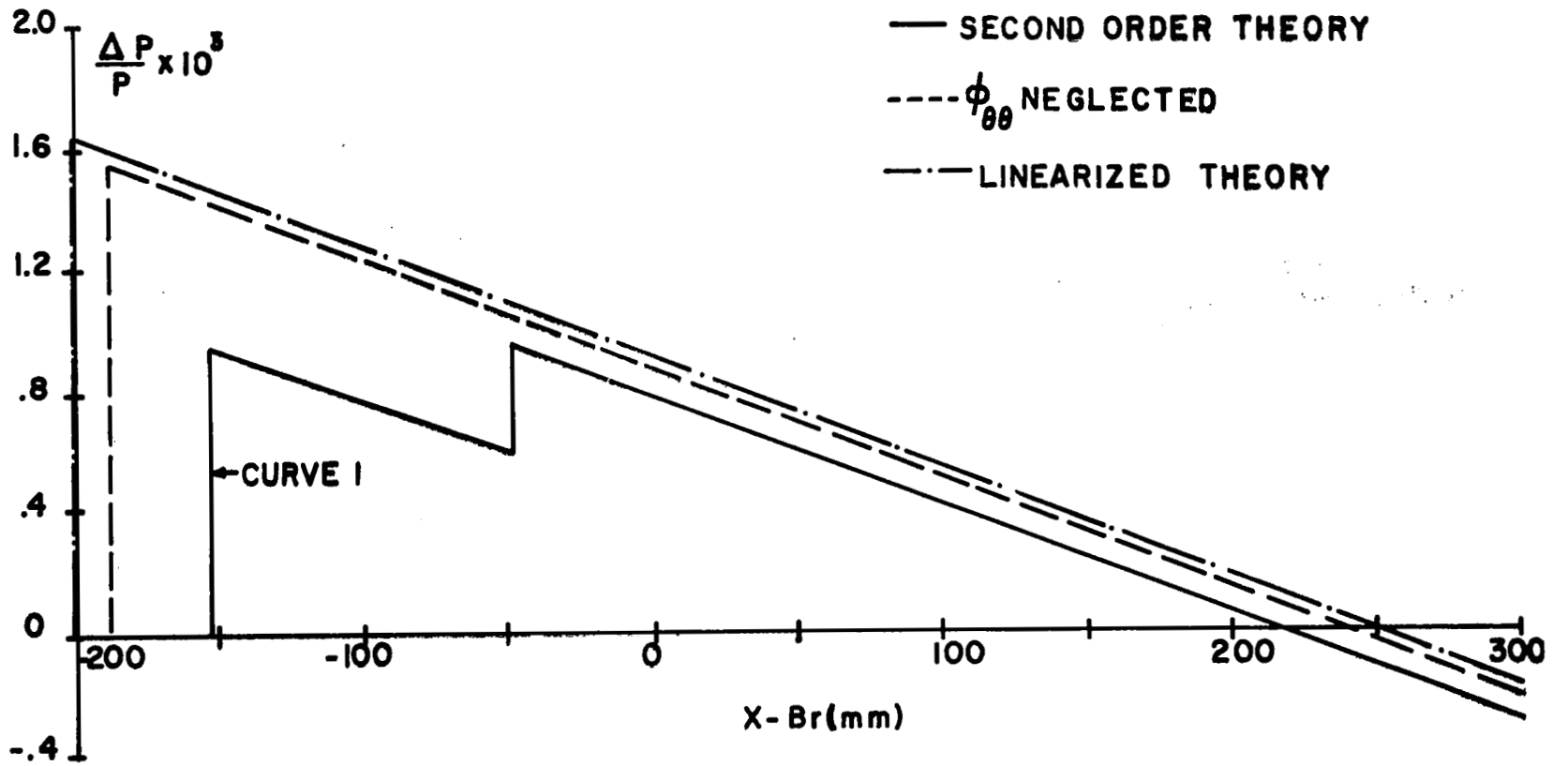

Fig. 36 Comparison of Sonic Boom Signatures for several types of analyses r/L = 200

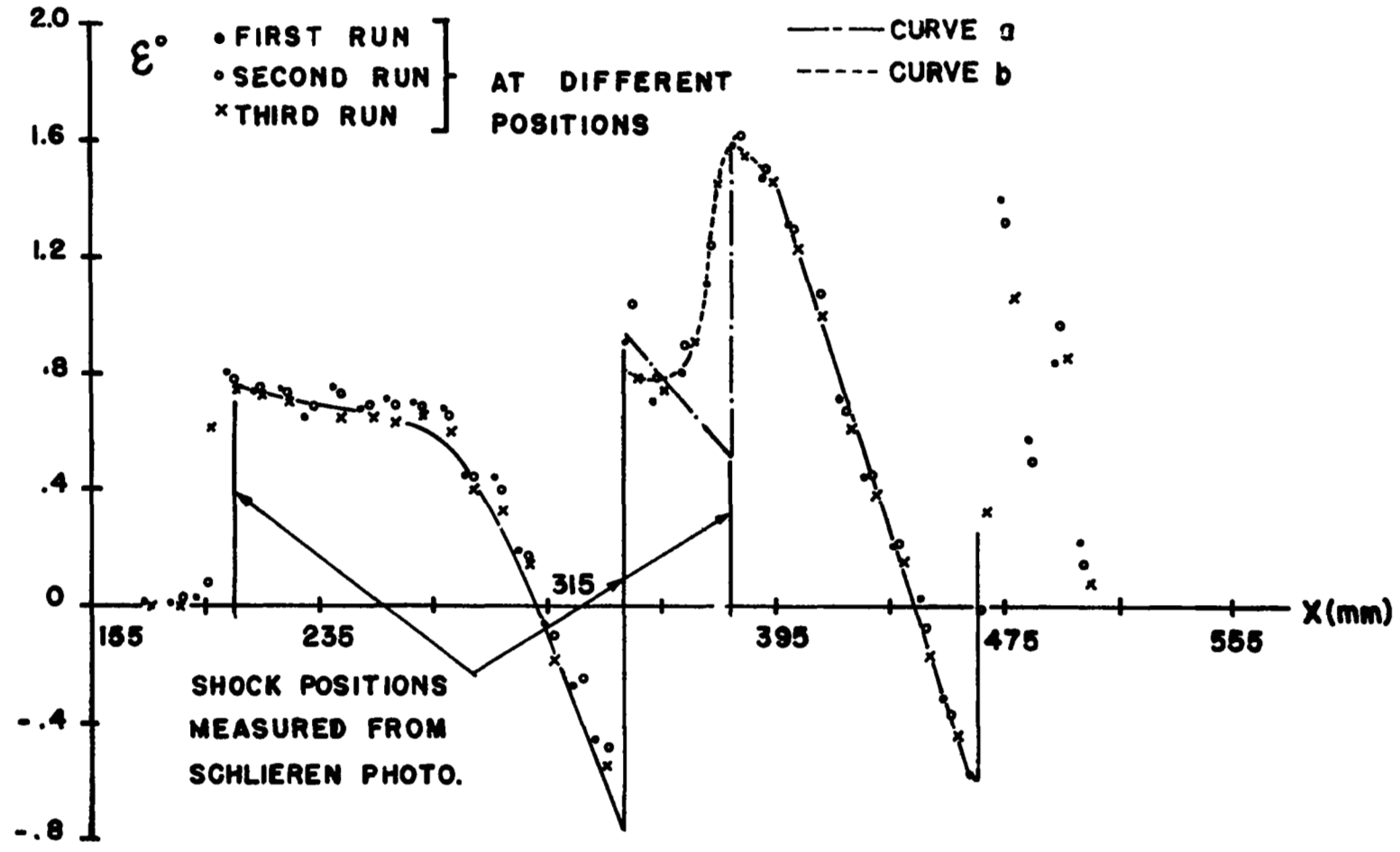

Fig. 37 Measurements of deviation angle of SST model at $r/L_o = 0.271$, $\bar{\epsilon} = 0.055$, $\alpha = 2.6^\circ$ at several positions

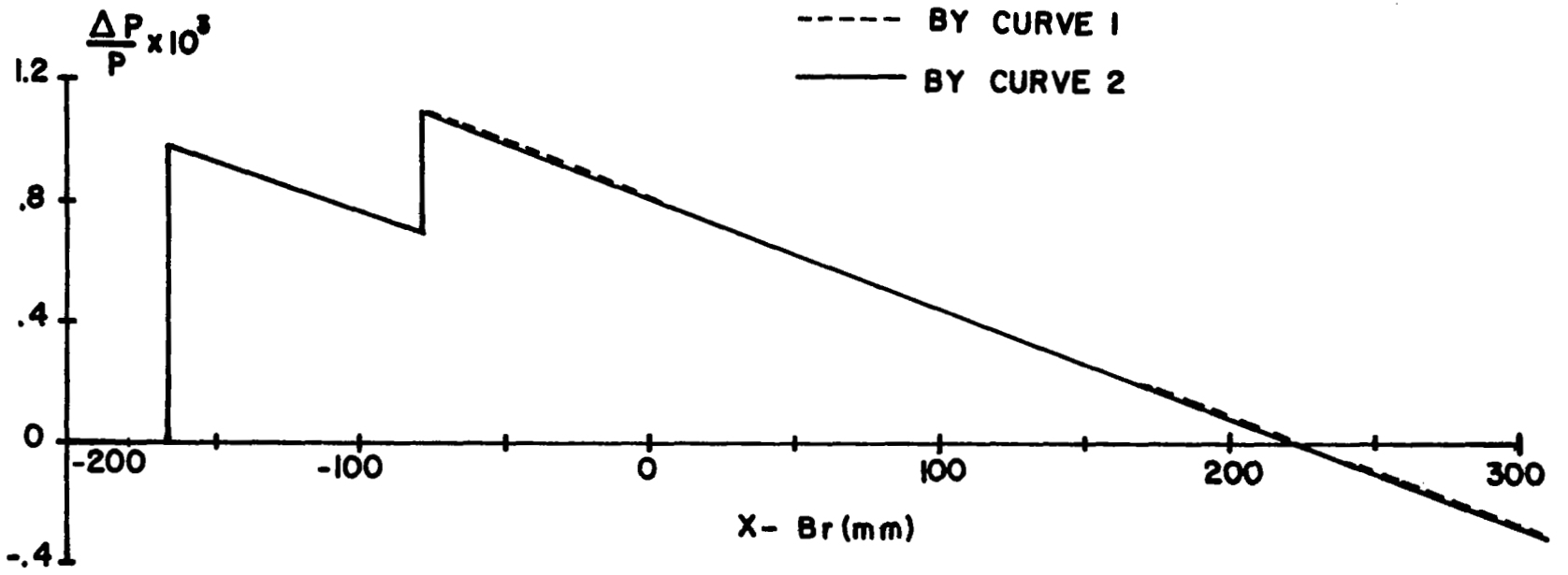

Fig. 38 Sonic boom signature for $\alpha = 2.6^{o}$, $\mathbb{C}_{L} = 0.055$ at $r/L_{o} = 200$ from data at $r/L_{o} = 0.271$, Kp = 1017 lb/ft^{2}

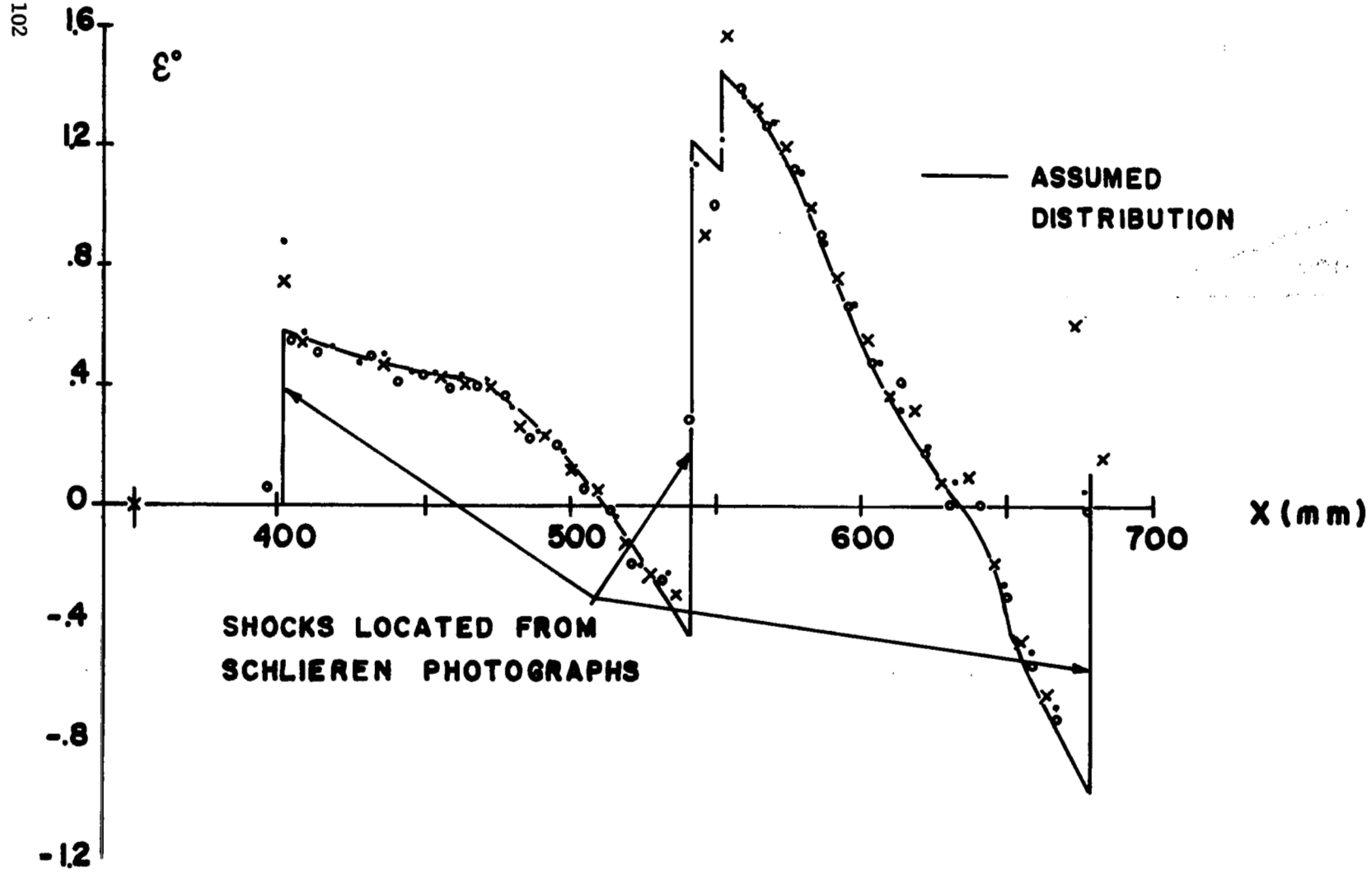

Fig. 39 Assumed distribution of ϵ at $r/L_o = 0.558$ $\mathfrak{L} = 0.066$, $\alpha = 3.2^o$

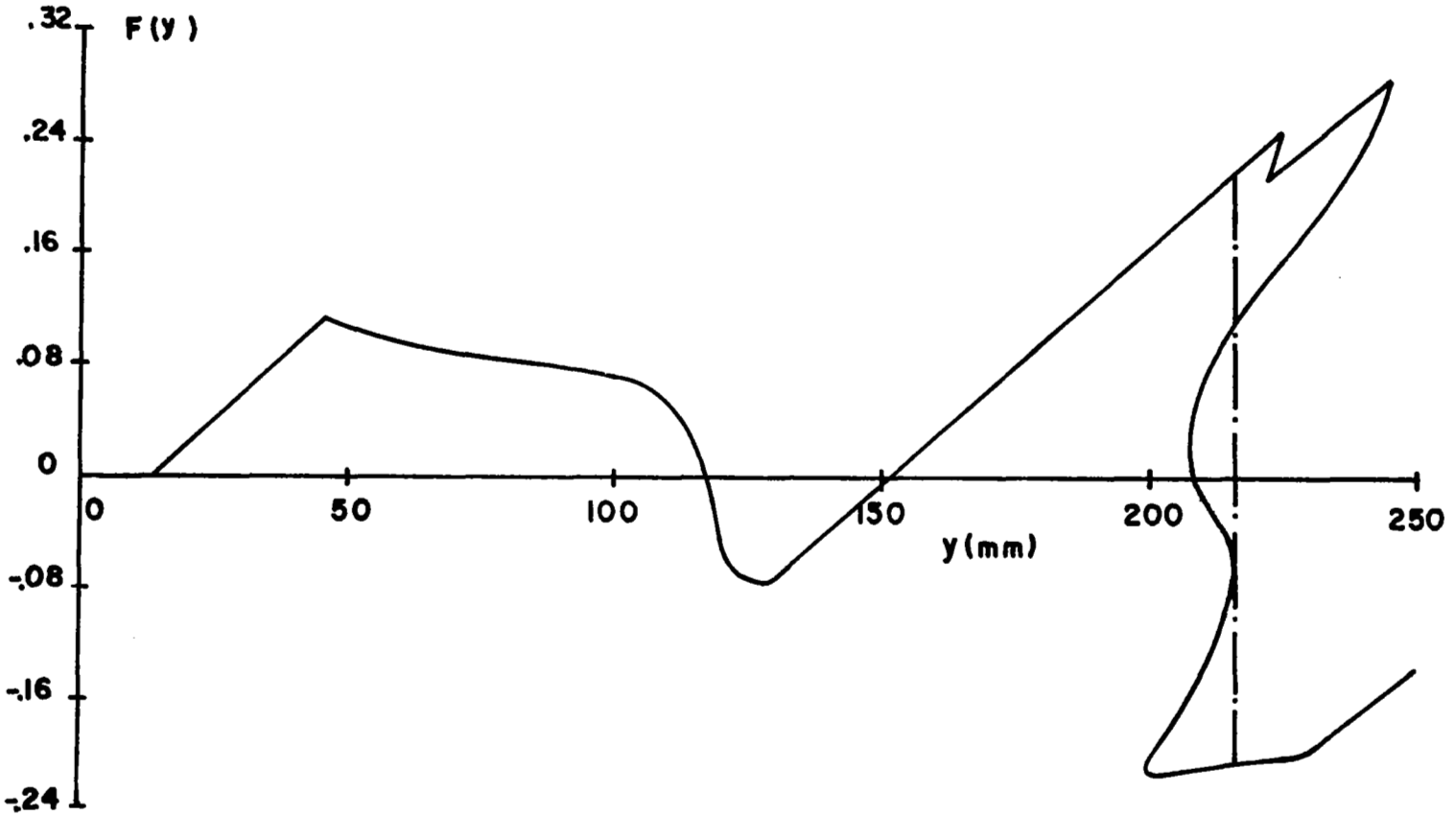

Fig. 40 F(y) curve for $\alpha = 3.2^{o}$ from data at $r/L_o = 0.558$

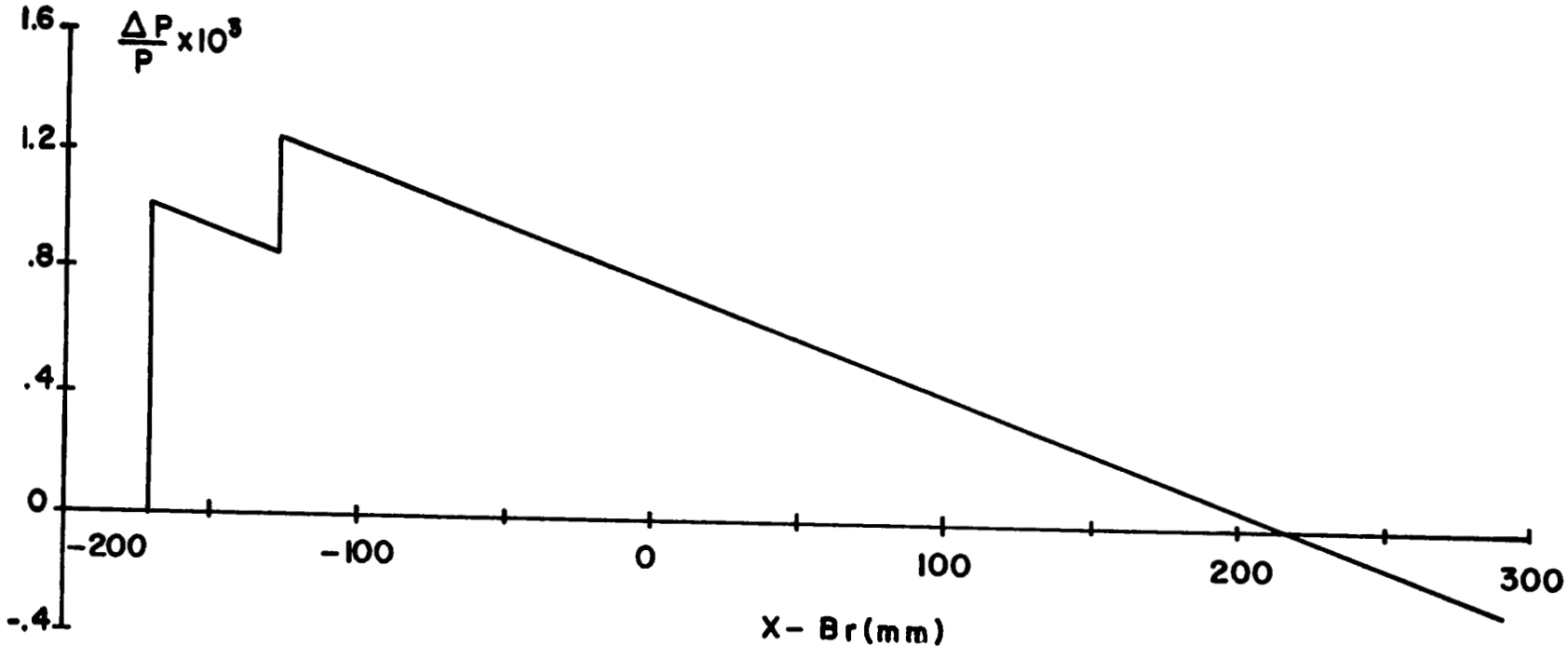

Fig. 41 Sonic boom signature for $\alpha = 3.2^{o}$, $\mathfrak{C}_L = .066$ r/L = 200 Kp = 1017 lb/ft^2